Study of Relaxation Dynamics and Ion Conduction Mechanism of Composite Polymer Electrolyte and Gel Polymer Electrolyte

Tapabrata Dam

Department of Physics & Astronomy
National Institute of Technology Rourkela

Study of Relaxation Dynamics and Ion Conduction Mechanism of Composite Polymer Electrolyte and Gel Polymer Electrolyte

Thesis submitted in partial fulfillment

of the requirements of the degree of

Doctor of Philosophy

in

Physics

by

Tapabrata Dam

(Roll Number: 511PH103)

based on research carried out

under the supervision of

Prof. Dillip K. Pradhan

and

Prof. Sidhartha S. Jena

March, 2017

Department of Physics & Astronomy

National Institute of Technology Rourkela

Department of Physics & Astronomy
National Institute of Technology Rourkela

March 24, 2017

Certificate of Examination

Roll Number: *511PH103*
Name: *Tapabrata Dam*
Title of Dissertation: *Study of Relaxation Dynamics and Ion Conduction Mechanism of Composite Polymer Electrolyte and Gel Polymer Electrolyte*

We the below signed, after checking the thesis mentioned above and the official record book (s) of the student, hereby state our approval of the thesis submitted in partial fulfillment of the requirements of the degree of *Doctor of Philosophy* in *Physics* at *National Institute of Technology Rourkela*. We are satisfied with the volume, quality, correctness, and originality of the work.

Sidhartha S. Jena Co-Supervisor	Dillip K. Pradhan Principal Supervisor
Simanchala Panigrahi Member, DSC	Garudadhwaj Hota Member, DSC
Ranabrata Mazumder Member, DSC	Suneel Kumar Srivastava External Examiner
Dilip Kumar Bisoyi Chairperson, DSC	Pawan Kumar Head of the Department

Department of Physics & Astronomy
National Institute of Technology Rourkela

Prof. Dillip K. Pradhan
Assistant Professor

Prof. Sidhartha S. Jena
Associate Professor

March 24, 2017

Supervisors' Certificate

This is to certify that the work presented in the thesis entitled *Study of Relaxation Dynamics and Ion Conduction Mechanism of Composite Polymer Electrolyte and Gel Polymer Electrolyte* submitted by *Tapabrata Dam*, Roll Number 511PH103, is a record of original research carried out by him under our supervision and guidance in partial fulfillment of the requirements of the degree of *Doctor of Philosophy* in *Physics*. Neither this thesis nor any part of it has been submitted earlier for any degree or diploma to any institute or university in India or abroad.

Sidhartha S. Jena	Dillip K. Pradhan
Associate Professor	Assistant Professor

Dedication

Dedicated to my
Family and Friends

Signature

Declaration of Originality

I, *Tapabrata Dam*, Roll Number *511PH103* hereby declare that this thesis entitled *Study of Relaxation Dynamics and Ion Conduction Mechanism of Composite Polymer Electrolyte and Gel Polymer Electrolyte* presents my original work carried out as a doctoral student of NIT Rourkela and, to the best of my knowledge, contains no material previously published or written by another person, nor any material presented by me for the award of any degree or diploma of NIT Rourkela or any other institution. Any contribution made to this research by others, with whom I have worked at NIT Rourkela or elsewhere, is explicitly acknowledged in the dissertation. Works of other authors cited in this dissertation have been duly acknowledged under the sections "Reference" or "Bibliography". I have also submitted my original research records to the scrutiny committee for evaluation of my dissertation.

I am fully aware that in case of any non-compliance detected in future, the Senate of NIT Rourkela may withdraw the degree awarded to me on the basis of the present dissertation.

March 24, 2017
NIT Rourkela

Tapabrata Dam

Acknowledgment

At the end of my Ph.D. work, it is a pleasant task and honour to express my sincere thanks to all those who contributed in many ways for my doctoral thesis.

First of all I would like to thank my thesis supervisors Prof. Dillip K. Pradhan and Prof. Sidhartha S. Jena for giving me the opportunity and freedom to work on this project. I would also like to express my deep sense of gratitude and indebtedness to my supervisors for their constant encouragement, constructive guidance and inspiration during my research work. I thank you teachers for your help, inspiration and blessings.

I would like to express my gratitude to my doctoral scrutiny committee members: Prof. D. K. Bisoyi, Prof. S. Panigrahi of Department of Physics & Astronomy; Prof. G. Hota of Department of Chemistry and Prof. R. Mazumder of Department of Ceramic Engineering for their valuable, insightful comments and suggestions that improved the quality of this work. I also must acknowledge my institute National Institute of Technology, Rourkela for providing me the necessary platform and facilities to carry out this research.

My special note of appreciation is for Prof. B. K. Chowdhury of Department of Physics & Astronomy for his immense support during the design and fabrication of low-temperature measurement system and to Prof B. G. Mishra of Department of Chemistry for helping and guiding me during the synthesis of my samples. I would also like to thank all the faculty members of Department of Physics & Astronomy for their fruitful suggestions during various seminars I have presented related to this work.

My sincere thanks to Prof. Marian Paluch from Institute of Physics University of Silesia and Central facility MEMS IIT Bombay, for necessary low-temperature dielectric measurements for polymer electrolyte samples. I would like to thank every present and past members of Ferroics Laboratory and Polymer Physics & Soft Matter Laboratory for maintaining such a good workable atmosphere in the laboratories and for bearing with me. Special thanks to Dr. Satya Narayan Tripathy and Mr. Hari Sankar Mohanty for their friendly cooperation and help in various ways and making my stay at NIT, Rourkela filled with a lot of memorable moments.

I am very much thankful to Dr. S. Naresh Kumar, Dr. Karan Kumar Pradhan, Mr. S. R. Mohapatra, Miss. S. Khandai, Mrs. Krushna Raut, Miss. Mithra K and Mr. Binayak Saho for all the help and good moments that we shared.

I bow my head to my teachers, Mr. Biplab Roy, Mr. Shaymol Kanti Roy, Dr. Manoj Kumar Laha, Prof. Dhiraj Kumar Basak, Prof. Chandana Acharya, Dr. Sujit Kumar Ghosh

and Prof. Raman Kumar Jha without whose inspiration and blessings, I would not have been able to come to the present position. Special thanks to all my High School, College, and University friends for their love and support throughout. Special thanks to Mr. Sourav Moitra, Mr. Sauvik Das and Mr. Suman Kumar Sen for giving mental support and keeping me pumped up.

I express my deep gratitude to my parents Mrs. Sefali Dam and Mr. Ujjwal Kumar Dam; wife Mrs. Keya Roy; grandparents Mrs. Kanan Bala Paul and Mr. Narendra Kumar Paul; in-laws Mrs. Dipali Roy and Mr. Tushar Kanti Roy; whose patience, understanding, support and love have been a key driver in this entire journey of work.

I would also like to thank Ministry of Human and Resource Development (MHRD), Govt. of India, for providing me financial assistance through NIT Rourkela during my Ph.D. work.

Above all, I sincerely thank Almighty **GOD** for his/her blessings

March 24, 2017 *Tapabrata Dam*

NIT Rourkela Roll Number: 511PH103

Abstract

The increasing demand for miniaturized portable electrical energy sources has led towards intensive research on developing efficient electrochemical energy storage/conversion devices. Based on the capability of delivering continuous energy for a longer period of time or quick charge-discharge capabilities, these devices can be divided into energy and current sourcing devices. Among these devices, batteries show intermediate power density along with energy density. At present in most of the commercially available devices, liquid organic carbonate electrolytes having conductivity values close to 10^{-3} Scm^{-1} are being used. Although liquid electrolyte shows a high conductivity value, they possess a serious safety concern. Therefore, prior importance is given to developing a polymer electrolyte with comparable ionic conductivity at ambient temperature. Polymer electrolyte has the prospect to improve various key properties of lithium based batteries when used as the electrolyte. These properties include design flexibility, safety, cyclability, energy and power density etc. However, polymer electrolytes are having a serious drawback of low ionic conductivity limiting its potential application. Therefore primary interest is given in the preparation of polymer electrolytes with high ionic conductivity at room temperature. Achievement of the desired level of ambient temperature ionic conductivity ($\approx 10^{-3}$ Scm^{-1}) is still an open problem. Literature suggests that to improve the ionic conductivity of polymer electrolytes several strategies such as plasticization, copolymerization, fabrication of composite/nano-composite etc. have been studied extensively. These techniques mainly concentrate on increasing the amorphous content of polymer electrolytes in order to favour ion mobility to increase the ionic conductivity. In this regard, optimization of ionic conductivity of polymer electrolytes is carried out in the present investigation for composite polymer electrolytes and gel polymer electrolytes. In addition to the process of optimization, prior importance is also given on the understanding the ion conduction mechanism in these two class of polymer electrolytes.

In this study three different series of polymer composite electrolytes are prepared using polyethylene oxide as the host polymer, lithium triflate as salt and nanocrystalline zirconia, titania and organo-modified hydrophobic montmorillonite clay as fillers. In addition to this a series of gel polymer electrolyte is also prepared by blending polymer host and 1 molar lithium triflate electrolyte solution consisting of a mixture of ethylene carbonate and diethyl carbonate as solvent. Phase formation of the filler materials, composite nature of polymer composite electrolytes and blended polymer host matrix prepared for gel

polymer electrolytes are studied using X-ray diffraction technique. Surface morphology of all these materials is studied using FE-SEM. Polymer salt interactions are investigated using FTIR. Ionic conductivity is measured over a wide range of temperature for getting proper idea about its temperature dependent behaviour. In all these electrolytes, we have achieved room temperature ionic conductivity up to the order of 10^{-5} S cm^{-1}. This is nearly two order higher in magnitude than conventional polymer-salt complexes at room temperature. Though we are successful in increasing the ionic conductivity by almost two orders in magnitude at room temperature, there exist a huge scope for further improvement in terms of the magnitude of the ionic conductivity. For this reason, a proper understanding of ion conduction mechanism is necessary. Ionic transport mechanism is probed using broadband dielectric spectroscopy over a wide range of frequency and temperature. Relaxation dynamics at different length and time scale is analyzed using broadband dielectric spectroscopy in order to get a proper idea about the ion conduction processes taking place at the microscopic level. The physical parameters that aids in increasing the ionic conductivity of these materials are also studied with observations made from broadband dielectric spectroscopy.

An in-depth step by step analysis of the data obtained from electrical characterizations are carried out. The temperature-dependent ionic conductivity for polymer composite electrolytes are found to follow VTF behaviour, indicating there exist coupling between ionic conductivity and polymer segmental motion. Segmental relaxation time also follow similar behaviour. To explain and investigate the coupled nature of ion conduction mechanism, ion diffusivity analysis is carried out by employing Trukhan model. The outcome of these analysis also supports the coupled nature of ion conduction process. Empirical laws like Jonscher power law, double power law and different models like RFEBM, Ngai coupling model, MIGRATION model are used to describe the frequency and temperature dependent ionic conductivity of polymer electrolytes. Havriliak -Negami expression is used to analyze the relaxation phenomenon present in polymer electrolytes. Study of ion conduction mechanism in polymer nanocomposite electrolyte suggest ionic conduction and segmental relaxation are coupled physical process. In the case of polymer gel electrolytes, polymer host does not play any significant role in ionic conduction but only provide the mechanical stability to the absorbed liquid electrolytes.

Proper understanding of ion conduction mechanism will help us for preparing good quality polymer electrolytes with high room temperature ionic conductivity, excellent mechanical, thermal and electrochemical stability. By achieving the aforementioned desired properties, the solid polymer electrolytes can replace the organic carbonate liquid based electrolytes commonly used in most of the portable energy storage/conversion devices.

***Keywords*: *polymer electrolyte*; *ion conduction mechanism*; *relaxation dynamics*; *first and second universality*; *ionic conductivity*.**

Contents

List of Figures

List of Tables

Chapter 1

Introduction

1.1 Preamble

With technological advancement and economic prosperity, the demand for energy is increasing rapidly. At present, the global energy economy is predominantly based on fossil fuels namely petroleum, coal, oil, natural gas, etc.[1] These are classified as the non-renewable sources of energy and are also depleting rapidly. Moreover, CO_2 and NOX emissions associated with the use of fossil fuel causes air pollution and global warming which affect our environmental sustainability severely.[2] Therefore, extensive research works are prioritized worldwide for the exploration of renewable, clean and environmentally benign energy resources. Particular interests are given to solar, wind, geothermal and oceanic current based power generation systems.[3–5]

However, energy production is only one aspect of alternative energy paradigm.[6] Another equally important aspect is energy storage/conversion devices to store the harvested energy so as to make it readily available and portable in necessity. Supercapacitors, fuel cells, secondary batteries are some of the important energy storage/conversion devices.[7] Secondary batteries have many advantages as an alternative source of energy storage/conversion devices. Lithium-based secondary batteries are showing good prospect for their reliability and other technological benefits among various energy storage/conversion devices.[8, 9] The reasons behind are as follows; lithium being the lightest and most electropositive metallic element facilitating very high energy density. These batteries have been found to be stable over 500 cycles and compared to the other batteries require less maintenance. Lithium batteries can also be manufactured in different shapes and sizes.[10, 11]

Polymer electrolyte is one of the key components to prepare efficient and durable energy storage/conversion devices like secondary batteries, supercapacitors, fuel cells etc.[12, 13] When used in different energy storage/conversion devices polymer electrolytes are having beneficial properties over their liquid counterpart like free from leakage, high energy density and processability . The functionality, working principle and importance of polymer electrolytes in Li-poly batteries will be discussed in section (1.2.1). Optimization of conductive properties of polymer electrolytes is essential for preparing

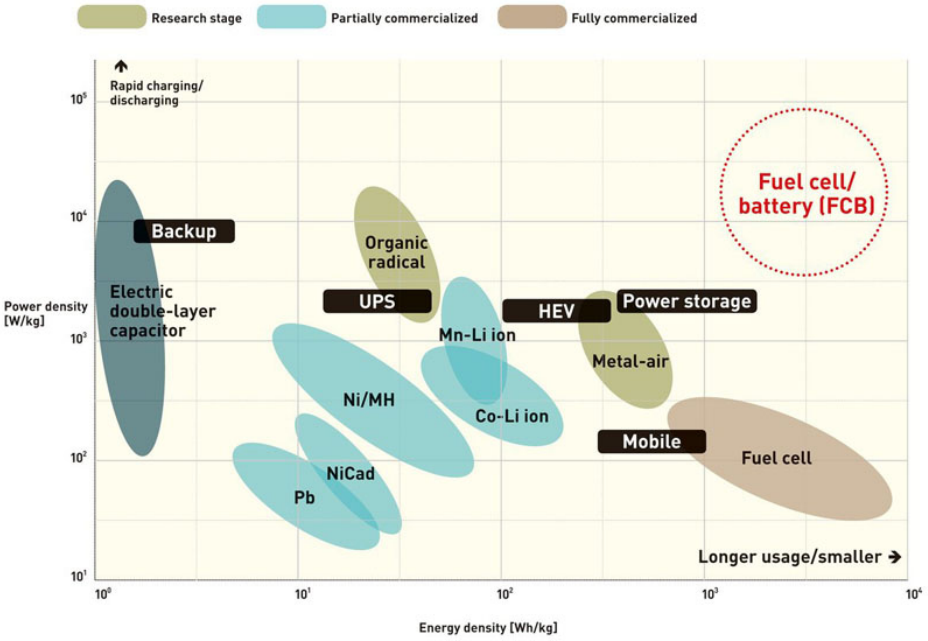

Figure 1.1: Ragone plot representing a comparative study of energy density and power density of different electrochemical storage-conversion devices.

better electrochemical energy storage/conversion devices. This process of optimization also demands an in-depth understanding of ion conduction mechanism in polymer electrolytes. The present investigation is focused on optimization of ionic conductivity along with investigation of the ion conduction process in polymer electrolytes.

1.2 Brief Introduction to Energy Storage and Energy Conversion Devices

The ever-increasing demand for portable and eco-friendly electrical energy is the main driving force behind the recent development in the field of energy storage/conversion devices. The difference between electrochemical energy storage and conversion device is; in case of storage devices reactants are sealed in the container and for conversion devices oxidant and reductant are fed into the electrochemical cell so that a continuous flow of electricity can be achieved.[14] Supercapacitors and batteries are the examples of electrochemical energy storage device and fuel cell is an example of electrochemical energy conversion device.[15] To get a broader perspective of these devices we need to study the Ragone plot. This plot maps power density as a function of energy density. The mapping of energy density and power density for various electrochemical energy storage/conversion devices is shown in figure (1.1).[16] It can be observed form Ragone plot that fuel cells and electrochemical double layer capacitors are at two extreme ends on Ragone plot. Fuel cells are having high energy density but at the same time they exhibit very low power density. This property indicates that using fuel cell one can draw energy for a longer duration of

time but if high energy is required in very short span of time, fuel cell will not be able to deliver the required energy effectively. Similarly using electrochemical double layer capacitors (EDLC) one can achieve very high amount of output current but its availability is for a very short period of time.[17] On Ragone plot, batteries are positioned in between these two extreme limiting ends. Batteries can deliver moderately high energy and power density.[16] The energy density of secondary batteries are increasing continuously due to property optimization and refinement of its constituent materials. A brief discussion on the structural and functional properties of these devices are required for a better understanding of their functionality and understanding the importance of polymer electrolytes in these devices. In this section, discussion will be focused on various types of energy storage/conversion devices.[14] It will also include how R&D in polymer electrolytes has become necessary for further development in the field of electrochemical energy storage/conversion devices. Required properties of polymer electrolytes for the particular application will also be stated after a brief description of these devices.

1.2.1 Battery

Electrochemical cells are capable of generating electrical energy from chemical reactions or can facilitate chemical reactions through the application of electrical energy. An individual or a set of electrochemical cells connected in series or parallel to deliver required output voltage is termed as a battery. Based on the functionality and reusability batteries can be classified into two major categories

- **Primary Batteries:** This class of batteries can be used only once. Here chemical energy is converted to electrical energy and the chemical reaction associated with electricity generation is not reversible in nature. Leclanché cell, zinc-chloride cell, alkaline manganese cell, zinc-mercuric oxide cell, cadmium-mercuric oxide cell, metal-air cell etc. are examples of primary batteries.

- **Secondary Batteries:** This class of batteries can be used for multiple discharge-charge cycles. Here the chemical reaction associated with electricity generation is reversible *i.e.* one can reverse the chemical reaction using externally applied electrical energy. Cadmium-nickel oxide cell, metal hydride-nickel oxide cell, iron-nickel oxide cell, zinc-nickel oxide cell, zinc-silver chloride cell, lithium-ion cell, lithium-polymer cell etc. are examples of secondary batteries.

Due to technological advancement in portable electronic gadgets, the global market demand for secondary batteries are increasing continuously as shown in figure (1.2a).[18] The chronological development of secondary lithium ion battery over the years is shown in figure (1.2b).[11] Also, the figure gives a comparative representation of volumetric and gravimetric energy densities among various secondary batteries. Clearly lithium-ion

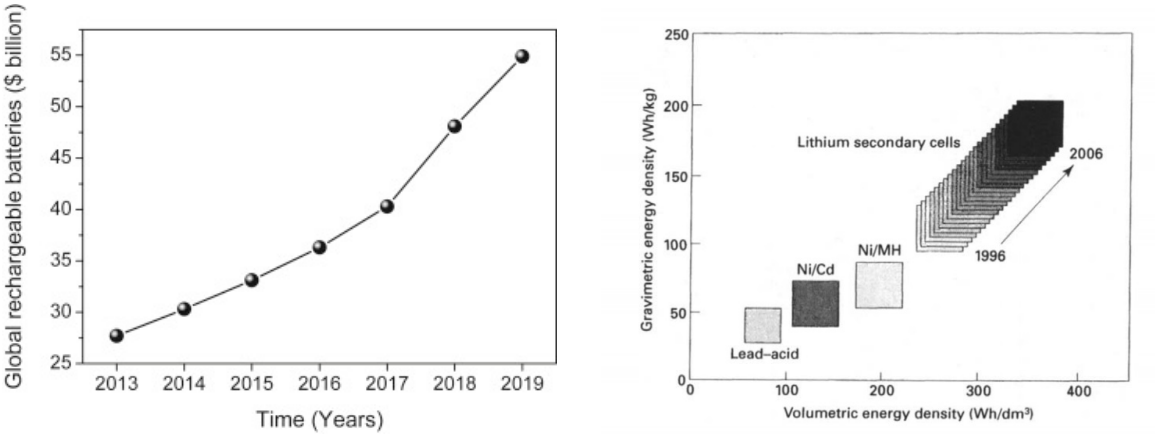

Figure 1.2: (a) Global Market Trend of secondary rechargeable batteries, emphasizing the consumer demand. (b) Comparative study of gravimetric and volumetric energy density of different types secondary batteries.

batteries showed an evolutionary improvement in both volumetric and gravimetric energy density over the years. Therefore, the focus is primarily given on the lithium based polymer electrolytes which are the key constituents of lithium-based secondary batteries.

The basic components of lithium ion batteries like anode, cathode, electrolytes and current collectors along with charge discharge operations are depicted in figure (1.3).[19] As anode and cathode take active participation in potential or voltage generation, these are termed as active components. On the other hand, electrolyte is termed as passive component because it do not take active participation in voltage generation. Polymer electrolytes help in transferring ions from one electrode to another during charge discharge processes.

During discharge, an external load is added between the electrodes of the battery. At the anode, metallic lithium after releasing one electron moves through the electrolyte and gets intercalated to the cathode; and free electron completes the circuit externally through the load. The opposite phenomenon occurs while lithium battery is charged with externally applied electrical energy. During charging process, Li^+ ions de-intercalate from the positive electrode, they diffuse through the electrolyte and intercalated or deposited back to the anode. Based on the nature and type of the constituents used, lithium ion batteries are termed in different manners.[20] In general, an intercalation compound is always taken as the cathode. The anode could be either metallic lithium or another intercalation compound. When metallic lithium is used as an anode, it is called lithium battery. If an intercalation compound, like lithiated graphite, is used as anode the resulting battery is termed as the lithium-ion battery.[21] Till date, in most of the commercialized lithium-ion batteries, organic carbonate based liquid electrolytes are used. These liquid electrolytes are having problems like flammability, leakage, electrode corrosion, high specific gravity, a limited temperature range of operation etc. Use of polymer electrolytes has significant advantage over the use of its liquid counterpart. Polymer electrolytes have improved

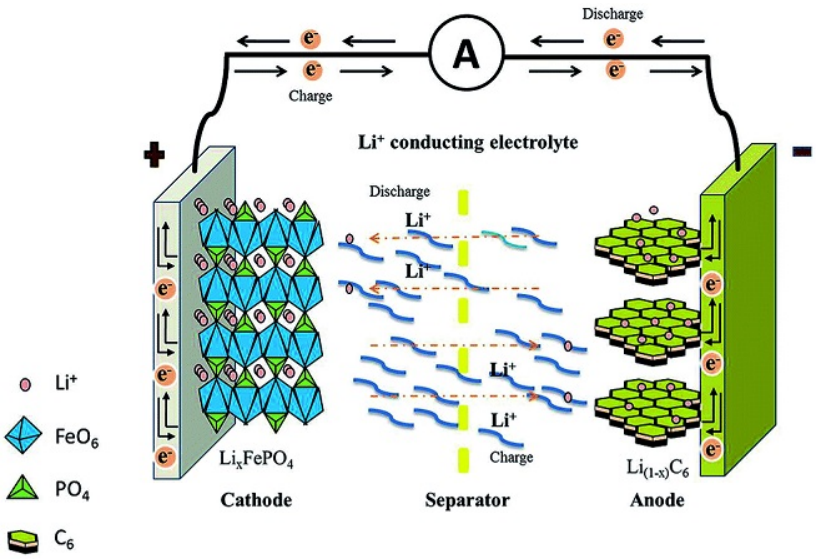

Figure 1.3: A representative diagram to elaborate the constructional building block of lithium batteries and charge-discharge process in secondary lithium batteries.

safety, enhanced endurance to varying electrode volume during charge-discharge cycling, better shape flexibility, reduced electrode reactivity etc. This kind of enhanced property parameters in polymer electrolytes draw the attention of researchers towards it. If the polymer electrolytes are used as the electrolyte in lithium based batteries, then they are termed as lithium polymer battery. Lithium polymer batteries are possessing superior properties along with better safety standards to other conventional secondary batteries for practical applications.[22] In the next section, the required properties of polymer electrolytes are described for a successful realization of lithium polymer batteries.

Performance requirement of Polymer Electrolytes in Batteries

As described in the constructional block diagram of lithium batteries shown in figure (1.3), polymer electrolytes are sandwiched between the anode and cathode materials. It fulfills the purpose of acting as the separator and electrolyte. To be successfully used in lithium batteries they should possess the properties given below

- **High ionic conductivity:** Polymer electrolytes should show a high ionic conductivity and high electronic resistivity. A high value of ionic conductivity facilitate ionic transport whereas a high value of electronic resistivity minimize self-discharge. To achieve rapid charge/discharge capabilities in batteries, the polymer electrolyte should have ionic conductivity of the order 10^{-4} Scm^{-1} or higher at ambient temperature.[23, 24]

- **Good Li^+ ion transference number:** In the polymer electrolytes the Li^+ ion transference number should be close to unity. A high value of transference number ensures reduced concentration polarization effect during the charge/discharge

processes. Therefore the prepared batteries should be capable of producing high power density.[25, 26]

- **Excellent mechanical strength:** Instead of showing the brittle characteristics like ceramic conductors, polymer electrolytes should be flexible. They should be capable to compress elastically when stress is applied on them during charge/discharge and ion transport process. To increase the mechanical stability and strength of electrolyte films various attempts are made such as adding inorganic fillers, cross-linking, introduction of additional physical support membrane etc.[27, 28]

- **Appreciable chemical and thermal stability:** Other battery components such as the electrodes, additives, cell separator and current collectors should not be chemically reactive to polymer electrolyte during charge/discharge process. The electrolyte should also posses thermal stability over a wide range of temperature.[29]

- **Wide electrochemical stability window:** The difference between the potentials of the reduction reaction and the oxidation reaction is defined as electrochemical stability window. Electrolyte should be be inert to both cathode and anode materials. This suggests that the oxidation potential must be higher than the embedding potential of Li^+ in the cathode. Again, the reduction potential should be low when the lithium metal stays in the anode during battery operation. Therefore, to become compatible with both electrode materials polymer electrolytes should have a wide electrochemical stability window of 4–5 V vs. Li/Li^+ transformation.[30–32]

1.2.2 Supercapacitor

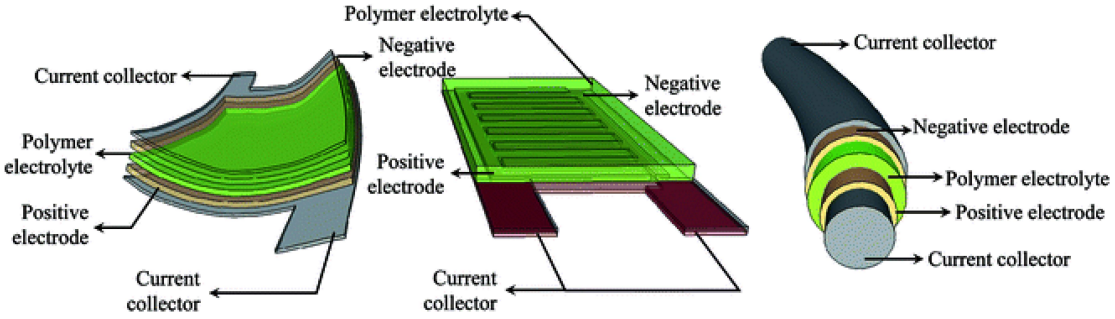

Figure 1.4: A representative diagram of polymer electrolyte-enabled supercapacitors in flexible sandwiched cell configuration (left), interdigitated finger cell configuration (middle) and coaxial fiber cell configuration (right).

The supercapacitor is another portable electrochemical energy storage device which is having high power density. From Ragone plot shown in figure (1.1) it can be observed that supercapacitor can be charged and discharged very rapidly.[33, 34] These devices can also withstand more charge-discharge cycles as compared to secondary rechargeable batteries

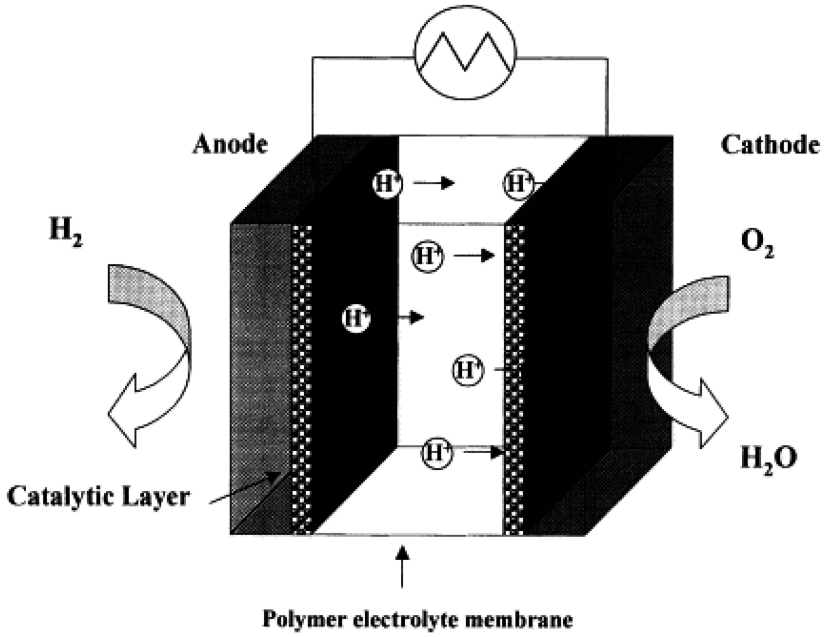

Figure 1.5: A representative diagram to elaborate the functionality of polymer electrolyte fuel cell and its constructional building block.

without losing their energy storage capacity. For these two properties, a supercapacitor is mainly used in the hybrid electrical vehicle, trains, cranes and elevators where burst-mode power delivery or short-term energy storage and regenerative breaking is required. In a supercapacitor, an electrically insulating ion-permeable membrane is placed between two electrodes filled with a liquid electrolyte.[35] As the leakage of liquid electrolytes is a matter of concern efforts are made to change these liquid electrolytes by using solid electrolytes. These next generation supercapacitors are safe and also provide high performance, bear less weight and can take flexible form factors. Among solid electrolytes, polymer electrolytes are ideal candidates for flexible solid supercapacitors. Different geometry and construction diagram of supercapacitors are shown in figure (1.4) where polymer electrolytes are used as solid electrolyte.[36]

1.2.3 Fuel Cell

In 1959 Grubb and his co-workers put forward the idea of using the organic cation exchange membrane in electrochemical fuel cells.[37] In terms of mode of operation the polymer electrolyte fuel cell (PEFC) is one of the most promising candidates among all fuel cell systems.[38] Therefore, a brief discussion on the constructional and operational aspect of PEFC is given in this section. PEFC consists of two electrodes and a solid polymer membrane as shown in figure (1.5).[38] Between two platinum-porous electrodes the polymer electrolyte membrane is sandwiched. Single cell PEFC assemblies can be mechanically compressed with using separators to fabricate stacks of PEFC. PEFCs can operate in a temperature range of 80 °C to 110 °C using H_2 as fuel and air/O_2 as oxidizer.

PEFCs can achieve upto 60% of efficiency.[39]

As far as the materials are concerned perfluorinated polymer electrolyte films made of FLEMION and NAFION is extensively used for fabricating PEFCs. These membranes possess good electrochemical properties, chemical, mechanical and thermal stabilities. PEFCs constructed with FLEMION and NAFION membranes are marginally expensive. It also show several problems when used in motor vehicles. These challenges can be overcome only if new proton-conducting polymer electrolytes can be prepared for extensive applications. It includes sulfonated aromatic polymers, Hydrocarbon polymers, alkyl sulfonated aromatic polymers, acid–base polymer complexes etc. Polymer electrolyte membranes for the use in PEFCs should have the following properties[38, 40]

- high conductivity values over a wide range of temperature
- durability
- water resistivity

1.3 Ionic Conductors: Brief Overview

Before the detailed discussion on polymer electrolytes, it is worth mentioning different classes of ionic conductors as a whole. It will serve the purpose of background study for the discussion of polymer electrolytes. Solid materials having high ionic conductivity (10^{-5} to 10^{-1} Scm^{-1}) and negligible electronic conductivity (10^{-9} Scm^{-1} or lower) are termed as ionic conductors. From the perspective of conductivity values in this class of materials, it is clear that the principal charge carrier must be ions resulting in a near unity value of ionic transference number. These materials exhibit activation energy less than 0.3 eV. Ionic conductors can be classified in various ways depending upon the types of charge carriers, the magnitude of conductivity, microstructure and different physical properties. Here the classification is carried out on the basis of microstructural properties. These are as follows

- **Framework crystalline/poly crystalline materials:** Framework crystalline materials consist of a rigid crystalline skeleton of mobile ions. These materials are further divided into two categories (a) soft framework crystals and (b) hard framework crystals. In soft framework crystalline materials bonds are ionic in nature and in general are polarizable. These materials also possess low Debye temperature where in between the low and high conducting phases a sharp ionic order-disorder phase transition appear. Silver iodide (AgI) is the most studied material in this category. In the case of hard framework crystalline materials bonds are covalent in nature. Debye temperatures are relatively high for these class of materials. NASICONS, montmorillonite, β - alumina, stabilized zirconia, $LiAlSO_4$ etc. are some of the examples of these class of materials.[41]

- **Amorphous-glassy electrolytes:** Using melt-quench techniques with various quenching rates or sol-gel methods these class of ionic conductors are prepared. Ion-conducting glasses have the following characteristic advantages over other solid ionic conductors. These class of materials possesses high isotropic ionic conductivity at room temperature with a low activation energy for ion migration, extremely low electronic conduction, the absence of grain boundary and high processability, greater thermal stability below the glass transition temperature.[42–44]

- **Composite or dispersed phase electrolytes:**The composite electrolytes are solid multiphase systems in which two or more materials are mixed to achieve desirable property, namely an enhancement in the ionic conductivity at room temperature. These two-phase composite electrolyte systems are prepared by dispersing sub-micrometer sized particles of chemically inert and insulating materials (e.g. Al_2O_3, SiO_2, ZrO_2, Fe_2O_3, SnO_2 etc.) into a moderate ion conducting solid host matrix (e.g. LiI, LiBr, LiCl, CuCl, $SrCl_2$, AgI, AgBr, AgCl, HgI_2, CaF_2, etc.). The ionic properties heavily depend on the surface properties and size of the dispersion phase.[45]

- **Polymer electrolytes:** Polymer electrolyte is an ionically conducting and electronically insulating solid phase. It is prepared by the dissolution of alkali metal salt in ion-coordinating polymers. This process of dissolution of alkali metal salts in ion-coordinating macromolecules are also termed as complexation. Conventional polymer salt complex in strict terms should be free from additives and or contaminants having low molecular weight.[46–49]

1.4 Polymer Electrolytes: Introduction and Classification

Based on the diverse and important field of application as discussed in section (1.2) and the cardinal role played by polymer electrolytes as a building block of those devices, the emphasis is to be given on polymer electrolytes. Based on the structure and constituent components, in general polymer electrolytes can be classified into the following categories

- **Polymer Salt Complex:** This is the first of its kind, which forms due to the complexation between a high molecular weight polymer and alkali metal salts having low dissociation energy. The room temperature ionic conductivity of polymer salt complex (PSC) are usually low, of the order of 10^{-9} Scm $^{-1}$ 10^{-7} Scm^{-1}. [50, 51]

- **Plasticized Polymer Electrolyte:** Organic carbonate or glycol based liquid having low molecular weight or ionic liquids are added to conventional polymer salt complex to prepare this class of electrolytes. Ionic liquids are nothing but salts in liquid state. They posses high dissociation constant, so gets easily dissociated leading to the enhancement of ionic conductivity.[52, 53]

- **Polyelectrolyte Membranes:** Polymers are in general neutral and in solution they don't undergo dissociation, but there exist some polymers which are having ionic backbone. The polyelectrolytes are polymeric single-ion conductors where the polymer backbone is charged. They release negative or positive ions when dissolved in a proper solvent and the polymer backbone also become negatively or positively charged. From the viewpoint of energy applications, generally the negative backbone based polyelectrolytes are favoured.[54]

- **Composite Polymer Electrolyte:** Nano particles having high surface area, added to conventional polymer salt complex to prepare this class of electrolytes. These class of polymer electrolyte show excellent mechanical strength, high electrical conductivity and electrochemical stability.

- **Gel Polymer Electrolyte:** These are nothing but liquid electrolytes trapped in a physical structure of a neutral polymer host. Gel electrolytes show solid like properties when characterized macroscopically and liquid like properties when characterized microscopically.[55–58]

Among these five above mentioned different classes of polymer electrolytes, plasticized polymer electrolytes and gel polymer electrolytes show excellent electrical properties having ionic conductivity (10^{-3} Scm^{-1}) with reduced mechanical and electrochemical stability. Whereas conventional polymer salt complex, polyelectrolyte membranes and composite polymer electrolytes show excellent mechanical properties along with moderately acceptable electrical properties having ionic conductivity (10^{-5} Scm^{-1}).

1.5 Brief History of Development and Current Status

In 1973 polymer electrolytes are first studied by P. V. Wright and co-workers[59, 60] and in 1978 M. B. Amrand and co-workers demonstrated their extensive potential to be used as materials for energy storage/conversion devices.[61] Therefore, this materials are having a history of more than four decades now. Over the time these materials have evolved and specific researches are carried out to overcome their various limitations. One of the most important property of these materials are that the conductivity behaviour is ionic in nature,[62] that is actually the main reason for extensive research on these class of materials. Here in the following sections a comprehensive discussion will be portrayed on various types of polymer electrolytes and techniques adopted to improve their properties for practical applications in energy storage/conversion devices.

1.5.1 Conventional Polymer Salt Complex

Polymer salt complex is the simplest polymer electrolyte. It is made of complexation between high molecular weight polymer having high dielectric constant and low activation

energy based alkali salts. Although conventional polymer salt complex has shown a promising prospect in terms of its field of applications, it is having the setback of very low values ionic conductivity. When salt is dissolved in a polymer matrix, the free energy change is governed by Gibb's free energy given by the following expression

$$\Delta G = \Delta H - T\Delta S \tag{1.1}$$

where, ΔH is the change in enthalpy, T is the temperature in absolute scale and ΔS is the change in entropy. The formation of polymer-salt complex will be thermodynamically favorable only if the Gibbs free energy reduces or ΔG assume negative values. At ambient temperatures for most of the alkali metal salt based polymer-salt complexes are having ionic conductivity ranging from 10^{-9} Scm^{-1} to 10^{-7} Scm^{-1}. Therefore at initial stage focus is given mainly on polymer-salt interaction, easy dissociation of salt in the host matrix, elevation of glass transition temperatures, polymer architecture and its influence to increase the value of ionic conductivity. The way these properties are affecting the ionic conductivity of the polymer salt complex at macroscopic scale is also studied at great length by various research groups. Considering the ability to dissociate lithium salts and the electrochemical stability of the formed polymer salt complex; polyethers are one of the best materials acting as host polymer. The process of dissolution of salt into host polymer matrix occurs via coordination bond formation between the ether oxygens of polymer and the alkali cations of salt. Polyethers possess flexible ethylene oxide segments and ether oxygen atoms, which have a strong electron pair donor characteristics *i.e.* they act as a Lewis base and therefore readily solvate Li^+ cations. The polyether polyethylene oxide (PEO) is the most investigated material and it is easily available in a relatively pure state at low cost. Among other polymers polypropylene oxide,[51] poly[bis(methoxy-ethoxy-ethoxy)phosphazene], polysiloxane etc. are also investigated. They possess low glass transition temperature and also show semi-crystalline nature at ambient temperature.

After the demonstration of M. B. Armad *et. al.* about the potential of polymer salt complex, comprising PEO and alkali metal halide salts, to be used in devices applications a lot of work was focused on these class of materials; particularly related to the improvement of ionic conductivity and ion conduction process in PEO-alkali halide systems. In 1981 J. M. Parker *et. al.* proposed that the morphology of the sodium and lithium ion based complexes with PEO are best described by a double strand helical arrangement of the PEO chains.[63] A schematic of a helical structure of PEO is shown in figure (1.6a) and schematic for the interaction between polymer and ions are shown in figure (1.6b). In the same year, D. F. Shriver *et. al.* particularly mentioned that polymer electrolytes with alkali metal complexes of polyethers are found to have considerable cationic mobility. This large magnitude of mobility may be a result of large-amplitude motions of the polymer.[64] E. Strauss *et. al.* demonstrated in their work with PEO-LiI based system, that the nature of ionic conductivity depends on the ratio of EO to Li. They optimized EO:Li over the range 9 to 80 and reported

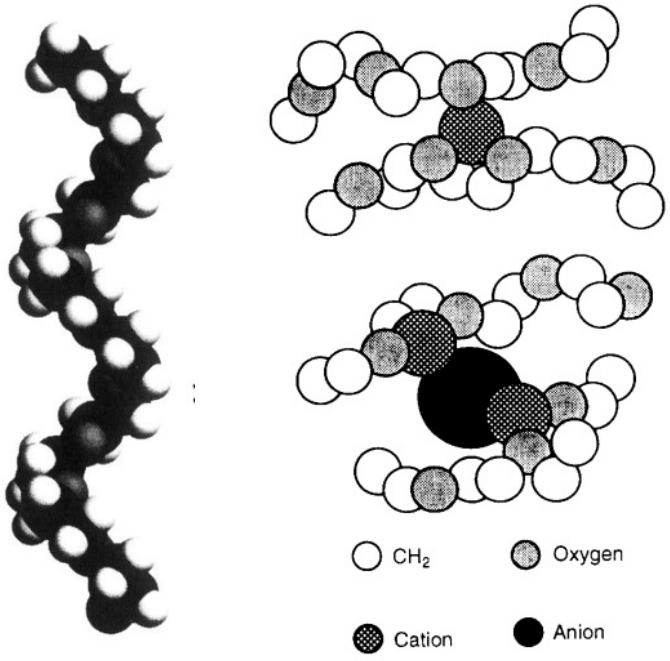

(a) (b)

Figure 1.6: (a) Polyethylene oxide viewed parallel to the 7/2 helix which is the basis of the structural unit in the crystalline phase having two turns of a fiber identity period of 1.93 nm. (b)Formation of transient cross-links via a cation and anion.

in that range the conduction process mainly depends on the diffusion coefficient of cations. The ionic conductivity value remains nearly similar in that range. However, a maxima was observed at EO:Li ratio 20.[50]

The change in glass transition temperature with the addition of metallic halide salts is discussed by D. B. James *et. al.*. They found an increase up to 140 K in glass transition temperature can be obtained with the addition of $ZnCl_2$ salt at different concentration.[65] Glass transition temperature of polymer salt complex is a crucial physical parameter as it controls the polymer segmental motions. Recently Joh Motomatsu *et. al.* studied ionic conductivity and dielectric properties of polymer electrolytes based on poly(ethylene carbonate) and lithium bis(trifluoromethane sulfonyl)imide. They reported the variation in polymer segmental relaxation with varying salt concentration in polymer electrolyte system.[66]

Though a different combination of polymer and salt are studied, but ionic conductivity of these conventional polymer-salt complexes can not be increased beyond 10^{-7} Scm^{-1}. Therefore, to increase the ionic conductivity various types of additives are added to polymer-salt complexes. Because of different kinds of additives a diverse range of polymer electrolytes were made and investigated by the researchers. A brief overview is presented in the following sections.

1.5.2 Plasticized Polymer Electrolytes

To increase the amorphous content in a polymer electrolyte as well as promote segmental mobility of polymer liquid plasticizers are added to the polymer salt complex. Using this technique ionic conductivity of the polymer electrolytes can be increased. A plasticizer can be low molecular weight organics,[30, 67–69] organic solvents or ionic liquids.[70] In this section, an overview of organic low molecular weight based plasticizer will be given first. Thereafter recently evolving ionic liquid based plasticized polymer electrolyte will be focused.

Charles W. Walker *et. al.* reported that with the addition of diethyl phthalate as plasticizer the ionic conductivity increases from 7.7×10^{-5} Scm^{-1} to 4.6×10^{-3} Scm^{-1} at 60 °C.[71] M. S. Michael *et. al.* reported the optimized ionic conductivity for the plasticized polymer electrolytes having composition PEO_8-$LiClO_4$: DOP $(99.9 : 0.1)$ is 4.305×10^{-3} Scm^{-1}, PEO_8-$LiClO_4$: DBP $(99.9 : 0.1)$ is 4.994×10^{-3} Scm^{-1}, PEO_8-$LiClO_4$: DMP $(99.9 : 0.1)$ is 1.331×10^{-4} Scm^{-1}. Here, DOP, DBP and DMP stands for dioctyl phthalate, dibutyl phthalate and dimethyl phthalate respectively.[52] Yuki Kato *et. al.* prepared polymer electrolyte plasticized with polyethylene glycol and borate ester and reported ionic conductivity is of the order of 10^{-5} Scm^{-1} at 20 °C. They also reported the electrolytes are electrochemically stable up to 4.5V vs. Li^+/Li and thermally stable up to 300 °C.[53] M. Z. A. Yahya *et. al.* studied chitosan based plasticized polymer electrolyte with lithium acetate as the salt and oleic acid as the liquid plasticizer. They reported that with the addition of 10 wt.% oleic acid, ionic conductivity increases upto the order of 10^{-5} Scm^{-1}.[72] A. A. Mohamad *et. al.* prepared alkaline solid polymer electrolytes using poly(vinyl alcohol), potassium hydroxide, α-Al_2O_3 and different amounts of propylene carbonate. With the addition of plasticized propylene carbonate composite electrolyte phase made of poly(vinyl alcohol), potassium hydroxide and α alumina its conductivity increases to the magnitude of the order 10^{-4} Scm^{-1}.[73] M. F. Z. Kadir *et. al.* studied chitosan-poly(vinyl alcohol) blend polymer electrolyte and reported that with the addition of 70 wt.% EC, maximum ionic conductivity 1.6×10^{-3} Scm^{-1} is achieved.[74] In recent times ionic liquid based polymer electrolytes are getting attention. Ionic liquids can be considered as salts in liquid phase. Addition of ionic liquid increase the ionic conductivity and at the same time it reduces dual ion conduction, which is one of the causes of premature failure of devices made of these class of materials.

Over all, it can be clearly observed that ionic conductivity of plasticized polymer electrolytes are much higher than conventional polymer salt complexes, but there exist serious drawbacks in terms of mechanical and electrochemical stability in this class of materials. Addition of low molecular weight additives also affect the energy density properties of the prepared devices.

1.5.3 Polyelectrolyte Membranes

The study on polyelectrolytes and salt complexes can be traced back to 1974, where N. L. Kuzntsova *et. al.* studied the gel structure of polyelectrolytes using poly-(1,2-dlmethyl-5-vinylpyridinium methylsulphate) and sodium polystyrenenesulphonate as specimens. The study reported the formation of a heterogeneous perforated continuous framework like structures interconnected polymers creating spherical voids. This study deals only the physical properties. Electrical properties are not analyzed at all in this early stage of study.[54]

The higher mobility of LI^+ causes an accumulation of anions around the electrode. The resulting gradients in the salt concentration formed in this process are responsible for the electrode polarization and it deteriorate the device performances. Dual ion conduction has been identified as one of the major reasons for premature device failure. Some attempts have been made to overcome this drawback during these last decades. As an example the use of large and heavy anions or of anion receptors like boron, linear and cyclic azo-ether compounds helped in reducing the concentration gradient effect.. In this context various techniques has been adopted to reduce the anion transport. Alkali metal salts of poly(methacrylic acid) and polysulfonic acid and their blends with polyethylene oxide with different molecular weights are used.[75] H. Ohno *et. al.* proposed PEO-methacrylic acid and poly(oligo-oxyethylene)methacrylate based systems as polyelectrolytes for lithium batteries. For different polymer structure the obtained ionic conductivity at 50 °C is found in the range 10^{-6} Scm^{-1} to 10^{-4} Scm^{-1}. Reduced anion movement through electrolytes may helps in increasing the self discharge duration of batteries.[76] Keeping these in mind recently focus has been given to poly-electrolyte films for probable use in energy storage/conversion devices and these class of materials has to be explored in detail before any possible move for device fabrication. [77–79]

1.5.4 Polymer Composite Electrolytes

There exist a major problem of low ionic conductivity in conventional polymer salt complex. Various combinations are tried to improve the ionic conductivity like used of low dissociation energy based salts, a salt having bulky anions, high dielectric constant based polymer host, a polymer having high glass transition temperature etc. However, much success could not be achieved in terms of improvement of ionic conductivity. The conductivity values remained well below the accepted level to be used in the electrochemical energy storage/conversion devices. Plasticized polymer electrolytes was also an another way to improve the electrical properties which had already been discussed. Though using these technique conductivity values can be increased easily up to the range 10^{-2} Scm^{-1} to 10^{-4} Scm^{-1}, but this technique compromises on other beneficial attributes like mechanical and electrochemical stability.[80] Loosing these advantageous properties are also not acceptable as well, while the goal is

to develop all solid state electrochemical energy storage/conversion devices. Therefore, different solid non-conducting additives are added to conventional polymer salt complex to find their influence on electrical properties. These includes nanocrystalline ceramic materials and modified layered clays. These class of materials are termed as polymer composite electrolytes and showed increased ionic conductivity as compared to polymer salt complex. At the same time, polymer composite electrolyte retains the beneficial properties like mechanical, electrochemical and interfacial stability properties as required for device applications.[46–49] Depending upon the nature of the interaction of filler with host polymer salt matrix and their roles played in ion conduction process, these can be classified into two major categories (i) active and (ii) passive. W. Wieczorek *et. al.* had shown the difference between these two types of fillers in their study using $AlCl_3$ as active and β-Al_2O_3 as passive filler.[81] Active fillers participate via interaction with salt and polymer in the ion conduction process *i.e.* it affects ionic conductivity and cationic transport number irrespective of the type of basic system of polymer electrolyte used. On the other hand, passive fillers are not involved in the ion conduction process directly. In passive class, there exist several types of fillers including inert oxides, ferroelectric materials, clays, carbonaceous materials etc. These fillers have been used in combination to different polymeric matrices to increase the ionic conductivity as well as improve various properties like interfacial stability, mechanical strength and electrochemical stability. These fillers can also influence the ion transport mechanisms in a variety of indirect ways such as speeding up segmental dynamics, inhibiting polymer crystallization and increasing the free volume.[82, 83] In the present study focus is given on the passive fillers. In this section, a detail literature review is carried out regarding the development on ceramic and clay based composite polymer electrolytes. At first discussion will be centered around the ceramic additives and thereafter focus will be given on modified layered clay additives to prepare composite polymer electrolytes.

Polymer Composite Electrolytes: Ceramic Filler Based

Ceramic fillers are added to polymer salt complex to prepare these type of electrolytes. These fillers do not take active participation in ion conduction process but modify the local environment of the polymer host at the microscopic level to increase the conductivity values. Study on these class of material can be traced back to 1989 where F. Corce *et. al.* elucidated the effect of addition of β-alumina on the ionic conductivity of PEO- NaI.[84] In another study J. Płocharski *et. al.* investigated solid polymer electrolytes having composition PEO-NaI mixed with Nasicon and Al_2O_3 powders. They concluded the increase in ionic conductivity is due to the presence of higher concentration of amorphous phase which resulted from a higher nucleation rate during the solidification process.[85] Here, a brief progress of ceramic filler based polymer composite electrolytes is described for a broader understanding.

M. A. K. L. Dissanayake *et. al.* investigated PEO-$LiCF_3SO_3$-Al_2O_3 based composite

polymer electrolyte system and reported a substantial increase in the ionic conductivity. The optimized room temperature ionic conductivity is approximately 10^{-4} Scm^{-1}. This increasing dc conductivity is because of the large surface area of the filler.[86] S. Klongkan *et. al.*, studied system of PEO - $LiCF_3SO_3$ - Al_2O_3 composite electrolytes and found with the addition of 15 wt.% Al_2O_3, ionic conductivity reach a maxima of 8.86×10^{-5} Scm^{-1} at room temperature.[67]

J. W. Park *et. al.* investigated PEO, $LiClO_4$, different organic acids like malonic, maleic, and carboxylic acids based electrolytes with alumina as filler in composite polymer electrolytes and reported an optimized ionic conductivity of 3.81×10^{-4} Scm^{-1} at 20 °C with the addition of 20 wt. % Al_2O_3 filler to the PEO_8-$LiClO_4$ + 5 wt.% carboxylic acid based polymer electrolyte is achieved.[87] Jin-Kyung Lee *et. al.* prepared PEO-$LiClO_4$-TiO_2 based organic-inorganic hybrids using sol-gel processing. The hybrid films containing 10 wt.% TiO_2 show the highest ionic conductivity 3.3×10^{-5} Scm^{-1} at room temperature.[88] S. Y. An *et. al.* prepared composite solid PEO - $LiClO_4$-(PAA/PMAA)-Al_2O_3 based polymer electrolytes, where PAA and PMAA stands for polyacrylic acid and polymethacrylic acid respectively. They reported the maximum ionic conductivity of 9.87×10^{-4} Scm^{-1} at 20 °C.[89] E. M. Masoud *et. al.* studied PEO- $LiClO_4$-Al_2O_3 based composite electrolyte samples and found that 1.25 mol of nano-Al_2O_3 based sample give rise to the highest conductivity value of 8.3×10^{-5} Scm^{-1}at room temperature.[90]

G. Nagasubramanian *et. al.* studied system of PEO based polymer composite electrolytes with LiI as salt and Al_2O_3 as ceramic filler. In their study they reported the optimized ionic conductivity 6×10^{-4} Scm^{-1} at 120 °C for 3 wt.% of the Al_2O_3 filler.[91] W. Krawiec *et. al.* studied polymer composite electrolyte system having PEO as polymer, $LiBF_4$ as salt and Al_2O_3 as ceramic filler. They reported the maximum ionic conductivity for PEO_8-$LiBF_4$-10 wt.% Al_2O_3 is of the order of 10^{-5} Scm^{-1} at room temperate.[92] J. H. Ahn *et. al.* studied system of PEO based polymer composite electrolytes with different combination of salts, $LiCF_3SO_3$, $LiClO_4$ and $LiPF_6$. This group used Al_2O_3, TiO_2 and ZrO_2 as ceramic fillers. They observed that the ionic conductivity become maximum when $LiPF_6$ is added as salt and Al_2O_3 is dispersed as filler particles. The optimized conductivity values were reported around 10^{-5} Scm^{-1} at room temperature, for PEO- 15 wt.% $LiPF_6$- 10 wt.%Al_2O_3 composition of polymer composite electrolyte.[93] A. Ahmad *et. al.* studied system of PVC-$LiClO_4$ based composite polymer electrolytes. The ceramic fillers used are ZnO, TiO_2 and Al_2O_3. They reported the optimized ionic conductivity 3.7×10^{-7} Scm^{-1} for the sample containing 20 wt.% ZnO.[94] S. Das *et. al.* studied system of PEO based polymer composite electrolytes with lithium (bis) trifluoromethanesulfonate imide as salt and Al_2O_3. They reported that with 5 wt.% Al_2O_3 addition optimum conductivity 3.3×10^{-5} Scm^{-1} can be achieved.[95] Y. Liu *et. al.* studied PEO-$LiBF_4$- TiO_2 based composite polymer electrolyte and reported a wider electrochemical stability 4.5 V Li^+/Li and ionic conductivity 7×10^{-5} Scm^{-1} at room temperature for 10 wt.% TiO_2 composition.[32]

B. Scrosati *et. al.* studied PEO-$LiCF_3SO_3$ based electrolytes with differnt types of alumina filler. They found for both acidic and basic types of alumina ionic conductivity increases as compared to neutral alumina filler.[96] Hucheng Zhang *et. al.* studied the effect of nano-sized Al_2O_3 and ZnO fillers on PEO_{20}-NaSCN based composite polymer electrolytes. The interactions between the filler and polymer salt complex are discussed according to the grain boundary effects, epitaxial effects and as per Lewis acid-base interactions. They concluded that soft Lewis acid groups of fillers are capable of forming stronger complexation with anions of the salt and thereby affect the ionic conductivity values and improved Li^+ transference number.[97] A. Bac *et. al.* also conducted similar studies using PEO_{20}-$LiCLO_4$- TiO_2 based polymer composite electrolytes.[98]

Y. W. Chen-Yang *et. al.* studied poly [bis (methoxyethoxyethoxy) phosphazene] - $LiClO_4$-α Al_2O_3 based composite polymer electrolyte and reported optimized conductivity of the order 10^{-4} Scm^{-1} at ambient temperature, for 2.3 wt.% filler concentration.[99] Z. Li *et. al.* studied P(VDF-HFP)- $LiClO_4$-α Al_2O_3 based composite polymer electrolytes and reported that with the addition of 10 wt.% Al_2O_2 nano-particles, polymer electrolyte achieve maximum ionic conductivity up to 1.95×10^{-3} Scm^{-1}. They also found a relatively high lithium ion transference number to 0.73.[100] M. Morita *et. al.* studied (PEO-PMA)- $Li(CF_3SO_2)_2N$ based polymer composite electrolytes with $BaTiO_3$, α-Al_2O_3, γ-Al_2O_3 as filler. The optimized ionic conductivity for 15 wt.% of α-Al_2O_3 composite polymer electrolyte is found 4.7×10^{-5} Scm^{-1} at 60 °C. Here PEO-PMA stands for poly(ethylene oxide)-modified poly(methacrylate).[101] Prasanth Raghavan *et. al.* reported that electrospun membranes of P(VdF-HFP) based polymer electrolytes loaded with safe and non-volatile bis(trifluoromethanesulfonyl)imide and nano-sized ceramic $BaTiO_3$ fillers show very good room temperature electrical conductivity, of the order of 10^{-3} Scm^{-1}.[102]

So far the discussion is related to a quantitative description of ionic conductivity values obtained by different groups. The mechanism of increase in ionic conductivity is also very important, hence it also drawn a greater attention by different research groups. W. Wieczorek *et. al.* studied a series of composite polymer electrolytes with PEO, $NaClO_4$ and α-Al_2O_3. They reported that strong interaction between surface oxygens of Al_2O_3 and the cations reduces the number of transient cross-links between cations and ether oxygens of polymer chains. Hence, the increase in conductivity of these composite polymer electrolytes can be associated with inter-phase phenomena between filler and polymer salt complex.[103] In an another study by W. Wirczorek *et. al.* with PEO, $LiClO_4$ and α-Al_2O_3 composite electrolyte system they reported that the addition of fillers leads to changes in the degree of crystallinity of the PEO - $LiClO_4$ matrix and the glass transition temperature which leads to changes in the ionic conductivity.[91] A. S. Best *et. al.* studied a series of composite polymer electrolytes with PEO as host polymer, $LiCF_3SO_3$, $LiClO_4$ as salt and Al_2O_3, TiO_2 as ceramic fillers. In the investigation they reported that the number of free ions available for conduction is not the leading cause for the increase in ionic conductivity in amorphous and semi-crystalline

polymer electrolytes. Instead, they argued from the results of Raman scattering and dielectric spectroscopy experiments that the increased ionic conductivity is due to filler influence on both the polymer chain and the salt ion mobility. They also investigated these effects using various modeling of dielectric interactions. [104] A. J. Hill *et. al.* investigated PEO-$LiCF_3SO_3$-TiO_2 based composite polymer electrolyte system and reported that ion conduction takes place mainly through the inter-facial region of polymer and TiO_2.[105] J. Zhou *et. al.* investigated PEO_{20}-[$LiN(CF_3SO_2)_2$] based systems and reported that there are two possible pathways for Li^+ ion transport in composite polymer electrolytes. Those are Li^+ ions hopping from one polymer segment to another dependent on their flexibility and Li^+ ions transfer along the filler surface. It is considered that the Lewis acid-base interactions between salt ions and filler surface generate additional favourable sites for ion-migration, which in-turn improve conductivity at temperatures below the melting temperature by increasing the ion mobility in the polymer composite electrolyte.[82] C. Karlsson *et. al.* investigated polymer electrolyte consisting (trihydroxypoly(ethylene oxide-co-propylene oxide), $LiClO_4$ and TiO_2 as filler. Their findings provide structural support for the idea that the conductivity enhancement in amorphous nano-composite polymer electrolytes is due the percolating network formation of lithium conducting pathways in inter-phase regions.[106] B. K. Money *et. al.* investigated polymer electrolyte consisting PEO-$LiClO_4$ and α-Al_2O_3, and reported that the increase in conductivity can be correlated to increase segmental relaxation or α relaxation of the polymer host. This conclusion was described using the correlated dielectric spectroscopy and differential scanning calorimetry data.[107]

Polymer Composite Electrolytes: Layered Clay Filler Based

In literature we can find the existence of clay based polymer composite electrolytes from the early ninety of twentieth century. Primarily the investigations are carried out for the potential application in electrical double layer capacitors.[108] T. Kanbara , T.J. Pinnavaia, R. A. Vaia and E. P. Giannelis are among the prominent researchers who have worked extensively on clay based polymer composite electrolytes in its early stage of development.[92, 109, 110] A detailed discussion of montmorillonite clay structure, different clay modification, polymer composite electrolyte preparation processes etc. will be discussed in chapter (2). The most important aspect of these composites is that along with the improvement in electrical properties other parameters like mechanical strength, thermal stability and molecular barrier properties are found to be improved. These improvements can be obtained at very low values of clay loading percentage ranging from 2 wt.% to 5 wt.%, with respect to the host polymer. It can be observed that from a detailed literature review; the extent of improvement in electrical and mechanical properties are directly related to the dispersion of the clay layers in the polymer matrix. Here, in brief the important findings of clay based polymer composite electrolytes are described for a broader understanding.

H. W. Chen *et. al.* have demonstrated that with the addition of optimum amount of

modified montmorillonite (D-2000) clay there is manifold increase in ionic conductivity. Investigation is carried out using polymer electrolyte system PEO-$LiCF_3SO_3$. With the addition of 3 wt.% clay the ionic conductivity of polymer electrolyte having EO/Li $= 6$, increases from 5×10^{-8} Scm^{-1} to 1.4×10^{-5} Scm^{-1} at room temperature.[111]

S. Kim *et. al.* have studied the polymer electrolyte system having composition PEO-$LiClO_4$-EC-Organo MMT. The modification of MMT was carried out using dihydrogenatedtallow quaternary ammonium ion as modifier. Using this organo modified MMT clay the maximum obtained conductivity is found approximately 9×10^{-5} Scm^{-1}. A firm conclusion is drawn from the results about the influence of organic MMT on the conductivity of the PEO-$LiClO_4$ based polymer electrolyte systems.[112] Another new approach is represented by S. Kim *et. al.*, in their work, where instead of modifying the Na^+-MMT form hydrophilic to organophilic they substituted Na^+ using Li^+ in montmorillonite clay gallery. Using this technique they are able to increase the ionic conductivity of PEO-$LiClO_4$ based polymer electrolyte systems upto the order of 10^{-5} Scm^{-1}. They also achieved a ionic transport number around 0.55 for 20 wt.% clay based composite electrolytes.[113] Y. P. Huang *et. al.* in the PEO-$LiClO_4$-montmorillonite system found that, the clay layers were exfoliated and act as Lewis base centers at low clay mineral contents. The negative charges of smectite layers yield the highest ionic conductivity since more cations could be mobilized for conduction. The obtained maximum ionic conductivity for 3 wt.% clay loading was 2.7×10^{-6} Scm^{-1}.[114]

Recently, S. Choudhary *et. al.* performed a comprehensive study taking different lithium salts including $LiClO_4$, $LiCF_3SO_3$, $LiBF_4$ and PEO as polymer host. The study focused mainly on the enhancement of ionic conductivity values. They reported for PEO_{20}-$LiBF_4$ electrolyte with the addition of 2 wt.% montmorillonite clay the achieved ionic conductivity at room temperature is 6.32×10^{-7} Scm^{-1}.[115]

In addition to PEO based systems other polymer based polymer composites are also investigated by various research groups. H. W. Chen *et. al.* have studied the electrical properties of PMMA-$LiClO_4$ based polymer composite electrolytes. Montmorrilonite clay modification was carried out using dimethyldioctadecylammonium chloride. Optimized ionic conductivity at room temperature is found 6×10^{-5} Scm^{-1} for the composition $P(MMA)_8LiClO_4$(25)-EC(75)- 5 wt.% modified clay.[116] Y. Ma *et. al.* investigated clay based polymer composite electrolytes where a blend of PVdF and PVA is used as intercalation polymer. Authors observed a higher ionic conductivity up to 4.32×10^{-4} Scm^{-1} at room temperature when 4.0 wt.% MMT clay was added to the electrolyte system. The maximum lithium ions transference number achieved for the system was 0.40.[117]

Proper understanding of interlayer structure is also necessary to understand the origin of increase in ionic conductivity of polymer clay composite electrolytes. Marc X. Reinholdt *et. al.* have studied Clay-PEO based nano-composites with natural and synthetic montmorillonite clays using X-ray diffraction (XRD), TGA-DTA and ^7Li and ^{23}Na NMR

techniques. An increase in basal d_{001}-spacings demonstrates successful intercalation of PEO in all samples and X-ray line narrowing shows that this intercalation improves the layer stacking order. The basal spacings of $17.9 - 19.4$ Å are consistent with a helical or bilayer structure of PEO in the interlayer.

1.5.5 Gel Polymer Electrolyte

Gel polymer electrolytes (GPEs) are obtained by trapping liquid electrolytes into a host polymer network. This concept was first proposed in 1975 by Feuillade *et al.*.[118] The transport of lithium ions is not dominated by the segmental motion of polymer chains, but occurs in the swollen gelled phase or liquid phase. GPE should possess the properties of good mechanical strength, capability of holding a liquid electrolyte, high ionic conductivity and electrochemical stability toward both electrodes. Polyvinyl chloride,[119, 120] poly(methyl methacrylate), [121, 122] polyvinylidene fuoride,[55–57] polyacrylonitrile [123, 124] and poly- (vinylidene fuoride-hexafuoropropylene) copolymer [125, 126] etc. have been widely studied by various research groups as the frameworks for gel polymer electrolytes. Here in this section some related literature is mentioned.

S. Panero *et. al.* prepared a gel polymer electrolyte formed by trapping $LiPF_6$ -propylene carbonate solution into a poly acrylonitrile matrix and achieved ionic conductivity of of the order 10^{-3} Scm^{-1} at 10 °C.[127] Y. H. Liao *et. al.* studied gel polymer electrolyte having PEO with P(VdF-HFP) doped with nano-Al_2O_3 and supported by polypropylene as host and 1 M $LiPF_6$ in ethylene carbonate, dimethyl carbonate, ethylmethyl carbonate ($1 : 1 : 1$ in volume) as liquid electrolyte. They reported that with the addition of 10 wt.% nano-Al_2O_3 to the host matrix maximum ionic conductivity 3.8×10^{-3} Scm^{-1} at 30 °C can be achieved.[128] Se-Hee Kim *et. al.* in his work reported mechanically stable dendrite growth free gel polymer electrolytes with acceptable ionic conductivity for device fabrication. Materials used are UV cured ethoxylated trimethylolpropane triacrylate as host polymer in combination with nano-Al_2O_3 and 1 M $LiPF_6$ liquid carbonate electrolyte (mixture of ethylene carbonate and propylene carbonate). [129] P. Sun *et. al.* prepared gel polymer electrolyte using poly(methyl methacrylate-acrylonitrile-ethyl acrylate) (P(MMA-AN-EA)) as a polymer matrix and nano-SiO_2 and nano-Al_2O_3 co-doped simultaneously as filler. They reported the ionic conductivity of 2.2×10^{-2} Scm^{-1} at room temperature and an enhanced oxidative stability up to 5.5 V (vs. Li/Li^+).[58]

1.5.6 Study on Ion-Conduction Mechanism

So far, the discussion was entirely centered on the aspects of materials and different techniques to increase the ionic conductivity of polymer electrolytes. Though over four decades of extensive research has been carried out still there is a lot of scope to further increase the ionic conductivity of solid polymer electrolytes and for that understanding of ion

conduction mechanism is very important. The concepts of ion conduction mechanism can be broadly classified into two major categories: (a) phenomenological concepts and (b) physical interaction based theoretical model analysis. In this section a brief overview on different models attempting to explain the ion conduction mechanism in polymer electrolyte is shown. Jonscher's power law and power law in Almond-West formalism are the most commonly used formalism to describe the frequency dependent conductivity spectra. [107, 130] These equations are formulated based on the phenomenological observations to describe the frequency dependent data. Experimental observation deviate significantly from Jonscher's power law at low temperature and high frequency regime. Therefore, double power law is introduced to analyze the experimentally obtained data. Though these two equations are having various shortcoming, still they are used to explain the frequency dependent conductivity spectrum. To explain the electrical properties as a function of temperature in polymer electrolytes VTF equation is mostly preferred. It gives the concept of Vogel temperature, at which molecular motion completely ceases.

On the other hand various mathematical and physical interaction based models are also present which try to describe the variation of different physical parameters as a function of frequency, temperature, ion mobility etc. These are Ngai's coupling model,[131–134] Deitrich's counter ion model, Percolation model, [135–137] Bunde's monte carlo simulations,[138] jump relaxation models,[139] random free energy barrier model[140] etc. In these models focus is given on finding the explanation for the variation of electrical properties. An in-depth discussion regarding these formalisms will be presented in chapter (3).

1.6 Motivation

Since from the inception of the idea of a polymer can conduct ions in early 80s and the introduction of polymer electrolytes as a potential material for energy storage/conversion device, a considerable amount of research has already been attempted for developing new electrolyte system. Mainly, the focus is given to increase room temperature ionic conductivity, enhancement of thermal, electrochemical and mechanical stability, better processability, increased lifespan etc. Though significant efforts were made, still there exist problems mainly related to electrical, mechanical, electrochemical properties of different polymer electrolytes. From literature the following drawbacks have been taken as motivation for carrying out this project

- Till date in most of the lithium ion battery, low molecular weight organic carbonate based liquid electrolytes are used. The presence of flammable organic liquid raises a serious safety concern. Polymer electrolytes being solid will be able to solve this issue.

- Room temperature ionic conductivity of polymer salt complex is found of the order 10^{-9} Scm^{-1} to 10^{-7} Scm^{-1} for PEO-based solid polymer electrolytes. This low value of ionic conductivity is far from the minimum acceptable range of ionic conductivity, 10^{-3} Scm^{-1} or better, to be used in various energy storage/conversion device.

- Mechanical, electrochemical and thermal stability of plasticized polymer electrolytes are not up to the desired level. Therefore composite polymer electrolyte and gel polymer electrolyte are chosen for the investigation.

- The ion conduction mechanism of polymer electrolytes are not adequately understood. A proper understating of ion conduction mechanism will help to increase the ionic conductivity of polymer electrolytes further. Using different phenomenology and model-based analysis, a comparative and comprehensive, study on ion conduction mechanism is required.

1.7 Objective and Scope

The objectives of the present investigation are based on the problems, challenges and current status of development of solid polymer electrolytes as found in the literature review. A brief outline of objective for the entire work is given below

- Synthesis of polymer nanocomposite electrolytes using conventional solution casting technique and gel polymer electrolyte using phase inversion technique.

- To study the structural and microstructural properties of the materials using X-ray diffraction technique. It helps to understand the formation of the nanocomposite electrolytes. Surface morphology is investigated using scanning electron microscopy. The interactions between polymer, salt and filler in case PNCEs and polymer, salt, organic carbonates in the case of GPEs are to be explored using FTIR spectroscopy.

- To study the relaxation phenomena observed in PNCEs by analyzing frequency dependent electrical modulus spectra using Bergmann modified Kohlrausch-Williams-Watts (KWW) and Havriliak-Negami (HN) approach. Frequency dependent dielectric spectra are also required to be analyzed using Havriliak-Negami and dc conduction-free dielectric loss approach for the in-depth understanding of relaxation process.

- To study the first universality also known as universal dielectric response (UDR) and second universality also known as nearly constant loss(NCL) phenomena commonly observed in disordered ionic conductors like PNCEs.

- To analyze the of frequency and temperature dependent conductivity spectra with the help of coupling and MIGRATION models for understanding the ionic transport mechanism at the microscopic level.
- The role of segmental relaxation in ion conduction process is to be studied with a comparative study between random free energy barrier hopping model and phenomenologically derived relations like power laws. The concept of coupled ion conduction mechanism is also needed to be investigated using Ratner's classical theory of coupling.
- To investigate the change in electrical conductivity as a function of blend percentage of host polymer matrix in gel polymer electrolyte.
- To investigate the ion conduction mechanism in gel polymer electrolytes.

1.8 Materials Under Present Investigation

In the present investigation, the focus is given on electrical properties and relaxation phenomenon to understand the ion conduction mechanism of polymer electrolytes. At the same time using different types of filler, the variation of ionic conductivity is studied. Polymer composite electrolytes and gel polymer electrolytes are prepared for ionic conductivity optimization and detailed study of ion conduction process. Lithium triflate is chosen as salt for electrolytes for its low activation energy value. PEO is chosen as the host polymer to prepare composite polymer electrolyte because of its high solvating power for lithium-based salts and its compatibility with the lithium electrodes. To prepare blend based gel polymer electrolytes PVdF-HFP and PMMA are chosen due to their excellent miscibility. PMMA is having good capability of absorbing and holding liquid electrolytes during gel formation. PVdF-HFP provides excellent mechanical strength to the blend system.

The materials under investigation are divided into following groups:

- PEO_{20}-$LiCF_3SO_3$- x wt.% ZrO_2 (x = 0, 3, 5, 8, 10 and 20).
- PEO_{20}-$LiCF_3SO_3$- x wt.% TiO_2 (x = 0, 2, 3, 5, 8, 10 and 15).
- PEO_{20}-$LiCF_3SO_3$- x wt.% mMMT (x = 0, 2, 3, 5, 8, 10 and 15).
- $(100 - x)$ PVDF-HFP- x PMMA- 1 M $LiCF_3SO_3$ in $(1 : 1)$ EC and DEC. (x = 30, 40, 50, 60, and 70)

First, three of them are polymer composite electrolytes and the fourth one is a blend polymer gel electrolyte. Fillers, ZrO_2 and TiO_2 act as dispersed phase filler. ZrO_2 is a neutral filler and TiO_2 is having the tendency to weakly attract the cations.[141] Montmorillonite clay-based polymer composite electrolyte is an intercalation based polymer composite

electrolytes. The used filler materials for the preparation of polymer composite electrolytes are either synthesized or modified using different chemical routes which will be discussed in chapter (2).

1.9 Organization of Thesis

This thesis consists of chapters as following:

- **Chapter 1:** A brief introduction to the energy storage and conversion devices are included in this chapter. Working principle and functional building blocks of secondary lithium batteries are discussed along with other energy storage/conversion devices. This chapter also covers a brief classification of different classes of ionic conductors and electrolytes. Summarized reviews of previous works are presented for various kinds of polymer electrolytes. On the basis of the available literature and importance of the materials, the primary objectives of the work have been formulated in this chapter.

- **Chapter 2:** This chapter elaborately presents various synthesis and characterization techniques used in the present investigation. The samples preparation techniques adopted for preparing different fillers, modification of hydrophilic montmorillonite clay is described in this chapter. The fabrication of polymer nanocomposites electrolytes using solution casting technique and gel electrolytes using phase inversion technique is discussed. The characterization techniques which includes XRD, FE-SEM, FTIR and Broadband Dielectric Spectroscopy are discussed here.

- **Chapter 3:** This chapter presents the idea and basic concepts of ion conduction mechanism presently available in the literature. Focus is given on various empirical relations and physical models used so far to analyze the experimentally observed electrical observations.

- **Chapter 4:** This chapter presents the study of structural, microstructural, morphological, vibrational, dielectric relaxation and electrical properties of PEO_{20}-$LiCF_3SO_3$- x wt.% ZrO_2 (x = 0, 3, 5, 8, 10 and 20) series of composite polymer electrolyte. The observed electrical behaviour is explained using Ngai Coupling Model. The observation of first and second Universality are discussed in depth. The cause behind the second universality is also explained with the help of Kramer-Krönig approach in combination to coupling model.

- **Chapter 5:** This chapter presents the study of structural, microstructural, morphological, vibrational, dielectric relaxation and electrical properties of PEO_{20}-$LiCF_3SO_3$- x wt.% TiO_2 (x = 0, 2, 3, 5, 8, 10 and 15) series of

composite polymer electrolyte. The observed electrical behaviour is explained using MIGRATION concept to explain the ion conduction mechanism.

- **Chapter 6:** This chapter presents the study of structural, microstructural, morphological, vibrational, dielectric relaxation and electrical properties of PEO_{20}-$LiCF_3SO_3$- x wt.% mMMT (x = 0, 2, 3, 5, 8, 10 and 15) series of composite polymer electrolyte. The observed electrical behaviour is explained using a comparative analysis between theoretical model based results and phenomenological concepts. The finding suggests how to improve the understandings of ion conduction process in polymer electrolytes.

- **Chapter 7:** This chapter presents the study of dielectric and electrical properties of gel polymer electrolyte series. The observed data are explained using phenomenological concepts. Ionic conductivity is correlated with liquid electrolyte absorbed by micro-porous membranes during the formation of GPEs. Frequency dependent dielectric and electrical modulus spectra are studied to describe ion conduction process. These findings suggest how to improve the understandings of ion conduction mechanism to increase ionic conductivity of gel polymer electrolytes further.

- **Chapter 8:** The collective concepts of ion conduction mechanism in different types of polymer electrolytes are mentioned in this chapter for a better understanding of long-range ion conduction process leading to dc conductivity. The difference in ionic conductivity values due to the nature of filler in polymer composite electrolytes are also shown here. In addition, brief outlines to the summary, main conclusions drawn and future scope of the present investigation are also discussed in this chapter.

Chapter 2

Materials Synthesis and Characterization Techniques

2.1 Introduction

Research and development in material science mainly focus on different types of material synthesis and their property optimization for potential device applications. Research work related to various materials to be used in energy storage/conversion devices has been given priority due to the growing demand for a reliable, safe and portable source of energy. In the present study, priority is given particularly on polymer electrolytes. The room temperature dc conductivity is optimized for both polymer composite electrolytes as well as gel polymer electrolytes. For polymer nano-composite electrolytes the electrical properties are optimized as a function of filler concentration and for blended gel polymer electrolytes the ratio of polymer blending is varied to get maximized electrical properties.

In this chapter, the focus is given on different synthesis techniques adopted to prepare the polymer electrolyte samples. Here the synthesis procedure of the ceramic oxides, used as filler, for polymer nanocomposite electrolytes is also described. Preliminary results on phase purity, surface morphology and micro-structural analysis of ceramic fillers are discussed in this chapter. A detailed description of the structure of montmorillonite clay along with its modification process is presented thereafter. Apart from material synthesis, characterization techniques also play a crucial role in the research of material science. Characterization techniques which are relevant to the present study are introduced and their basic working principles are discussed This includes X-ray diffraction (XRD), scanning electron microscopy (SEM), fourier transform infrared spectroscopy (FTIR) and broadband dielectric spectroscopy (BDS). Finally, all instruments used in this work are listed at the end.

2.2 Ceramic Filler Synthesis

Due to the potential multidisciplinary application, an increasing interest in ceramic powders and their derivatives can be observed.[142] Physical properties of these ceramics depend considerably on their size, shape and surface properties. Many synthesis techniques are available for the fabrication of ceramic materials.[143] They are broadly classified into

a top-down *i.e.* mechanical method and bottom-up *i.e.* chemical method approaches for ceramic synthesis.[144] For the present investigation, the bottom-up or chemical method is more suitable. In the chemical method, the starting materials are taken in solution form and different reactants used are mutually soluble with each other. It helps in preparing a homogeneous precursor solution. Powders prepared by chemical route show improved characteristics concerning purity, stoichiometry, homogeneity, reactivity as well as particle shape, size, agglomeration and surface properties.[145, 146] Different chemical routes used for the synthesis of ceramics are co-precipitation, sol-gel, hydrothermal, citrate gel method, auto-combustion, polymer template etc. A brief description of synthesis procedures are given below

- **Co-precipitation:** In co-precipitation reactions nucleation, growth, coarsening and or agglomeration processes occur simultaneously.[147] These reactions process are as follows
  - **Nucleation:** In these step small particles begin to form or nucleate.
  - **Growth:** In these step particle growth take place.
  - **Secondary processes:** In general, the final product obtained remain insoluble to the solvent used earlier to dissolve the reactants. Therefore, in this step final product can be separated using filtration and or centrifuge techniques.
- **Sol-gel:** A sol is a dispersion of the solid particles ($\approx 0.1 - 1$ mm) in a liquid where only the Brownian motions suspend the particles whereas, the gel is a state where both liquid and solid are dispersed in each other. Gel presents a solid network containing liquid components. Sol-gel process involves the transition of a system from a liquid sol to a solid gel phase.[148] The sol-gel process is as follows
  - The desired colloidal particles dispersed in a liquid to form a sol and the particles in sol are polymerized to produce gel in a state of a continuous network.
  - Heat treatments pyrolyze the organic or inorganic components and form an amorphous or crystalline coating
  - The materials used in the preparation of the sol are usually inorganic metal salts or organometallic compounds such as metal alkoxides. Thus producing ceramic materials.
- **Hydrothermal and Solvothermal:** In a sealed vessel, water or organic solvents can be brought to temperatures well above their boiling points by an increase in auto-generated pressures resulting from heating. Performing a chemical reaction under such conditions is referred to as solvothermal processing. If water is chosen as the solvent then the process is called hydrothermal reaction. In this case, also the final product can be separated using filtration and centrifuge techniques.[149]

- **Auto-combustion:** In this process a sudden release of energy in highly exothermic redox chemical reaction helps in preparing the ceramic nano-particles. It is a simple, rapid process and cost effective process, which can synthesize a variety of nano-sized materials. This process involves a homogeneous solution of different oxidizers like metal nitrates or oxynitrate solutions and fuels like urea, glycine and hydrazides. Based on the source of metal and flush point of the fuel different structures may get generated for either volume or layer-by-layer propagating combustion modes.[150, 151]

- **Polymer template:** Polymer gel template method is a simple synthesis technique and can provide ultra-fine ceramic powders at relatively low temperatures for synthesis of ceramic powders.[49] The commonly used polymers include polystyrene and its derivatives, formaldehyde resin, polyacrylamide and polymethyl methacrylate.[152] In this technique, ceramic particles grow in the voids of gel structure. Once gel structure is burnt, it provides a porous ceramic powder having high surface area.

In the present study auto-combustion and polymer template methods are used to prepare single phased zirconia and titania filler respectively. The synthesis procedure are optimized to achieve phase purity at minimum synthesis temperature. The synthesis procedures and reaction steps for the preparation of zirconia and titania filler are described in this section with the help of flow charts.

2.2.1 Synthesis of Zirconium Dioxide: Auto-combustion Synthesis

Auto-combustion technique is used to prepare ZrO_2 filler. The synthesis procedure in form of flow char is shown in figure (2.1). Stoichiometric amount of Zirconium Oxychloride ($ZrOCl_2$-$8H_2O$) and urea ($CO(NH_2)_2$), maintaining molar ratio $1:1$ is dissolved in distilled water. The clear solution thus obtained, is then kept in a preheated muffle furnace at 450°C, for 30 minutes. In this process, a white voluminous material is obtained. The XRD pattern, shown in figure (2.2), confirms the formation of tetragonal phased ZrO_2 and this tetragonal phase ZrO_2 is used as the filler to prepare PNCEs without any further heat treatment.

2.2.2 Synthesis of Titanium Dioxide: Polymer Gel Template Synthesis

Titanium isopropoxide ($Ti(OCH(CH_3))_4$) is taken as the source of titanium. Two and a half ml of titanium isopropoxide is added dropwise in a beaker filled with 50 ml of deionized water kept at 4°C under vigorous stirring. Instantaneously yellowish white precipitate of titanic acid ($Ti(OH)_4$) is observed. These precipitates are collected and dissolved in dilute nitric acid keeping the temperature of the solution below 4°C. With this clear solution of titanyl nitrate ($TiO(NO_3)_2$) is obtained. Optimized amount of acrylamide, N,N-methylene bisacrylamide are dissolved to this solution and mixed thoroughly. To initiate the gelation

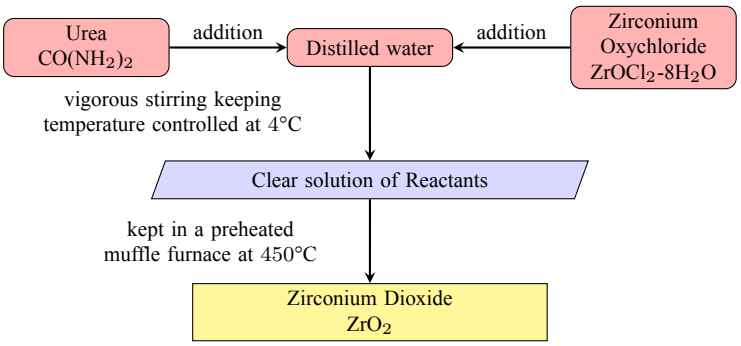

Figure 2.1: Synthesis of inorganic nano-crystalline ZrO_2 filler, represented in from of flow chart.

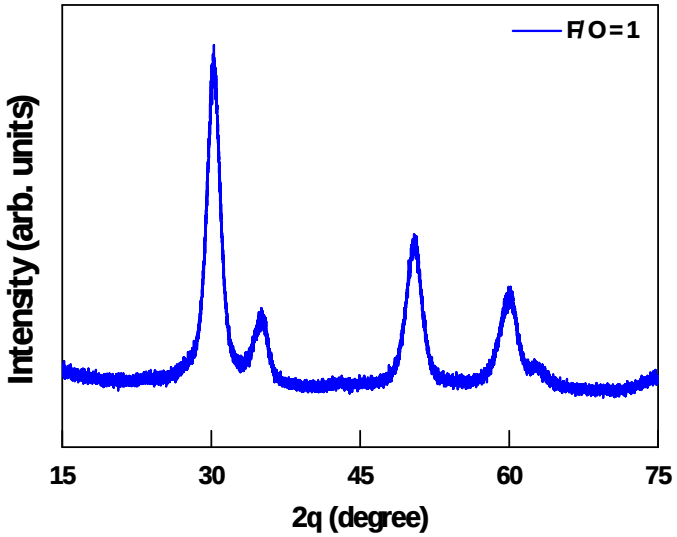

Figure 2.2: X-ray diffraction pattern for tetragonal phased zirconia synthesized using auto-combustion technique.

0.5 ml ammonium persulfate (10 wt.%) solution is added and mixed again. The mixture is kept at 40°C in a water bath for 5 h to get acrylamide hydrogel. Acrylamide hydrogel is then heat treated at 300°C for 2 h to get the black network like structure. This network like structure is then ground to get fine powder using mortar pestle and calcined at different temperatures ranging from 450°C to 650°C to obtain TiO_2 samples. The synthesis procedure of anatase TiO_2 is shown in form of flow chart in figure (2.3). Phase analysis of synthesized TiO_2 samples are carried out using XRD technique. Figure (2.4a) shows the XRD patterns of synthesized samples at various synthesis temperature. From the XRD patterns, it can be observed that till 500°C only anatase polymorphs of titania is synthesized, whereas if synthesis temperature increased further a mixed phase titania sample, containing anatase as well as rutile polymorphs, are obtained. Rietveld refinement is carried out for these XRD patterns using FULLPROF software. Figure (2.4b) shows the Rietveld analysis of titania sample synthesized at 650°C. The crystallographic information evaluated from Rietveld

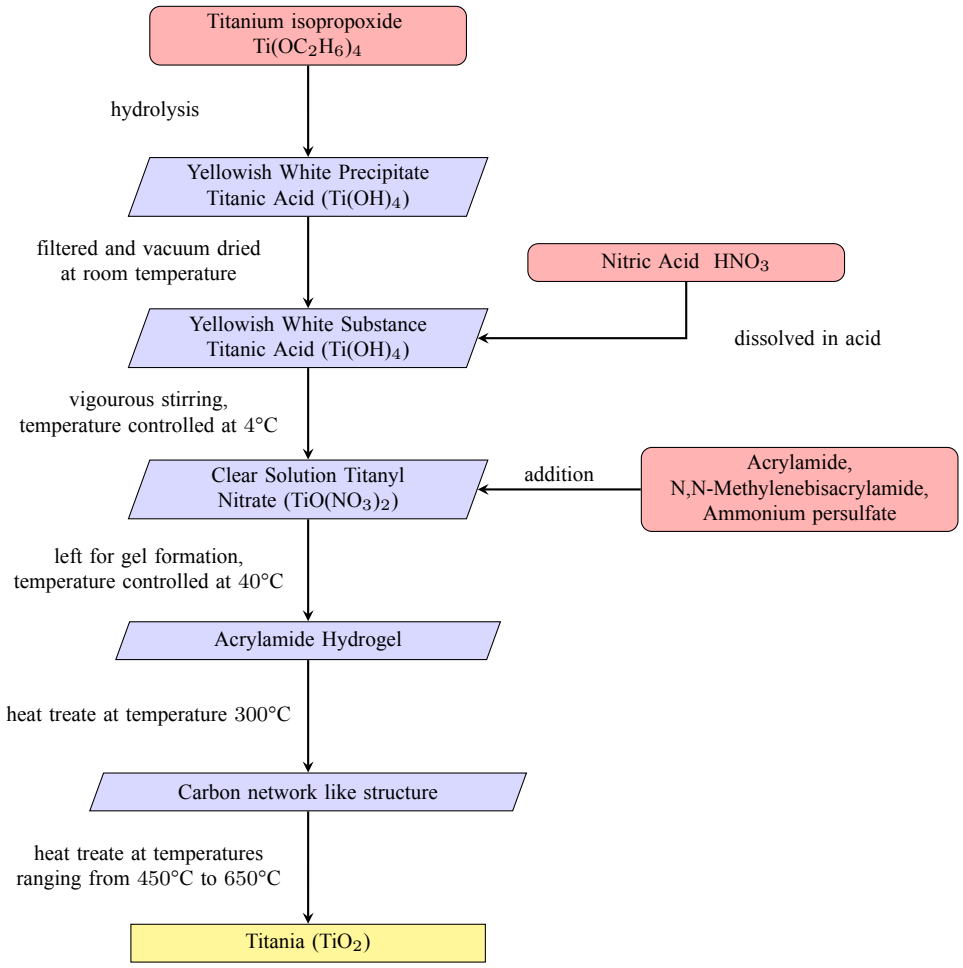

Figure 2.3: Synthesis of inorganic nano-crystalline TiO_2 filler, represented in from of flow chart.

refinement analysis are tabulated in the table (2.1).

2.3 Montmorrilonite Clay: Brief Description

Montmorillonite is a member of smectite group of clay having $2:1$ layer structure. It is having a central octahedral sheet of alumina sandwiched by two tetrahedral sheets of silica. Intercalation chemistry of montmorillonite clay is well understood; therefore environment-friendly modified montmorillonite clay is chosen as the intercalation filler to prepare polymer composite electrolytes. The layered structure of montmorillonite clay is shown in figure (2.5).[153] One of the characteristic properties of montmorillonite clay structure is that other molecules can enter between its unit layers easily. The c-axis of montmorillonite can expand and varies depending upon the condition of the surroundings. Because of this characteristic property of montmorillonite clay its X-ray diffraction pattern show two distinct types of reflections

- the basal $00l$ reflections exhibiting an interlayer series or orders varying in position as per the separation of structural layers

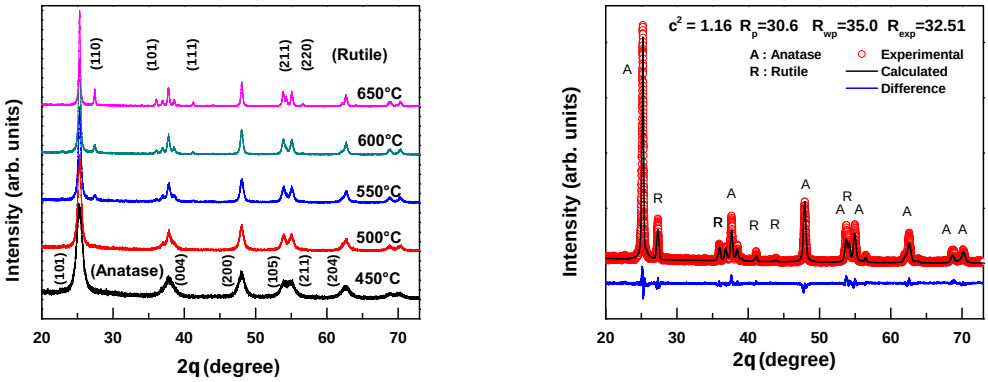

(a) X-Ray diffraction pattern for titania synthesized at different temperatures.

(b) Rietveld refinement of X-ray diffraction data for dual phased titania synthesized at 650°C (anatase + rutile).

Figure 2.4: XRD analysis of TiO_2.

- the general reflections from the $hk0$ plane which are characteristic of different minerals present.

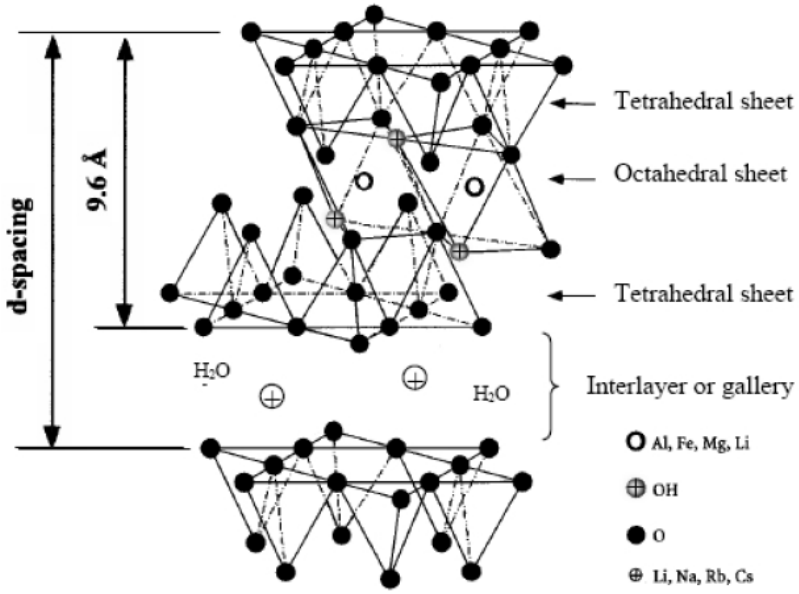

Figure 2.5: Schematic diagram of montmorillonite clay structure.

Modification of montmorillonite (MMT) clay from hydrophilic to organophilic in nature is required for easy intercalation of polymer chains into the clay layers and or to achieve a homogeneous distribution of montmorillonite clay into host polymer matrix. In this process, the Na^+ and Ca^{2+} residing in the interlayer regions are to be replaced by organic cations such as alkylammonium ions which modify the hydrophilic-layered silicate to be organophilic.[153] The stacked silicate sheets present a number of interesting properties such as cation exchange capacity, intercalation, swelling, porosity, catalytic activity, and

Table 2.1: Rietveld refined structural parameters of TiO_2 samples synthesized at different temperatures obtained using FULLPROF software.

Parameter		450°C	500°C	550°C	600°C	650°C
			Anatase ($I4_1/amd$)			
Lattice Constant (Å)	a	3.7834(6)	3.8026(4)	3.7945(4)	3.7933(3)	3.7916(3)
	c	9.5043(7)	9.5527(3)	9.5341(2)	9.5371(2)	9.5395(2)
Atomic Position	Ti(4a)	$0, 0.75, 0.125$	$0, 0.75, 0.125$	$0, 0.75, 0.125$	$0, 0.75, 0.125$	$0, 0.75, 0.125$
	O(8e)	$0, 0.75, 0.331$	$0, 0.75, 0.336$	$0, 0.75, 0.332$	$0, 0.75, 0.331$	$0, 0.75, 0.338$
Phase Percent		100	100	96.71	92.16	83.63
			Rutile($P4_2/mnm$)			
Lattice Constant (Å)	a	–	–	3.7945(4)	3.7933(3)	3.7916(3)
	c	–	–	9.5341(2)	9.5371(2)	9.5395(2)
Atomic Position	Ti(2a)	–	–	$0, 0, 0$	$0, 0, 0$	$0, 0, 0$
	O(4f)	–	–	$0.311, 0.311, 0$	$0.311, 0.311, 0$	$0.303, 0.303, 0$
Phase Percent		0	0	3.29	7.84	16.37
χ^2		1.85	1.77	1.30	1.13	1.16

sorption.[154] Especially, the high swelling capacity of MMT is significant for the efficient intercalation of the polymer. Polymer-clay composites have been actively studied since researchers discovered the possibility to build a nanostructure from a polymer and an organophilic clay. These composites are divided into three general types[155]

- conventional composite where the clay acts a conventional filler
- intercalated nanocomposite consisting of a regular insertion of the polymer in between the clay layers
- delaminated nano-composite where 1 nm-thick layers are dispersed in the polymer matrix, forming a monolithic structure.

In the present study synthesis of intercalated polymer, clay composite is targeted. To achieve this goal cetyltrimethylammonium bromide is used as the organic modifier. Here the modification procedure is described with the help of a flowchart shown in figure (2.6).

2.3.1 Montmorrilonite Clay Modification Using Cetyltrimethylammonium Bromide: Modification Process

Unmodified MMT clay with cation exchange capacity(CEC), 76.4 meq $/100$ g has been procured from the clay mineral society of Purdue University, Indiana. In general the cation exchange reaction follows the relation given as[156]

$$\frac{c \times y}{100} \times x = \frac{m}{M_s} \times 1000 \tag{2.1}$$

where, c is the cation exchange capacity of MMT per 100 g, y is the amount of MMT clay to be modified in g, x is the excess factor, m is the mass of surfactant required for modification

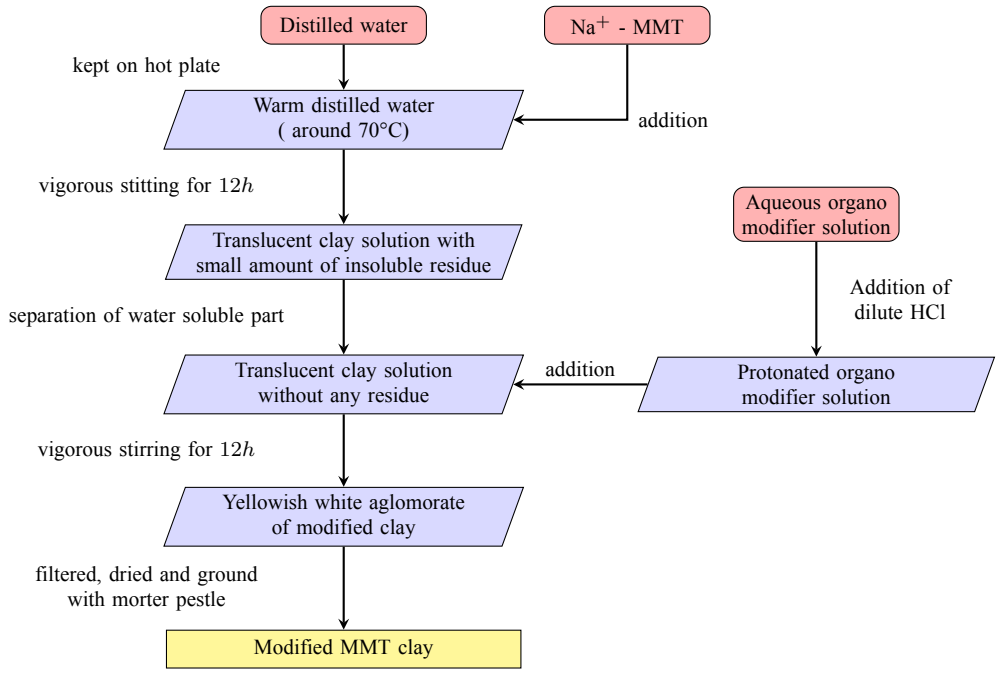

Figure 2.6: Na^+ - MMT modification process from hydrophilic to hydrophobic in nature represented in from of flow chart.

and M_s is the molecular weight of the surfactant used. Cetyl trimethyl ammonium bromide (CTAB) is used as the surfactant for clay modification. At first, unmodified MMT clay is dispersed in deionized water and stirred vigorously for 12 h. Only the translucent part of the solution is taken for further processing after discarding the insoluble residue. In a separate beaker stoichiometric amount of surfactant is dissolved in deionized water under continuous magnetic stirring and dilute hydrochloric acid is added dropwise to obtain a clear protonated solution, *i.e.* dilute hydrochloric acid added to the solution, of the surfactant. This protonated surfactant solution is added drop-wise to the translucent unmodified MMT clay solution under vigorous stirring keeping its temperature fixed at 333 K. The mixture is then kept under vigorous magnetic stirring for another 12 h to complete the cation exchange reaction. Thereafter a yellowish white precipitate is obtained upon filtration. The obtained precipitate is repeatedly washed with deionized water for removal of halide compounds, which is confirmed by a negative result in silver nitrate test. The precipitate is then vacuum dried at 373 K and grounded to get modified hydrophobic montmorillonite (mMMT) clay. The clay modification procedure is shown in form of flow chart in figure (2.6). This modified mMMT clay is used as the filler to prepare the clay filler based polymer nanocomposite samples.

2.4 Polymer Electrolyte Synthesis

Polymer electrolytes are in general consists of a broad group of materials. The classification of polymer electrolytes are described earlier in section (1.4) of chapter (1). Therefore, it is

needless to say the synthesis techniques of a different class of polymer electrolytes are quite different from each other. For the synthesis of polymer salt complex and composite polymer electrolytes usually, in-situ polymerization method, conventional solution casting and melt intercalation techniques are used. Again for the synthesis of polymer gel electrolytes, conventional gel preparation technique and phase inversion techniques are used by different research groups. In the present study conventional solution technique is used to prepare the composite polymer electrolytes and phase inversion techniques are used to prepare gel polymer electrolytes.

2.4.1 Synthesis of Composite Polymer Electrolyte Films: Conventional Solution Casting Method

Conventional solution casting method is one of the simplest techniques to prepare free-standing polymer electrolyte films. It ensures homogeneous mixing of the different constituent, which is an essential feature composite electrolytes.[157, 158] In this study, polyethylene oxide (M.W. = 6×10^5, Sigma-Aldrich), lithium trifluoromethanesulfonate ($LiCF_3SO_3$, Sigma-Aldrich), as prepared fillers, *i.e.* tetragonal phased zirconia, anatase titania and modified montmorillonite clay , are used to prepare composite polymer electrolytes. Analytical grade acetonitrile is used to as common solvent to these materials. Polyethylene oxide and $LiCF_3SO_3$ are vacuum dried before use whereas acetonitrile is dehydrated using the molecular sieve. Polyethylene oxide is added to acetonitrile and left to swell for 12 h. Then stoichiometric amount $LiCF_3SO_3$ is added to the swollen PEO and the mixture is stirred thoroughly for 12 h resulting in a viscous slurry of polymer salt complex. For all samples the $EO : Li^+$ is fixed at $20 : 1$. Thereafter required amount of fillers (ZrO_2 or TiO_2 or mMMT) is added to the polymer-salt complex maintaining different wt.% with respect to polymer host and stirred for another 12 h. The resulting slurry thus obtained is then cast on a glass petri dish and solvent is allowed to evaporate slowly at room temperature to prepare a free-standing film of polymer composite electrolytes. The entire operation is carried out inside PlasLabs controlled atmosphere chamber (855-AC/E) with a constant flow of dry nitrogen gas. The conventional polymer salt complex technique used here is shown in form of flow chart in figure (2.7a).

2.4.2 Synthesis of Gel Polymer Electrolyte Films: Phase Inversion Technique

In phase inversion technique at first, the porous polymer network is synthesized and thereafter the prepared porous polymer film is activated by dipping it into standard liquid electrolytes.[159–161] This process is often termed as charging. While charging porous polymer film with a liquid electrolyte, gelation takes place and gel polymer electrolyte film forms. Polymer gel electrolyte is prepared using phase inversion technique by blending

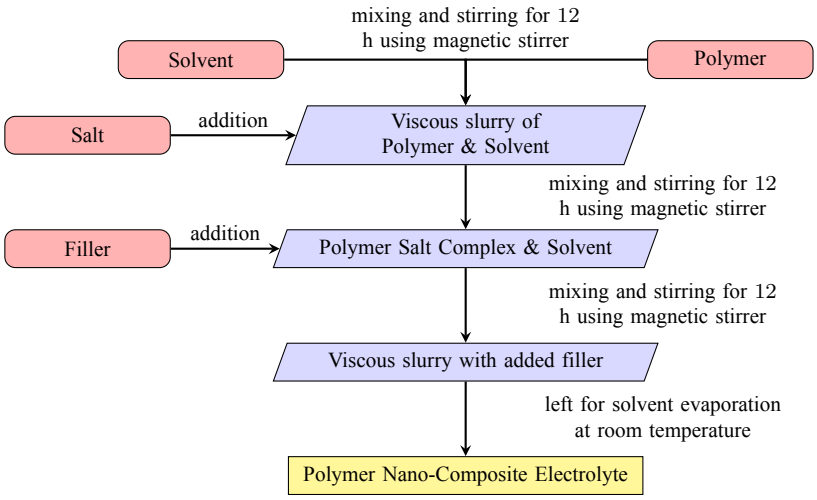

(a) Conventional solution cast synthesis technique for polymer nano-composite electrolyte.

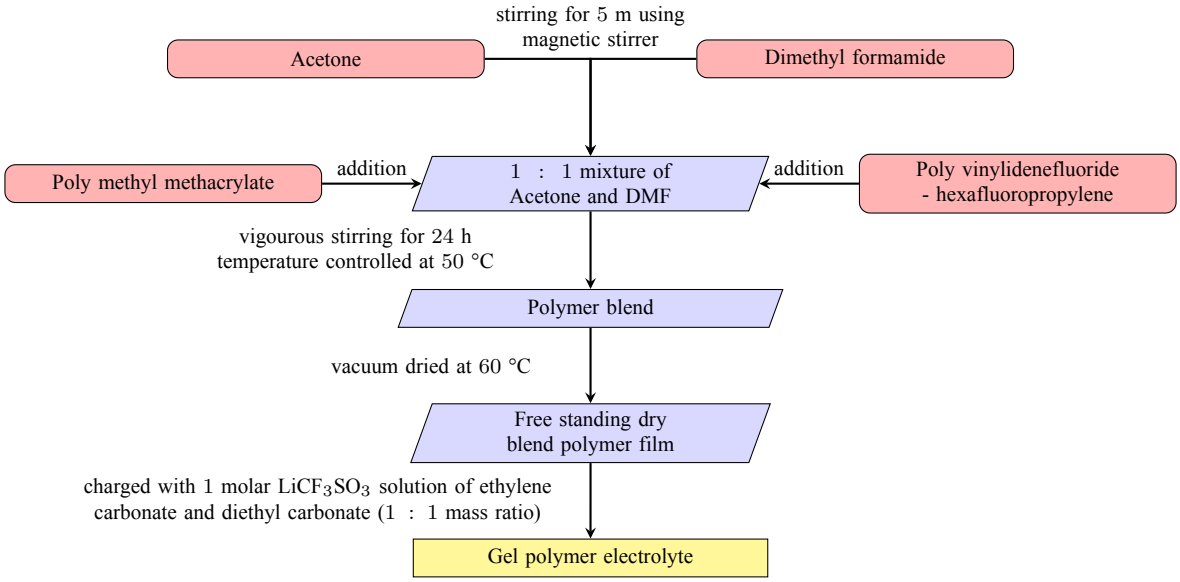

(b) Phase inversion synthesis of gel polymer electrolyte.

Figure 2.7: Flow chart for the synthesis of, (a) composite polymer electrolyte and (b) gel polymer electrolyte films.

polyvinylidene fluoride-hexafluoropropylene (PVdF-HFP) and polymethyl methacrylate (PMMA). At first, to prepare the microporous film, a stoichiometric amount of PVdF-HFP and PMMA are dissolved in the mixture of acetone and dimethylformamide (1 : 1). Once completely dissolved the solution is then cast on a glass petri dish and kept at 60 °C under vacuum to prepare a free standing blend polymer film. This film is then charged with the 1 molar solution of $LiCF_3SO_3$ dissolved in the mixture of ethylene carbonate and diethyl carbonate (1 : 1 mass ratio) for 24 h to prepare polymer gel electrolyte. The phase inversion technique used here to prepare gel polymer electrolyte is presented in form of flow chart in figure (2.7b).

2.5 Characterization Techniques

2.5.1 X-Ray Diffraction

X-ray diffraction (XRD) is a non-destructive technique; predominantly used to determine the atomic structure of the crystalline material along with the structural aspects of semi-crystalline materials.[162] It is one of the fundamental techniques to ascertain whether a desired phase of the intended material is successfully formed or not. X-rays are nothing but electromagnetic waves having a wavelength similar to the lattice spacing of the crystalline or semi-crystalline materials under study. For the structural information of the material under investigation monochromatic X-rays are impinged on the sample. They are scattered by the outer electrons of atoms or ions. It is found that the incident and scattered waves are having the same energy, hence termed as elastic scattering. These elastically scattered electromagnetic waves interfere and generate a diffraction pattern. The information about the nature of the sample can be obtained from this observed diffraction pattern. For a given inter-planer spacing (d) and wavelength (λ), the various orders (n) of reflection occurs only at the precise values of angle θ, which satisfies the Bragg condition given by[163]

$$2d \sin\theta = n\lambda \tag{2.2}$$

The present work includes not only the preparation and characterization of different types of polymer electrolytes but also the constituent fillers used to prepare those polymer nanocomposite electrolytes. Therefore, X-ray diffraction is a very much useful technique to check the phase formation of the single phase ceramic fillers, modification of hydrophilic montmorillonite clay along with the structural characterization of polymer electrolytes. Using XRD data the Rietveld refinement is carried out to get structural information of fillers. However, conventional indexing is performed and calculation of d- spacing have been carried out using the XRD patterns. X-ray diffraction patterns are recorded using Rigaku Ultima IV X-ray diffractometer operated at 40 kV potential and 40 mA current with Cu $K_{\alpha 1}$ radiation (1.5405 Å). Diffraction patterns are recorded with a scanning step of $0.002°$ and speed $3°$ per minute over a wide range of Bragg diffraction angle. A brief idea about Rietveld refinement is given below.

Rietveld Refinement

Detailed structural information can be extracted by performing Rietveld refinement of XRD pattern. The basic concept behind Rietveld refinement techniques is the comparison between the simulated XRD pattern based on the theoretical model structure with the experimentally obtained XRD pattern. This method consists of a least square reiterative refinement and its aim is to minimize the difference between the model predicted and the experimentally obtained XRD patterns. The difference between the model predicted and the experimentally

obtained data is represented by the following equation:

$$S_y = \sum W_i (y_i^{obs} - y_i^{cal})^2 \tag{2.3}$$

where, W_i is the weighing factor $(1/y_i)$ of the i^{th} data point, y_i^{obs} is the total observed intensity at the i^{th} point. The total calculated intensity y_i^{cal} at the i^{th} point is represented by the following equation:

$$y_i^{cal} = B + s.A.P.\xi \sum L_{hkl}.P_{hkl}.F_{hkl}^2.profile(2\theta_{hkl} - 2\theta_i) \tag{2.4}$$

where B, s, A, P and ξ are the parameters associated with background, scale factor, absorption, polarization and extinction of the experiment, respectively. L_{hkl} and P_{hkl} are the geometry and preferred orientation parameters.

In the course of pattern refinement, the position of reflections, intensity and profile parameters are refined. Though the refinement strategies change based on the type of data, but the success of refinement is usually predetermined by the quality of the initially assumed theoretical model. Typically background, scale factor, unit cell parameters and peak profiles are refined first. After the best possible fit is obtained from the starting model, structural parameters such as atomic coordinates, occupancies and thermal factor are also refined. Additional information can also be fed into the refinement program in form of constraints, to extract refined structural information such as site occupancies, multiplicities, thermal factor etc. All these parameters are continually varied in the refinement procedure, hence called an iterative process, until the best possible fit is obtained between the model predicted and the experimentally observed patterns. The fitting results generally represented as the goodness of fit using the following parameters.[164, 165]

$$R_p = \frac{\sum_i |y_i^{obs} - y_i^{cal}|}{\sum_i y_i^{obs}} \tag{2.5a}$$

$$R_{wp} = \left[\frac{\sum_i w_i (y_i^{obs} - y_i^{cal})^2}{\sum_i w_i (y_i^{obs})^2} \right]^{1/2} \tag{2.5b}$$

$$R_{exp} = \left[\frac{N - P}{\sum_{i=1}^{N} w_i (y_i^{obs})^2} \right]^{1/2} \tag{2.5c}$$

$$\chi^2 = \frac{R_{wp}}{R_{exp}} \tag{2.5d}$$

For a good refinement, one should get small values for the R_p (R pattern) and the R_{wp} (R weighted pattern) or must achieve a very close agreement between R_{wp} and R_{exp} (R experimental), leading χ^2 values close to unity. The Rietveld refined X-ray diffraction pattern for a dual phased titania (anatase + rutile) is shown is figure (2.4b) as indicative.

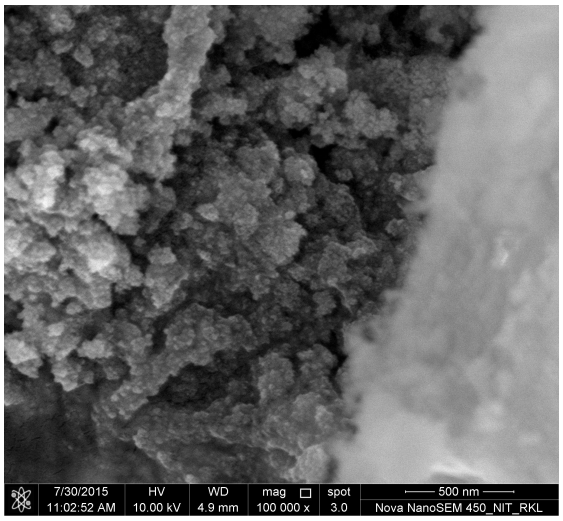

(a) Zirconium dioxide powder sample, synthesized using $1:1$ molar ratio of $ZrOCl_2$-$8H_2O$ and $CO(NH_2)_2$

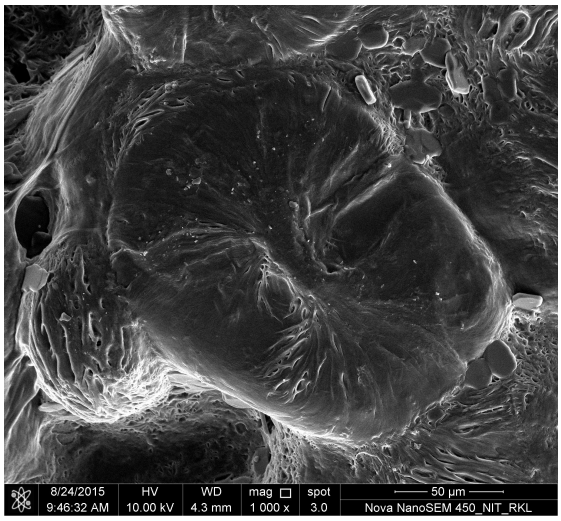

(b) Modified montmorillonite clay based polymer composite electrolyte having composition $PEO_{20}LiFC_3SO_3$-5 wt.% modified montmorillonite.

Figure 2.8: Scanning electron micrographs of zirconia filler and polymer electrolyte sample under investigation as representative.

2.5.2 Scanning Electron Microscopy

Scanning electron microscopy (SEM) is an extremely versatile technique for providing microstructural information over a wide range of magnification. Scanning electron microscopy helps for studying the texture, topography and surface features of samples.[166] It is a type of electron microscope that images the sample surface by scanning it with a high-energy beam of electrons in a raster scan pattern. Micrographs are rendered using the secondary electrons. In the present investigation, the micrographs are recorded using Nova Nano SEM 450 scanning electron microscope. Samples are gold coated before analysis and they are analyzed with varying resolutions for detailed morphological information. In figure (2.8), SEM micrographs of as prepared zirconia filler and modified montmorillonite-based polymer nanocomposite electrolytes for 5 wt.% mMMT composition are represented.

2.5.3 Fourier Transform Infrared Spectroscopy

Spectroscopy is the study of the interaction between matter and electromagnetic radiation. Infrared spectroscopy deals with the infrared region of the electromagnetic spectrum. It works on the fundamental principle that molecules absorb specific frequencies that correspond to the characteristic frequencies of normal mode vibrations of the molecule.[167] Although, photon energies associated with the infrared are not large enough to excite electrons, can induce vibrational excitation of covalently bonded atoms and groups. From the molecular structural viewpoint, it is clear that the covalent bonds in molecules are not rigid, but are more like stiff springs that undergo vibration such as stretching and bending. This

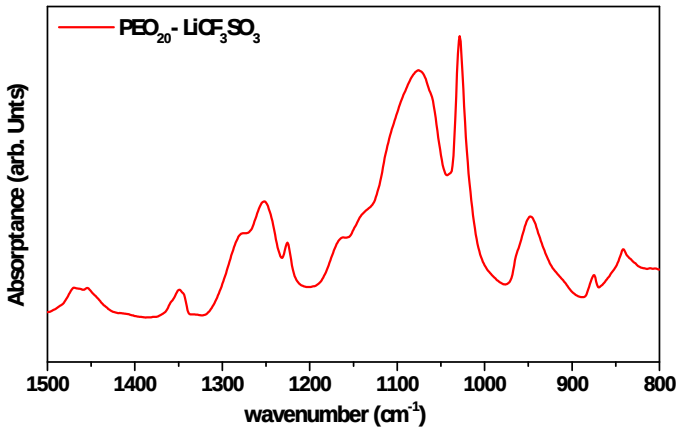

Figure 2.9: FTIR spectra of polymer salt complex film having composition PEO_{20}-$LiFC_3SO_3$ as representative.

different motion results in the change in bond length, bond angle or torsion angle. Certain frequencies of the radiation will be absorbed when the matter is irradiated by the infrared light. Polymer related characterization can be performed using infrared spectroscopy to get information on tacticity, 'mer' sequence distribution, chain branching or structure of radicals. These are collectively termed as chemical aspects of the material. In addition to these, using infrared spectroscopy information about chain orientation, crystallinity, chain conformation can also be found, which are termed as physical aspects of the materials. In the present study FTIR, spectra are recorded using Bruker Alpha-E spectroscope in the mid-IR region. In figure (2.9), FTIR spectra of polymer salt complex having composition PEO_{20}-$LiFC_3SO_3$ is shown as indicative.

2.5.4 Dielectric Spectroscopy

Dielectric spectroscopy measures the dielectric properties of a medium as a function of frequency. It is a widely accepted technique to characterize electrical properties of both the liquid and solid electrolytes along with a variety of other materials starting from conductors to insulators.[168, 169] This technique is one of the versatile technique to characterize ionic conductors in terms of electrode polarization, ionic conductivity, ion conduction mechanism, relaxation dynamics etc of polymer electrolytes. To characterize the samples using this technique a capacitive arrangement is prepared using two non-blocking electrodes. The sample is kept between the electrodes and a small ac signal is imposed on the sample. The output current is measured along with the phase difference. For the temperature dependent electrical property analysis, usually sets of isothermal frequency sweeps are carried out and electrical properties at various temperatures are compared for a particular frequency. This approach provides information about the electrical properties as a function of frequency as well as temperature. From frequency dependent data, a detailed overview different

relaxation phenomenon present in the system can be studied.

Broadband dielectric spectroscopy provides the basic information of the capacitance, phase difference, loss tangent etc. When a dielectric is placed in an alternating electric field the strength of the electric field $E(t)$ and the electric displacement $D(t)$ are described as follows[168]

$$E(t) = E_0 \exp(j\omega t) \tag{2.6}$$

$$D(t) = D_0 \exp(j\omega t - \theta) \tag{2.7}$$

where E_0 and D_0 are system constants, ω is the angular frequency, and t is time. $D(t)$ is normally out of phase with $E(t)$ by the phase angle θ. In complex notation, the dielectric constant ε^* is expressed as

$$\varepsilon^* = D(t)/E(t) = D_0/E_0 \exp(-j\theta) = \varepsilon_0(\cos\theta - j\sin\theta) \tag{2.8}$$

$$\varepsilon^* = (\varepsilon_0 \cos\theta) - j(\varepsilon_0 \sin\theta) = \varepsilon' - j\varepsilon'' \tag{2.9}$$

and

$$\tan\delta = \varepsilon''/\varepsilon' \tag{2.10}$$

where ε' is the dielectric constant or permittivity and ε'' is the dielectric loss; $\tan\delta$ is the dissipation factor or loss tangent and is independent of sample geometry. Here ε_0 is the permittivity of the free space *i.e.* $8.8541878 \times 10^{-12}$ F/m and $j = \sqrt{-1}$. Other electrical parameters can be evaluated using the following relations. The real and imaginary part of ac conductivity are calculated using the following relation[168]

$$\sigma^*(f) = \sigma'(f) - j\sigma''(f) = j2\pi f\varepsilon_0(\varepsilon' - j\varepsilon'') \tag{2.11}$$

The complex dielectric modulus, $M^* = M' + jM''$ is obtained from the complex dielectric permittivity using

$$M^*(f) = 1/\varepsilon^*(f) = \varepsilon''/(\varepsilon'^2 + \varepsilon''^2) + j\varepsilon'/(\varepsilon'^2 + \varepsilon''^2) \tag{2.12}$$

As mentioned earlier, broadband dielectric spectroscopy is an effective tool to study relaxation dynamics of dielectric materials. Depending on the frequency range, from high frequency to low frequency, various polarization can be observed. These are electronic, atomic, orientational (dipolar) and interfacial (ionic) and electrode polarization. A schematic diagram is shown in figure (2.10) to show the approximate frequency range of these polarizations. Electronic and atomic polarizations is observed for very high values of frequency. The ionic polarization, which is seen at the low-frequency spectrum, is usually can be related to the geometries and the interfaces of the domains in the sample. In these regions, space charge effect takes place which is creating macroscopic dipoles. The

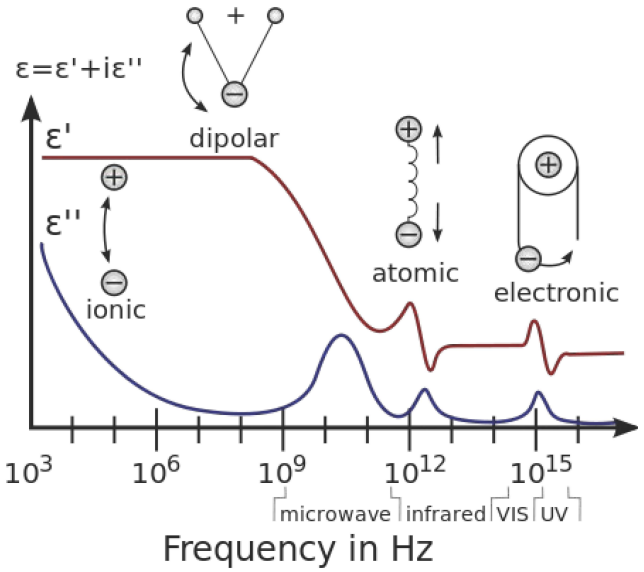

Figure 2.10: Schematic diagram of the complex permittivity spectrum vs. frequency, showing the several types of relaxation processes.

orientational polarization is responsible for the alignment of dipolar molecules under the external electric field, which reflects the dynamics of the polymer chains or segmental relaxation dynamics. Segmental relaxation does play an important role in ionic transport in polymer electrolytes. Electrode polarization is observed at very low frequency. Using Ratner's classical approach coupling between ion conduction mechanism and segmental relaxation is investigated. In that formalism concepts of electrode polarization in terms of Mcdonald -Trukhan approach do play an important approximation. These are described in detail in subsequent chapters.

2.6 Instruments Used in the Present Study

All the samples under investigation are prepared inside the inert atmospheric chamber, PlasLab 855-AC/EXP, equipped with a dehumidifier, nitrogen gas circulation system, electronic weighing balance and stirring units. These are the following instruments used for characterizing the samples:

- **X-ray Diffraction:** Rigaku Ultima IV
- **Scanning Electron Microscopy:** Nova- Nano SEM 450
- **Fourier Transform Infrared Spectroscopy:** Bruker Alpha-E FTIR Spectroscope
- **Broadband Dielectric Spectroscopy:**
  - Novocontrol α analyzer
  - PSM 1735 impedance analyzer

Chapter 3

Ion Conduction Mechanism in Polymer Electrolytes:Phenomenological concepts, Physical models and Universalities

3.1 Introduction

The basic concepts to analyzing and interpret the experimental observations related to electrical properties and conduction mechanism are presented in this chapter. Nearly four decades have passed when M.B. Armand *et. al.* first proposed that these class of materials has potential to be used in energy storage/conversion devices. Till date, various measures has been taken to increase the ionic conductivity of polymer electrolytes along with enhancing its other physical properties like mechanical, thermal and electrochemical stability etc. suitable for device application.[10, 94, 170, 171] Unfortunately, even with a lot of efforts to improve the ionic conductivity of polymer electrolytes, keeping it mechanically stable, is not achieved so far.[69, 77, 172] Therefore, the study of ion transport mechanism is much required to further improve its electrical properties, from the fundamental point of view. In this chapter, different approaches are presented to study and analyze the experimental observation and understand the ionic transport mechanism at the microscopic level.

3.2 Empirical Relations Developed

An extensive amount of research work has been carried out on electrical properties of disordered solids. The experimental observations were analyzed and interpreted to get an idea about the physical parameters associated with various properties, ranging from electrical, mechanical, thermal and chemical properties, of disordered solids. In this chapter, the focus is given on the development of phenomenological theories as well as physical model based theories used to describe electrical properties of ionic disordered solids in general and polymer electrolytes in particular.

3.2.1 Jonscher Power Law

It is found that the frequency dependence of the electrical conductivity (σ') in ionic conductors show a dispersive behaviour, which can be described by the Jonscher power law expression given by the following equation[173]

$$\sigma' = \sigma_{dc} + Af^n \tag{3.1}$$

where, σ_{dc} is the dc conductivity, A is temperature-dependent constant, f is frequency and n is power law exponent whose value should be within $0 < n < 1$. In general for ionic conductors, the value of "n"lies in between 0.4 and 0.7.[174] Frequency dependent dispersive behaviour is mainly observed for disordered materials, *e.g.*, ionically conducting glasses, conducting polymers and amorphous semiconductors etc. and is termed as "universal dielectric response" or "first universality". Jonscher power law mentioned above can also be represented in Almond-West formalism given by the following equation[107]

$$\sigma' = \sigma_{dc}[1 + (f/f_c)^n] \tag{3.2}$$

where, the critical frequency f_c, termed as crossover frequency, represents the onset frequency of the dispersive behaviour. By fitting the ac conductivity data using power law expression in Almond West formalism, both dc conductivity (σ_{dc}) and crossover frequency can be estimated. In the present study, therefore, Almond-West form of power law will be used.

3.2.2 Double Power Law

While describing ac conductivity spectra over a wide range of temperature and frequency, it is observed that at very low temperature and or very high frequency experimentally observed data can not be fitted using power law expression shown in equation (3.2). Therefore, to describe the experimentally obtained data another term is added to power law, which is known as double power law given by the following equation [175, 176]

$$\sigma' = \sigma_{dc}[1 + (f/f_c)^n] + Bf \tag{3.3}$$

where, B is a weakly temperature dependent constant. This added term, *i.e.* Bf, is having linear frequency dependence and the modified power law expression can successfully explain the ac conductivity spectra over a wider range of frequency and temperature. This modified equation also gives the concept of nearly constant loss, which will be explained in section (3.4.2). Clearly these power law relations given in equation (3.1) and equation (3.3) cannot be valid over the entire frequency range, since they give rise to divergences as $f \to 0$.

Conductivity isotherms are fitted using Jonscher power law and or double power law

to obtain dc conductivity at a particular temperature. DC conductivity as a function of temperature is explained with the help of Arrhenius or Vogel-Tamman-Fulcher (VTF) relations given in the following section.

3.2.3 Arrhenious and VTF Relations

The obtained dc conductivity as a function of temperature for disordered solids in general follows Arrhenius behaviour given by the expression below[177]

$$\sigma_{dc} = \sigma_0 \exp\left(-\frac{E_A}{k_B T}\right) \tag{3.4}$$

where, σ_{dc}, σ_0, E_A, k_B and T represents dc conductivity, pre exponential factor, activation energy, Boltzmann constant and temperature in absolute scale respectively. For the polymer electrolytes in general, the experimental data does not fit with this equation. Rather, the temperature dependent dc conductivity data fits well with another equation known as VTF equation given by[178]

$$\sigma_{dc} = \sigma_0 \exp\left[-\frac{E_A}{k_B(T - T_0)}\right] \tag{3.5}$$

where, T_0 the equilibrium glass transition temperature or Vogel temperature. At $T = T_0$, excess configuration entropy becomes zero, *i.e.* molecular motions cease. The VTF equation is an empirical relation originally developed to describe viscosity of super cooled liquids. The viscosity η was found to follow the relation [179]

$$\eta = \eta_0 \exp\left[\frac{E_A}{k_B(T - T_0)}\right] \tag{3.6}$$

where, η_0 is a pre-exponential factor. The above mentioned equation in combination with Stokes-Einstein relation for diffusivity of polymers and Nernst-Einstein expression can be expressed in the mathematical form given in equation (3.5)

3.2.4 WLF Relations

Williams, Landel and Ferry (WLF) developed an equation to study the dynamics of polymers and other glass–forming materials, which relate polymer chain viscosity to glass transition temperature as given by[180]

$$\log a_T = Constant + \log\left[\frac{\eta(T)}{\eta(T_s)}\right] = \frac{-C_1(T - T_s)}{C_2 + T - T_s} \tag{3.7}$$

where a_T is the shift ratio (ratio of any relaxation process like viscosity, diffusion, conductivity, etc. at temperature T to its value at some reference temperature T_s) and C_1 and C_2 are constants. This equation can be re-written for temperature dependence of

conductivity as

$$\log\left[\frac{\sigma(T)}{\sigma(T_s)}\right] = \frac{-C_1(T-T_s)}{C_2+T-T_s}$$

$$\sigma(T) = \sigma(T_s)\exp\left[\frac{-C_1(T-T_s)}{C_2+T-T_s}\right] \tag{3.8}$$

The WLF behavior is found to be universal for many disordered systems, including glasses and pure polymers.

3.3 Physical Models

Based on the physical interactions at microscopic levels, different models were also developed over the years to explain the ionic transport process in polymer electrolytes. In this section, a brief idea of these models is presented.

Dynamic Bond Percolation Model: In order to describe the local liquid-like motion of the ions in a polymer, which is rapidly changing conformation above glass transition temperature, Ratner and Nitzan's dynamic bond percolation model introduces the idea that the available paths (or bonds in the author's terminology) are constantly opening and closing. The physical picture is that the renewal processes corresponding to conformational changes in the polymer and surrounding ions that lead to ion transport.[135]

Monte Carlo Simulation Studies by Bunde: Using this formalism, two different class of physical conditions are examined. Firstly an amorphous structure and thereafter random mixtures, where pathways in the conducting network are partially blocked by an immobile component. In this simulation study, the appearance of approximate power laws in the dynamic response is closely related to strong backward correlations among subsequent hops of the ions to the properties of particle trajectories in space. The frequency and temperature dependent conductivity spectra are not investigated thoroughly in these studies.[181, 182]

Deitrich's Counterion Model: In this model, the diffusion dynamics of particles having some discrete charge $+q$ is studied in an energy landscape. The energy landscape is determined by immobile centers of charge $-q$, hence counter ion, which are distributed randomly in space. Monte Carlo simulations are carried out to understand the diffusion dynamics and ionic conductivity along with various observed relaxations. This model emphasizes on the dependence of transport properties based on carrier concentration and non-exponential relaxation effects. The assumption of having discrete charge based energy landscape is not suitable for polymer electrolytes as above glass transition temperature the polymer chain undergo significant segmental relaxation.[183]

Random Free Energy Barrier Model: This model assumes ion conduction occurs by hopping mechanism. The hopping charge carriers are subject to random energy barriers. The model has solved in the continuous time random walk formalism and in the effective medium approximation. Obtained solutions in both the techniques are found nearly the same. In

the random free energy barrier model, the frequency-dependent conductivity is completely determined by the dc conductivity and the dielectric loss strength. Random free energy barrier model is very much successful for disordered solids, solid ionic conductors where the lattice points are fixed and they don't evolve with time. The expressions for real part of ac conductivity as a function of angular frequency in this model is expressed as

$$\sigma' = \frac{\sigma_{dc}\omega\tau_e \tan^{-1}(\omega\tau_e)}{1/4\left[ln(1+\omega^2\tau_e^2)\right]^2 + \left[\tan^{-1}(\omega\tau_e)\right]^2} \tag{3.9}$$

where, σ', σ_{dc}, ω, τ_e are real part of complex ac conductivity, dc conductivity, angular frequency and relaxation time respectively. [139, 184]

Ngai Coupling Model: This model is applicable to inherently heterogeneous systems at the microscopic level. In this model intrinsic mobility of polymer chains along with local compositional heterogeneity is considered. These are arising due to concentration fluctuation and the segmental dynamics. Slowing down of these relaxation rates is described at macroscopic level by a time dependent factor $(\omega_c t)^{-n}$,which shows relaxation phenomena slows down after an average time $t_c = 1/\omega_c$. The coupling parameter n is found proportional to average coupling or interaction of the species. With this perspective, coupling model simplifies the collective complicated behaviour of individual relaxing species in a heterogeneous system. The coupling parameter can replace and simplify approximated relaxation time on macroscopic scale predicting the experimental observations. [131, 185]

MIGRATION Concept: The acronym MIGRATION stands for MIsmatch Generated Relaxation for the Accommodation and Transport of IONs. The physical picture conveyed in this model is related to the mismatch introduced by any hop of an ion and the ensuing relaxation (rearrangement) of the ionic neighbourhood. This phenomenon may or may not provide a stable accommodation of the ion at its new position. When a stable accommodation of moving ions are achieved at a new position, an elementary step of macroscopic transport has been completed by the ions. Based on these concepts hopping conductivity is presented in the following form[186]

$$\sigma_{hop}(\omega) = \frac{q^2 N}{3Vk_BT}\int_0^\infty \langle v(0)v(t)\rangle_{hop} \exp(-i\omega t)dt \tag{3.10}$$

where, q is the charge of mobile ions, V is the volume, N is the number of mobile ions of same kind, k_B is the Boltzmann constant, T is the temperature in absolute scale ω is the angular frequency, t representing time and $\langle v(0)v(t)\rangle_{hop}$ is the velocity autocorrelation fuction for ion hopping. Time-dependent correlation factor is defined using the following relation[228]

$$W(t) = \frac{\frac{d}{dt}\langle r^2(t)\rangle_{hop}}{\frac{d}{dt}\langle r^2(t)\rangle_{hop}|_{t\to 0}} \tag{3.11}$$

where, $W(t)$ is the normalised time derivative of the mean square displacement of the mobile

ions. From the above mentioned equation (3.11) it can be seen that $W(0)$ is unity and $W(t)$ is the normalized integral of the velocity autocorrelation function for the hopping motion $\langle v(0)v(t)\rangle_{hop}$. Therefore the hopping ionic conductivity can be represented as[229]

$$\frac{\sigma_{hop}(\omega)}{\sigma_{HF}} = 1 + \int_0^\infty \dot{W}(t)\exp(-1\omega t)dt \tag{3.12}$$

where, σ_{HF} is the high frequency contribution part in ac conductivity. After integrating by parts the frequency dependent ionic conductivity can be rewritten as[228]

$$\sigma_{hop} = \sigma_{dc}\left[1 + i\omega\int_0^\infty W_s(t) - 1\exp(-i\omega t)dt\right] \tag{3.13}$$

This concept also provide variation of ionic conductivity as a function of temperature in the following form[186]

$$\sigma_{dc}(T) = \alpha\exp\left[-\frac{E^*}{k_BT} - \gamma\exp\left(\frac{E^*/K}{k_BT}\right)\right] \tag{3.14}$$

where, α and γ are pre-exponential factor and E^* is displacive activation energy. High frequency conductivity limit given can be represented in the following form

$$\sigma_{HF} = \frac{\alpha}{T}\exp\left\{-\frac{E^*}{k_BT}\right\} \tag{3.15}$$

The drawback of dynamic bond percolation, Monte Carlo studies by Bunde, Deitrich's Counterion, random free energy barrier model is that these models mostly do not focus on the intrinsic heterogeneity of the system and associated relaxation phenomena. These models also do not focus on the observed first and second universalities found in disordered solids in general. So in the present study emphasis is mainly given on Ngai coupling model and MIGRATION concept.

3.4 Universalities

Frequency dependent conductivity spectra show two universalities, namely first and second universality. First universality or Universal Dielectric Response behaviour is generally observed at high temperature and or low-frequency region of the conductivity spectra.[187–189] On the other hand, second universality or nearly constant loss is observed at very high frequency and or low-temperature regions.

3.4.1 First Universality: Universal Dielectric Response

The measurement of the ac conductivity generally as a function of frequency shows dispersion. This dispersive behaviour offers an opportunity to gain insight into the interaction of the migrating ion with other defects in the structure. This frequency dependent

behaviour can be observed over a wide class of highly disordered materials, such as glasses, polymers, amorphous semiconductors, heavily doped crystals etc. Mathematically this dispersive behaviour can be represented in form of a power law previously stated as Jonscher power law shown in equation (3.1). Such behaviour was first reported by A. K. Jonscher for such a wide variety of materials and he denoted this behaviour as the "universal dielectric response". The imaginary part, ε'', of the complex dielectric constant, ε^*, corresponding to UDR behaviour is given by[190]

$$\varepsilon'' = [\sigma(\omega) - \sigma(0)]/\varepsilon_0\omega = (A/\varepsilon_0)\omega^{-(1-n)} \tag{3.16}$$

where, ε_0 is the vacuum permittivity, σ is ac conductivity represented as a function of angular frequency, ω. Correspondingly, as a consequence of the Kramers-Kronig relation, the real part of complex permittivity, ε^*, is given by [190]

$$\varepsilon' = \varepsilon_\infty + (A/\varepsilon_0)\tan(n\pi/2)\omega^{-(1-n)} \tag{3.17}$$

where, ε_∞ is the high-frequency limiting value of $\varepsilon'(\omega)$.

3.4.2 Second Universality: Nearly Constant Loss

At sufficiently low temperatures the frequency response of σ' isotherms becomes linear or nearly linear. It also implies negligible frequency dependence of the imaginary part of dielectric permittivity. This can be expressed as, $\epsilon''_{NCL}(f) = B/2\pi f^a$ where, a is a positive constant having value nearly equal to zero and B is a constant with weak temperature dependence. Therefore this kind of response is named "second universality" or "nearly constant loss"(NCL) as described in various literatures. Contribution of NCL behaviour to σ' can be represented as, $\sigma'_{NCL} = 2\pi f\epsilon''_{NCL}(f) \approx Bf^{1-a}$[190]. It is already mentioned in section (3.2.2), that in order to accommodate this almost linear frequency dependent contribution in the low-temperature region addition of an another term is required to Jonscher power law. This term has a nearly linear dependence on frequency.

3.5 Scaling

3.5.1 Conductivity Scaling

Scaling studies of experimentally measured quantities are in general important. It gives better insight to the common underlying reasons for a particular physical property[140, 191]. With increasing temperature, if the onset of conductivity dispersion found shifting towards higher frequency values, then the conductivity spectra can be scaled to obtain a superimposed master curve for all isotherms. This scaling procedure is also known as time temperature superposition principle and its purpose is to probe whether conduction mechanism is temperature dependent or not. Different approach have been proposed to superimpose the

$\sigma'(f)$ isotherms to get a master curve and in general this can be represented by the following equation[192],

$$\frac{\sigma(f)}{\sigma_{dc}} = F\left(\frac{f}{f^*}\right) \tag{3.18}$$

where, F is the temperature independent scaling function, f^* is the frequency scaling parameter for each conductivity isotherm. In Summerfield scaling process for a given composition and different isotherms the frequency scaling parameter *i.e.*, f^* is chosen as $\sigma_{dc}T$[193]. Therefore in case of Summerfield scaling formalism equation(3.18) can be expressed as,

$$\frac{\sigma(f)}{\sigma_{dc}} = F\left(\frac{f}{\sigma_{dc}T}\right) \tag{3.19}$$

The Summerfield scaling approach is having the advantage of using directly accessible parameters *i.e.* d.c. conductivity (σ_{dc}) and temperature (T).[194]

3.5.2 Electrical Modulus Scaling: Maxima Normalization Technique

Electric modulus is usually investigated to analyze the conductivity relaxation phenomena in the polymer electrolyte. The analysis of frequency dependent electrical modulus data has the advantage of eliminating the electrode polarization effects in particular where ionically conducting samples are characterized with blocking electrodes. Successful formation of a single master curve for a particular composition of polymer electrolyte over a wide range of temperature suggest that the observed conductivity relaxation phenomenon is a temperature independent dynamic process. In this present study to form a master curve for the electrical modulus isothermal spectra, maxima normalization technique is used which can be represented by the following equation.

$$\frac{M''(f)}{M''_{max}} = F\left(\frac{f}{f_{max}}\right) \tag{3.20}$$

3.6 Coupling: Ratner's Classical Approach

Coupled ion conduction process can be represented using two different approaches, firstly using decoupling ratio and secondly using Ratner's classical approach. The decoupling ratio is defined as the ratio of segmental to conductivity relaxation time and can be expressed as

$$R = \frac{\tau_s}{\tau_c} \tag{3.21}$$

where, τ_s and τ_c are segmental and conductivity relaxation time respectively. For decoupled ion conduction process, the value of R should be as high as 1000, but for a coupled system in general the value of decoupling ratio should be small. Another approach to study the decoupling of ion conduction process is by using modified classical Ratner's approach,

where the relation between free ion concentration, p and dc conductivity, σ_{dc} is given by

$$p = \frac{\sigma_{dc} k_B T}{D q^2} \tag{3.22}$$

where, k_B is the Boltzmann constant, D is diffusivity and q is the ion charge. For coupled systems according to Stokes-Einstein (SE) relation, D is inversely proportional to the polymer segmental relaxation time, τ_s, *i.e.*

$$D \propto \frac{1}{\tau_s} \Rightarrow D\tau_s = constant \tag{3.23}$$

Combining equation (3.22) and (3.23) one can obtain

$$\sigma_{dc} \propto \frac{p}{\tau_s T} \tag{3.24}$$

If the effect of free ion concentration is neglected, from equation (3.24) one can get the classical theory proposed by Ratner and his co-workers.[195]

$$\sigma_{dc} \tau_s T = constant \tag{3.25}$$

Hence to validate whether ion conduction and host polymer segmental relaxation are coupled phenomena or not, equation (3.23) and equation (3.25) must be satisfied. Probing equation (3.23) will be a better choice as literature suggest the effect of free ion concentration, p may not be negligible over a wide range of temperature.[196]

3.7 Data Fitting

Experimentally obtained data are fitted with various equations to get an insightful analysis of different physical parameters under investigation. For this, χ^2 minimization technique has been employed and Originlab Origin 2015 software has been used. Fitted results are shown in form of fitted plot where-ever necessary.

Chapter 4

Investigations of Relaxation Dynamics and Observation of Nearly Constant Loss Phenomena in PEO_{20}-$LiCF_3SO_3$-ZrO_2 Based Polymer Nano-Composite Electrolyte[1]

4.1 Introduction

Conventional polymer salt complex do exhibit a very low range of ionic conductivity at room temperature, ranging from 10^{-9} Scm^{-1} to 10^{-7} Scm^{-1}. To increase the ionic conductivity of conventional polymer salt complex different types of nanocrystalline ceramic additives are added to it, which are named as polymer nanocomposite electrolytes (PNCEs). Based on filler concentration the ionic conductivity of these electrolytes needs to be optimized. Apart from this process of optimization; the ion conduction mechanism also needs to be explored in detail. Further increase in the conductivity values of polymer nanocomposite electrolytes can only be possible with a proper understanding of ion conduction process in these class of materials.

The existence of first universality or universal dielectric response can be observed in disordered solids; when their electrical properties are characterized as a function of frequency. Polymer nanocomposite electrolytes being a disordered ionic conductor also exhibit the characteristic presence of the universal dielectric response in its frequency-dependent dielectric and conductivity spectra. In addition to the presence of dispersive frequency dependent universal dielectric response (first universality), nearly constant loss (NCL) (second universality) behaviour can be observed in PNCEs. The cause of the presence of first and second universality is examined in this work. The relaxation dynamics and explanation for ion conduction mechanism is also investigated.

[1]Content of this chapter is partially published in : Tapabrata Dam, S. N. Tripathy, M. Paluch, S. S. Jena and D. K. Pradhan, "Investigations of Relaxation Dynamics and Observation of Nearly Constant Loss Phenomena in PEO_{20} - $LiCF_3SO_3$ -ZrO_2 Based Polymer Nano-Composite Electrolyte.", Electrochimica Acta, 2016 (202) 147-156.

In the present work, polymer nanocomposite electrolytes are prepared using polyethylene oxide as the host polymer, lithium triflate as salt and nanocrystalline zirconia as ceramic filler. Zirconia being a neutral passive filler, its influence on ionic conductivity is an interesting topic to explore. Therefore, PNCEs films are synthesized using solution casting technique having compositions PEO_{20}-$LiCF_3SO_3$ - x wt.% ZrO_2, with $x = 0$, 3, 5, 8, 10 & 20. Phase purity of used zirconia filler is first analyzed by X-ray diffraction technique, before using it as the filler for the composite electrolyte. Structural, vibrational, surface morphological and temperature dependent electrical properties are investigated using X-ray diffraction, FTIR, FE-SEM and broadband dielectric spectroscopy respectively. Variation of ionic conductivity as a function of temperature and filler concentration is studied. Emphasis has been given on the observed universalities in these class of materials. An in-depth study is carried out to explore the cause of the presence of the second universality at very low temperature and or high-frequency regime.

4.2 Experimental Procedure

The XRD patterns of the PNCE films are recorded using Rigaku Ultima IV X-Ray diffractometer operated at 40 kV and 40 mA current with Cu $K_{\alpha 1}$ radiation having wavelength 1.5405Å. The XRD patterns are recorded with a scanning step of 0.002° and scan rate of 3° per minute. Fourier transforms infrared spectra of the nanocomposites are recorded with FTIR spectrometer (Bruker Alpha-E spectroscope in ATR mode) from 4000 to 600 cm^{-1} with a resolution of 2 cm^{-1}. For FE-SEM micrographs, samples are first gold coated and images are recorded using Nova Nano-SEM 450 instrument. Dielectric measurements are performed using a Novo-Control GMBH Alpha dielectric spectrometer in the frequency range from 10^{-1} Hz to 10^6 Hz with perturbation potential of 10mV. Temperature is controlled with a stability better than 1 K, using Novo-Control Quattro Cryo-system, with the use of a nitrogen gas cryostat. The PNCE films are sandwiched between a pair of stainless steel electrodes and then placed in the sample holding assembly of the cryostat. The samples are heated to 323 K and kept for 1 hour before commencing the measurement. Thereafter the dielectric data is collected during cooling mode from 323 K to 173 K at every 5 K interval with 10 minute of equilibration time at each temperature.

4.3 Results and Discussion

4.3.1 Structural study

The XRD patterns provide information related to the complexation, composite formation, crystalline-amorphous phase contents for PNCEs.[197] Figure (4.1) represents the XRD patterns of PEO, PSC (PEO_{20} - $LiCF_3SO_3$) and different compositions of PNCEs. XRD pattern of PEO show several characteristic peaks at $2\theta = 19.2°$, 23.4°, 26.3° and 27°,

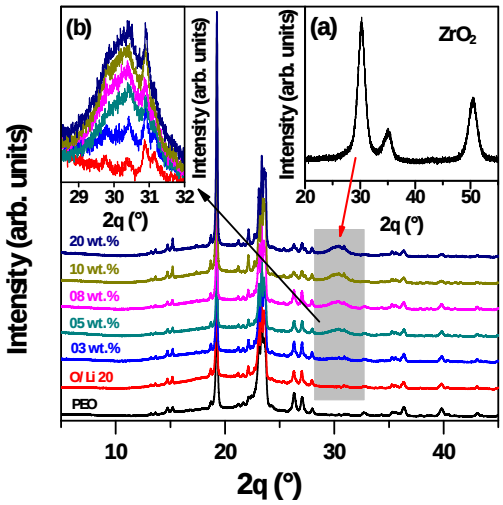

Figure 4.1: X-Ray diffraction pattern of poly ethylene oxide (PEO), polymer salt complex (PSC, O/Li 20) and polymer nano composite electrolytes (PNCEs) with different weight percentage of zirconia (ZrO_2) filler [PEO_{20}-$LiCF_3SO_3$- x wt.% ZrO_2 (x = 3, 5, 8, 10 & 20)]. Inset (a) showing the X-Ray diffraction pattern of nano-crystalline tetragonal phased ZrO_2 used as nano filler. Inset (b) showing the superimposed X-Ray diffraction pattern of polymer salt complex and polymer nano composite electrolytes.

corresponds to (120), (112)/ (032), $(21\bar{1})$ and (040) reflections respectively.[198] These reflections are also present in PSC and all compositions of PNCEs. In addition to these crystalline characteristic peaks, an amorphous background hump can also be observed in all XRD patterns. The appearance of background hump and crystalline peak together suggest the semi-crystalline nature of the samples. On comparing the XRD patterns of PEO and PSC it is observed that no additional XRD reflections corresponding to $LiCF_3SO_3$ (JCPDF # 81-0813) is observed in PSC, which is confirming proper complexation of PEO and $LiCF_3SO_3$. Inset (a) of figure (4.1) shows the XRD pattern of zirconia (ZrO_2) (JCPDF # 80-0965), confirming the formation of tetragonal zirconia phase with strongest peak around $2\theta = 30°$. With the addition of ZrO_2 in PNCEs, an additional peak is appearing around $2\theta = 30°$ for all PNCEs. On close observation with the superimposed XRD patterns shown in the inset (b) of the figure (4.1), it is observed that the peak intensity corresponding to ZrO_2 gradually increases with increasing ZrO_2 concentration. However, with the addition of ZrO_2 nano-crystalline fillers no significant change in the characteristic peaks of PEO at $2\theta = 19.2°$, $23.4°$, $26.3°$ and $27°$ is observed. This indicates, with the addition of $LiCF_3SO_3$ and ZrO_2 nano-crystalline fillers, the structure of polymer host remain unaffected. Moreover, the presence of characteristic reflections for both PEO and ZrO_2 confirms that the identity of both components preserved to function as a composite material system.[199]

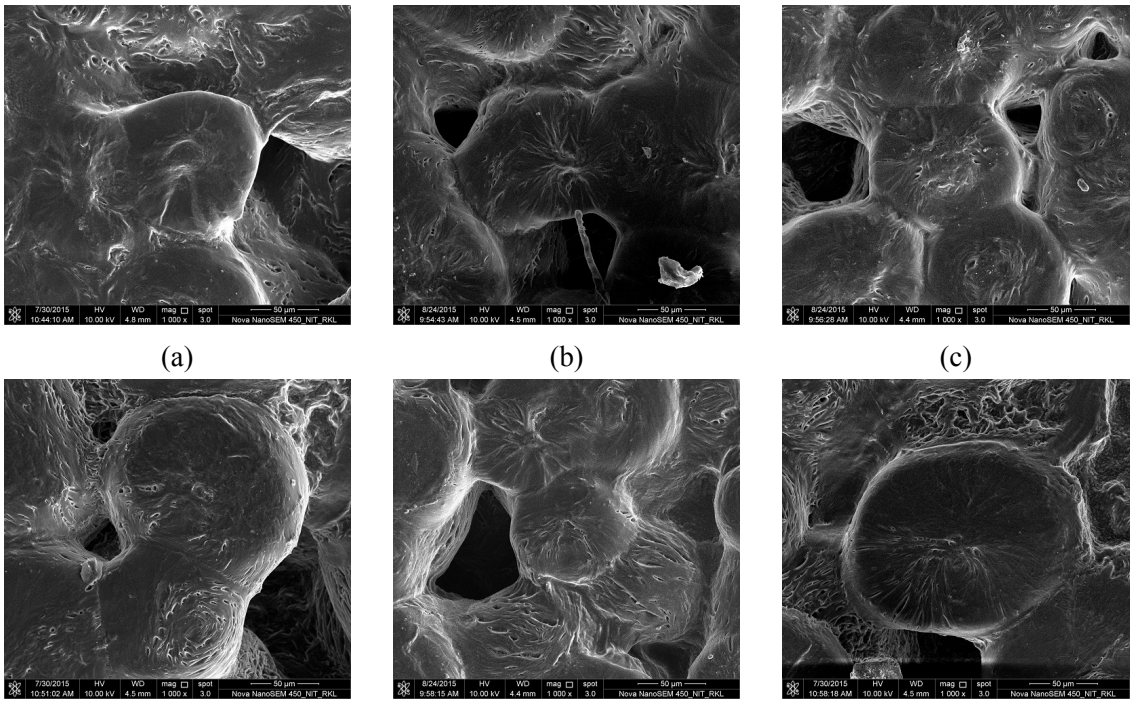

(a) (b) (c)

(d) (e) (f)

Figure 4.2: Scanning electron micrographs of polymer salt complex (PSC) and zirconia based polymer nano-composite electrolyte samples. (a) PSC, (b) 3 wt.% ZrO_2, (c) 5 wt.% ZrO_2, (d) 8 wt.% ZrO_2, (e) 10 wt.% ZrO_2 and (f) 20 wt.% ZrO_2 based compositions.

4.3.2 Surface Morphology

Figure (4.2) shows FE-SEM micrographs of the polymer salt complex and different PNCEs having compositions PEO_{20}-$LiCF_3SO_3$- x wt.% ZrO_2 ($x = 3, 5, 8, 10$ & 20). The FE-SEM micrographs of the polymer-salt complex and other PNCEs, shown in figure (4.2a), clearly depicts the presence of distinct spherulites. Characteristics lamellar microstructure can be observed in the spherulites. These lamellar structure represent the crystalline domain of the samples. The average size of the spherulites appeared for the polymer-salt complex is about $60 - 70$ μm in diameter. Not much variation in the spherulite sizes can be observed due to addition of fillers. The boundary between the spherulite represents the presence of amorphous phase in these samples. With the addition of ZrO_2 filler no substantial change in the morphological feature *i.e.*, spherulite texture can been observed as shown in from figure (4.2b) to (4.2f). Filler particles are found embedded in the polymer matrix forming a proper composite sample. These surface micrographs of PNCEs also indicate that the films are of semi-crystalline in nature, as suggested by X-ray diffraction pattern. Spherulites represent the crystalline and the boundaries represent the amorphous regions.

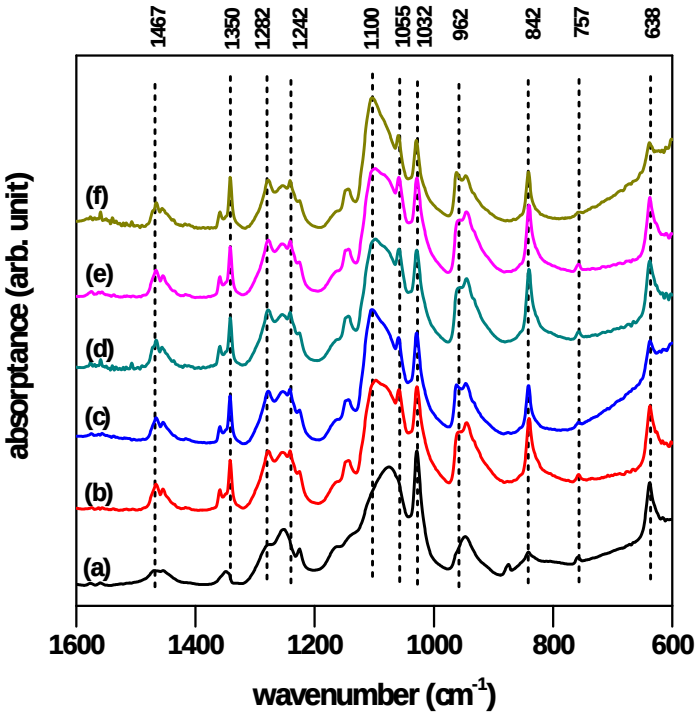

Figure 4.3: FTIR spectra of composite polymer electrolytes having composition PEO_{20}-$LiCF_3SO_3$- x wt.% ZrO_2 (a) PSC, (b) 3 wt.% ZrO_2, (c) 5 wt.% ZrO_2, (d) 8 wt.% ZrO_2, (e) 10 wt.% ZrO_2 and (f) 20 wt.% ZrO_2 based compositions.

4.3.3 Vibrational Study

Infrared (IR) spectroscopy is used to study interactions between the ions and host polymer. FTIR studies can help to study the effect of additive *i.e.* filler concentration on the polymer-salt complex. Polymer-salt complex exhibits characteristic bands around 638 cm^{-1} corresponds to cis C-H wagging mode, 842 cm^{-1} corresponds to cis C-H_2 wagging, 962 cm^{-1} corresponds to stretching of ether bond (C-O) of polymer, 1032 cm^{-1} corresponds to symmetric stretch SO_3 vibration of $LiCF_3SO_3$, 1100 cm^{-1} corresponds to stretching of ether bond (C-O) of polymer, 1242 cm^{-1} corresponds to C-F and CF_2- stretching, 1282 cm^{-1} corresponds to CH_2 twisting vibration of polymer and 1467 cm^{-1} corresponds to CH_2 scissoring mode.[200, 201] Comparing the FTIR spectra of PSC and different compositions of PNCEs it can be observed that all characteristic bands of PEO and $LiCF_3SO_3$ are present in the samples. Focus is to be given on mainly 1032 cm^{-1} and 1055 cm^{-1} bands, which corresponds to symmetric stretch SO_3 vibration of $LiCF_3SO_3$ under complexation.[202, 203] 1032 cm^{-1} is related to free anions and solvent separated pair vibrations whereas around 1055 cm^{-1} represents $Li_2CF_3SO_3^+$ aggregates. With varying concentration of ceramic additives these two band profile show slight variation, which suggests that ion dissociation do take part in enhancing the ionic conductivity of the composite electrolytes.[204]

4.3.4 Conductivity Study

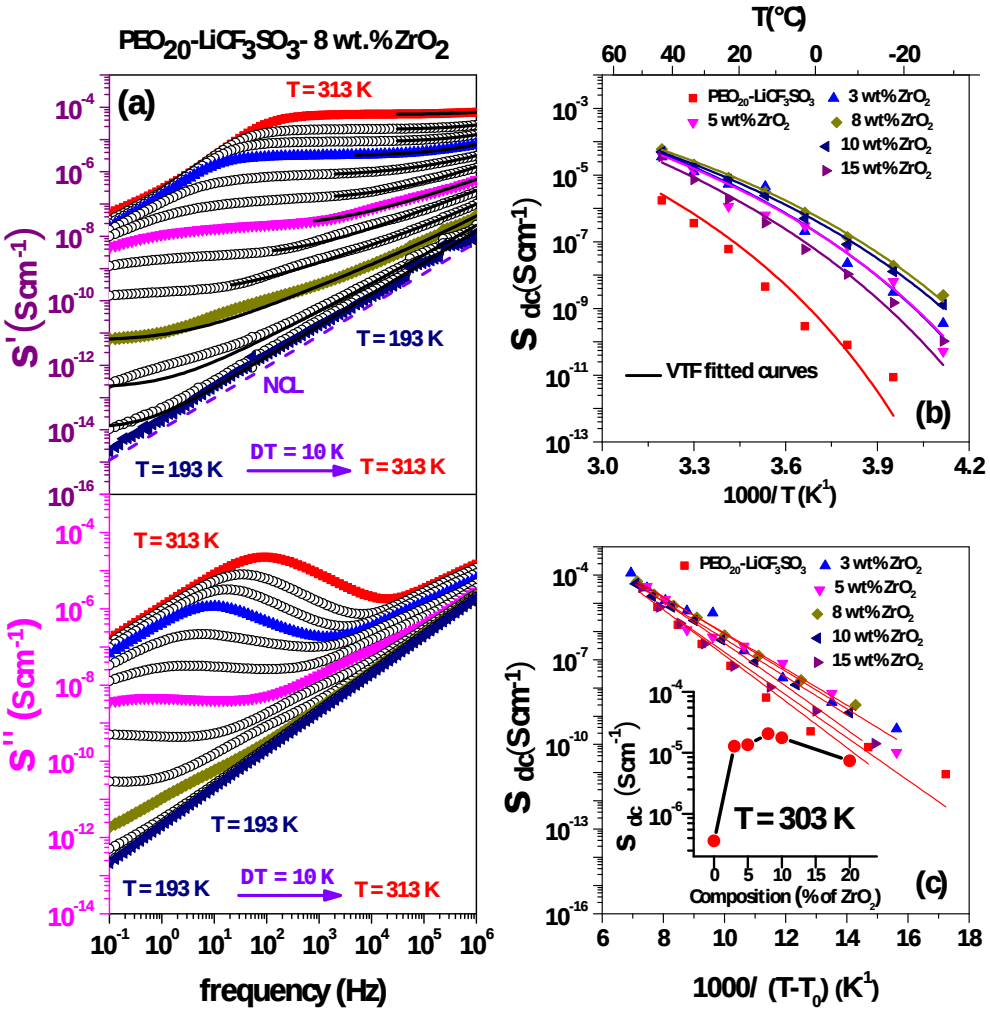

Figure 4.4: (a) Variation of real and imaginary part of ac conductivity as a function of frequency at different temperatures for PEO_{20}-$LiCF_3SO_3$- 8 wt.% ZrO_2 (representative). Solid lines representing Jonscher's power law (JPL) or double power law (DPL) fitted results. (b) Variation of dc conductivity (σ_{dc}) as a function of inverse of temperature in absolute scale for PEO_{20}-$LiCF_3SO_3$- x wt.% ZrO_2 (x = 0, 3, 5, 8, 10 & 20). Solid lines representing VTF fitted results. (c) Variation of dc conductivity as a function of inverse of reduced temperature for PEO_{20}-$LiCF_3SO_3$- x wt.% ZrO_2 (x = 0, 3, 5, 8, 10 & 20). Solid lines representing fitted results in reduced scale with inset showing the variation of dc conductivity as a function of nano-filler concentration at room temperature (303 K).

The variation of real and imaginary part of ac conductivity as a function of frequency at temperatures ranging from 313 K to 193 K with an interval of 10 K for PEO_{20}-$LiCF_3SO_3$- 8 wt.% ZrO_2 PNCE is shown in figure (4.4a). Similar observations are observed for all other compositions of PNCEs in the series under investigation. It is seen that the ac conductivity increases with increase in frequency for all temperatures. The frequency dependent real part of ac conductivity (σ'), show three distinct regions firstly low-frequency dispersion, then a frequency independent plateau, again followed by a high-frequency dispersion region.

The low frequency dispersion is attributed to fast ion migration *i.e.* electrode polarization (EP). This region can only be observed at a relatively higher temperature and disappears with the decrease in temperature. Frequency independent plateau region appears at a slightly higher frequency range than that of low-frequency dispersion region. This region is attributed to long-range ionic motion *i.e.* dc conductivity (σ_{dc}). Finally, the high-frequency dispersion region is attributed to the short range (hopping) ionic motion. With the decrease in temperature the plateau region shifts towards the lower frequency and ac conductivity spectra shows dispersive behaviour throughout the entire frequency range of investigation. The switch-over frequency from frequency independent plateau to high frequency dependent dispersive region is known as hopping crossover frequency. Hopping crossover frequency marks the onset of conductivity relaxation in PNCEs and it shifts towards lower value with decreasing temperature. Careful observation reveals a hump in the intermediate frequencies in the real part of ac conductivity spectra which is shifting to lower frequencies with decreasing temperature. The inherent inhomogeneous nature of the samples is proposed to be the cause of this kind of behaviour.[205] In the frequency dependent imaginary part of the ac conductivity (σ'') (figure (4.4a)), relaxation peaks can be observed in the low frequency region of σ'' spectra. The relaxations observed in the low-frequency region of the conductivity spectra are nothing but EP, which can also be observed in σ' spectra as a dispersive region. It occurs due to the accumulation of free ions in the vicinity of electrodes.[206] The onset of these relaxation peaks signifies the onset frequency of EP. With decreasing temperature, EP peak is shifting towards even lower frequency region and below 233 K we do not observe any relaxation peak due to EP.

To quantitatively describe the ion conduction process emphasis is given on frequency independent plateau and high-frequency dispersion regions. At relatively low frequency and/or high temperature, σ' can be represented using power law given by the following equation[175, 190]

$$\sigma' = \sigma_{dc}[1 + (f/f_c)^n] \tag{4.1}$$

The experimental data has been fitted with equation (4.1) excluding the regions of EP , for the temperature range 313 K to 233 K and a reasonably good fit has been observed. This behaviour is known as first universality or universal dielectric response (UDR). Microscopic jump relaxation model has been used to describe the behaviour of σ' spectra for various PNCEs.[199] According to this model at very low frequencies (without EP) an ion jumps from one site to its neighbouring favourable vacant site, contributing towards the dc conductivity. At higher frequencies due to the short time period available the correlated forward-backward hopping of mobile ions give rise to ac conductivity. The presence of the above-mentioned phenomena *i.e.* ion jumps and correlated forward-backward hopping, in σ' spectra is explained by UDR. On the other hand, at sufficiently low temperatures the behaviour of $\sigma'(f)$ becomes linear or nearly linear (becoming parallel to the dotted guideline shown in figure (4.4a)). It also implies negligible frequency dependence of the

imaginary part of dielectric permittivity. The mathematical background of nearly constant loss is described in chapter (3) section (3.4.2). In order to accommodate the observed linear frequency dependent contribution in the low-temperature region *i.e.* below 233 K, the σ'spectra is fitted by using double power law given by the following equation[175]

$$\sigma' = \sigma_{dc}[1 + (f/f_c)^n] + Bf \tag{4.2}$$

Below 233 K the $\sigma'(f)$ spectra is fitted with equation (4.2) and a reasonably good fit is observed. The origin of NCL is not properly understood and remain controversial with two possible explanation. First school of idea is that NCL arise from the motion of group of atoms in an asymmetric double well potential proposed by Jain *et al.*,[207] whereas the second school of idea is that NCL arise from slowing down of ionic motion in the cage like structure due to ion-ion interactions and correlation in a very short response time regime proposed by Ngai *et al.*[208, 209] Jonscher's power law or first universality (equation (4.1)) and UDR based double power law or second universality (equation (4.2)) together can successfully explain the frequency dependence of ac conductivity spectra in structurally disordered materials such as ionically conducting glass, conducting polymers etc. over a wide range of frequency and temperature. The σ_{dc} values are obtained from the σ' spectra using the above discussed fitting formalism. Figure (4.4b) show the variation of σ_{dc} as a function of inverse of temperature in absolute scale for different PNCE compositions. This temperature dependent dc conductivity for all compositions of PNCEs was analyzed using Vogel-Tammann-Fulcher (VTF) equation given below[210]

$$\sigma_{dc} = \sigma_0 \exp\left[-\frac{E_A}{k_B(T - T_0)}\right] \tag{4.3}$$

The solid lines in figure (4.4b) show the non-linear least square fitting of the conductivity data to equation (4.3), assuming the equilibrium glass transition temperature T_0 value on the basis of the boundary condition 60 K$\leq T_g - T_0 \leq$ 50 K as found in literatures.[211] The good fit of σ_{dc} to VTF equation over a wide temperature range signifies the close coupling among the ionic conductivity and the polymer chain mobility of the PNCEs. Equation (4.3) suggests linear temperature dependence of conductivity when a characteristic value T_0 is subtracted from temperature. So we have plotted the variation of conductivity on a logarithmic scale against the inverse of reduced temperature, *i.e.* $1000/(T - T_0)$ as shown in figure (4.4c). It reveals that temperature dependent conductivity value tends to superpose with each other for all the PNCEs under investigation. This suggests that the thermal energy in excess to this characteristic temperature T_0, (as opposed to the absolute thermal energy at any temperature in the Arrhenius case) provides actual mobility to the ions responsible for the observed macroscopic conductivity.[195] This also qualitatively supports the possibility of a close correlation between the ionic conductivity and segmental relaxation process in PNCEs. As far as the σ_{dc} is concerned, inset of figure (4.4c) show that, with

increasing ZrO_2 concentration, σ_{dc} increases and reached a maximum for 8 wt.% ZrO_2 composition. Thereafter σ_{dc} decreases with further addition of ZrO_2 nano-filler. At ambient temperature(T = 303 K) σ_{dc} of 8 wt.% ZrO_2 PNCE is found 2.04×10^{-5} Scm^{-1} which is higher by two order of magnitude when compared to σ_{dc} of PSC at same temperature *i.e.* 3.57×10^{-7} Scm^{-1}. Therefore with the addition of optimized amount of nano-filler the magnitude of σ_{dc} can be increased.

4.3.5 Dielectric Relaxation Study

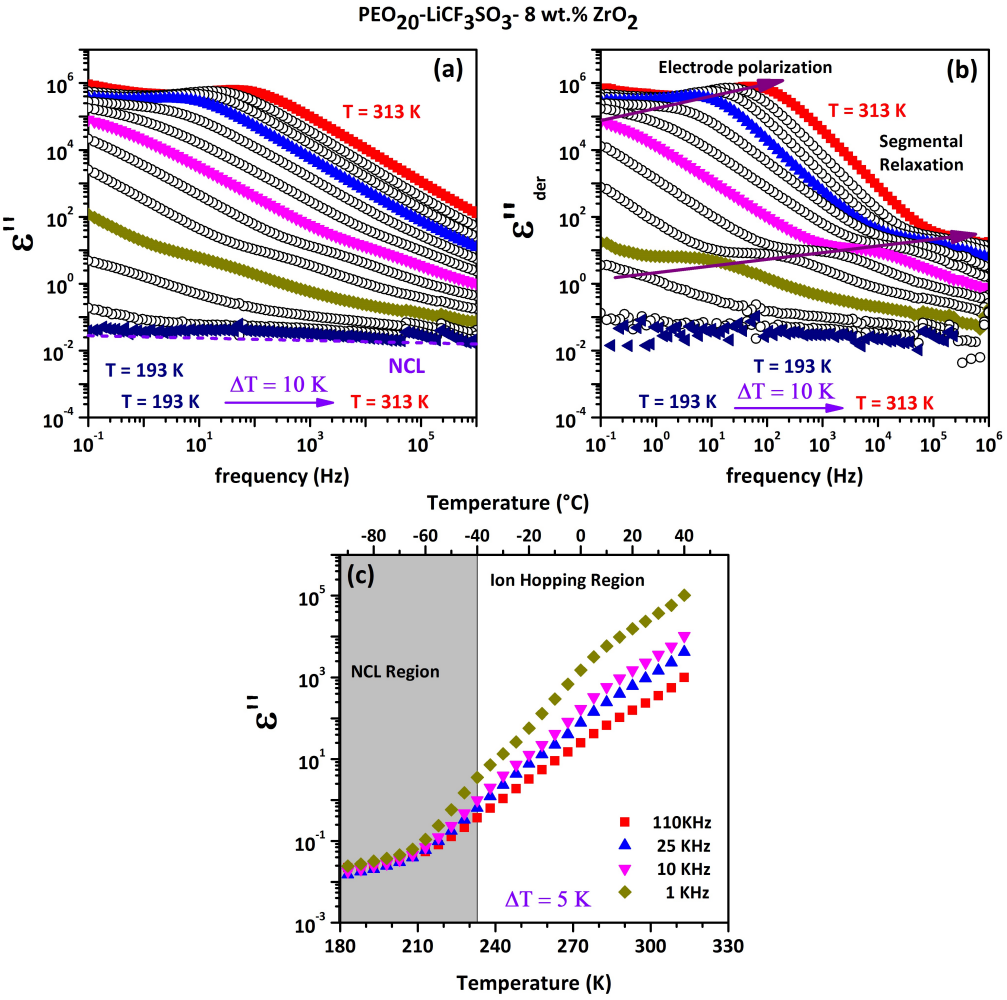

Figure 4.5: Variation of (a) imaginary part of relative permittivity or dielectric loss, (b) derived relative permittivity or dc conduction free dielectric loss as a function of frequency at different temperatures and (c) dielectric loss as function of temperature in absolute scale for PEO_{20}-$LiCF_3SO_3$-8 wt.% ZrO_2.

To investigate the different electrical relaxation phenomena, imaginary part of the relative permittivity or dielectric loss (ϵ'') is plotted as a function of frequency, shown in figure (4.5a) for the PNCE composition, PEO_{20}-$LiCF_3SO_3$-8 wt.% ZrO_2. Similar behaviour has also been observed for PSC and other PNCE compositions. Dielectric loss spectra

decrease monotonically with the increase in frequency throughout the frequency range of investigations. In general, at low frequency and high temperature, relaxation is occurring due to an accumulation of charge in the vicinity of electrodes *i.e.*, EP in polymer electrolytes. This phenomenon of EP is already described in the conductivity study section. The presence of high ionic conductivity masks the different relaxation effects, as a result, segmental relaxation processes are not clearly visible in this plot. To successfully resolve segmental relaxation phenomena and for accurate measurement of segmental relaxation time (τ_s), derived relative permittivity (ϵ''_{der}) formalism has been adopted.[199] This method is used to successfully de-convolute ionic conduction and segmental relaxation phenomena. ϵ''_{der} can be obtained by taking derivative of the real part of permittivity (ϵ') as stated below[212, 213]

$$\epsilon''_{der} = -\pi/2 \times \partial\epsilon'/\partial(ln\omega) \approx \epsilon'' \tag{4.4}$$

ϵ''_{der} represents dc conduction-free dielectric loss and allow the measurement of segmental relaxation process precisely. Two different relaxation processes are distinctly visible in ϵ''_{der} vs frequency plot, shown in figure (4.5b). The low-frequency relaxation process is due to the EP, whereas the high-frequency relaxation is attributed to the segmental relaxation of polymer chains in PNCEs. Figure (4.5a) also reveal that at low-temperature dielectric loss assume nearly constant values over a wide range of frequency. This phenomenon is indicating the presence of NCL behaviour, which is discussed earlier in conductivity spectra analysis. To draw a precise conclusion on NCL and ion hopping boundary, the variation of ϵ'' as a function of temperature is shown in figure (4.5c). It is observed that with increasing temperature, ϵ'' increases monotonically for all frequencies. At low temperatures, in the present study below 233 K, for a change in two decades of frequency (*i.e.* 1 kHz to 110 kHz) ϵ'' changes by less than one order of magnitude. Starting from this temperature (233 K) ϵ'' increases rapidly and ϵ'' as a function of frequency start to disperse. As ϵ'' assumes nearly constant value below 233 K for a wide range of frequency, it can be considered that below this temperature NCL phenomenon prevails.[214] For PSC it is observed that NCL prevail below 248 K. The crossover temperature from UDR to NCL region in all PNCEs are found lower than that of PSC. Decrease in crossover temperature with the addition of ZrO_2 filler suggest a reorientation of the local environment of host polymer, helping the caged Li^+ ion to overcome the potential barrier and contribute to ion conduction with successful ion hopping, which will be discussed later.[107] NCL phenomena will be further discussed using Kramer-Krönig formalism. In order to understand the relaxation phenomena in detail, modulus formalism is also investigated and discussed hereafter.

4.3.6 Electrical Modulus Formalism for Relaxation Study

In the case of ionic conductors, at low-frequency region, EP is reflected by a significant increase in the dielectric loss *i.e.* $\epsilon''(f)$ spectrum. Conductivity relaxation is entirely masked

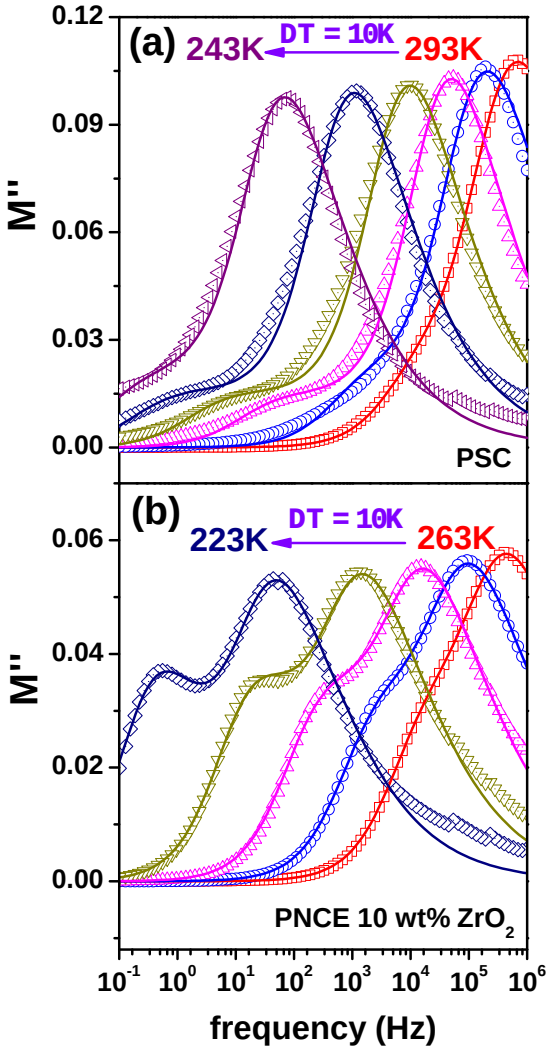

Figure 4.6: (a) Variation of imaginary part of electrical modulus as a function of frequency at different temperatures for PEO_{20}-$LiCF_3SO_3$ *i.e.* PSC (b) Variation of imaginary part of electrical modulus as a function of frequency at different temperatures for PEO_{20}-$LiCF_3SO_3$-10 wt.% ZrO_2. Solid lines representing KWW fitted results.

by electrode polarization in this frequency range as shown in figure (4.5a), but using modulus formalism the effects due to EP can be masked. The relationship between the electric modulus and relative permittivity is given by $M^*(f) = 1/\epsilon^*(f)$. Modulus formalism also helps to understand and interpret the ion dynamics and conductivity relaxation of ionic conductors with the probable decoupling between the conductivity and segmental relaxation processes. $M^*(f)$ can be obtained via Fourier transform of time-dependent correlation function of ion motion $\phi(t)$.

$$M^*(f) = M'(f) - M''(f) = M_\infty \left[1 - \int_0^\infty dt\ exp(-i2\pi ft)(-d\phi/dt)\right] \tag{4.5}$$

where, M_∞ is the reciprocal of high frequency dielectric constant and $\phi(t)$ is the relaxation function represented by $\phi_{KWW} = exp\left[-(t/\tau)^\beta\right]$. Kohlrausch-Williams-Watts (KWW) function is a convenient choice for fitting the data as the parameters $\phi(t)$ and β can be suitably adjusted. For a single exponential, Debye type relaxation β assumes the value 1 and decreases with the increasing stretching of the relaxation function *i.e.*, with increasing deviation from Debye type relaxation.[107] The fitting of each $M''(t)$ spectra is performed using the procedure described by Moyninhan *et. al.* According to the fitting algorithm the imaginary part of electrical modulus can be written as,

$$M''(f) = \sum_n \frac{M''_{max,n}}{(1-\beta_n) + \beta_n/(1+\beta_n)[\beta_n(f_{max,n}/f) + (f/f_{max,n})^{\beta_n}]} \tag{4.6}$$

Subscript $'n'$ is used to clarify that the $M''(f)$ spectra are having more than one relaxation process. In figure (4.6a) and (4.6b), the variation of imaginary part of electrical modulus as a function of frequency at different temperatures is shown for PSC (PEO_{20}-$LiCF_3SO_3$) and PNCE (PEO_{20}-$LiCF_3SO_3$-10 wt.% ZrO_2) respectively. With decreasing temperature peak of $M''(f)$ spectra is shifting towards the low-frequency side. $M''(f)$ spectra has been fitted with equation (4.6) and presence of two different relaxation phenomena is established. Among these two relaxation peaks (obtained from deconvolution process), one is a weak (low amplitude) low-frequency peak and the other one is strong (high amplitude) high-frequency peak. Low amplitude peak is attributed to conductivity relaxation whereas the strong peak is attributed to polymer segmental relaxation.[215] On comparing two sets of M'' spectra for PSC and 10 wt.% PNCE a marked difference can be observed around the low amplitude conductivity relaxation peak in the modulus spectra at a low-frequency region. In the case of PNCEs, the conductivity relaxation peak becomes prominent. This deviation in M'' profile of PSC and PNCE suggest that with the addition of filler local environment of the cation coordinating polymer gets modified resulting in the decoupling of conductivity and segmental relaxation processes.[107] The stretching parameter, β for conductivity relaxation peak is found around 0.45 whereas for segmental relaxation peak it is found around 0.55, which is reflecting the non-Debye type behaviour of these relaxations. Conductivity relaxation time (τ_c) can be obtained from fitted plots.[216] From deconvoluted spectrum, it is also found that with decreasing temperature conductivity relaxation peak shifts towards the low-frequency region. This indicates the conduction process in the ionic conductor is thermally activated phenomena. The long tail in the low-frequency region is due to large capacitance associated with EP. At low frequency $M''(f)$ spectra is approaching zero, suggesting a very high value of ϵ'' due to EP. The relation between the two different relaxation processes obtained from de-convoluted $M''(f)$ spectrum will be discussed later in section (4.3.9).

4.3.7 Relaxation Time and Impact of Vogel Temperature (T_0)

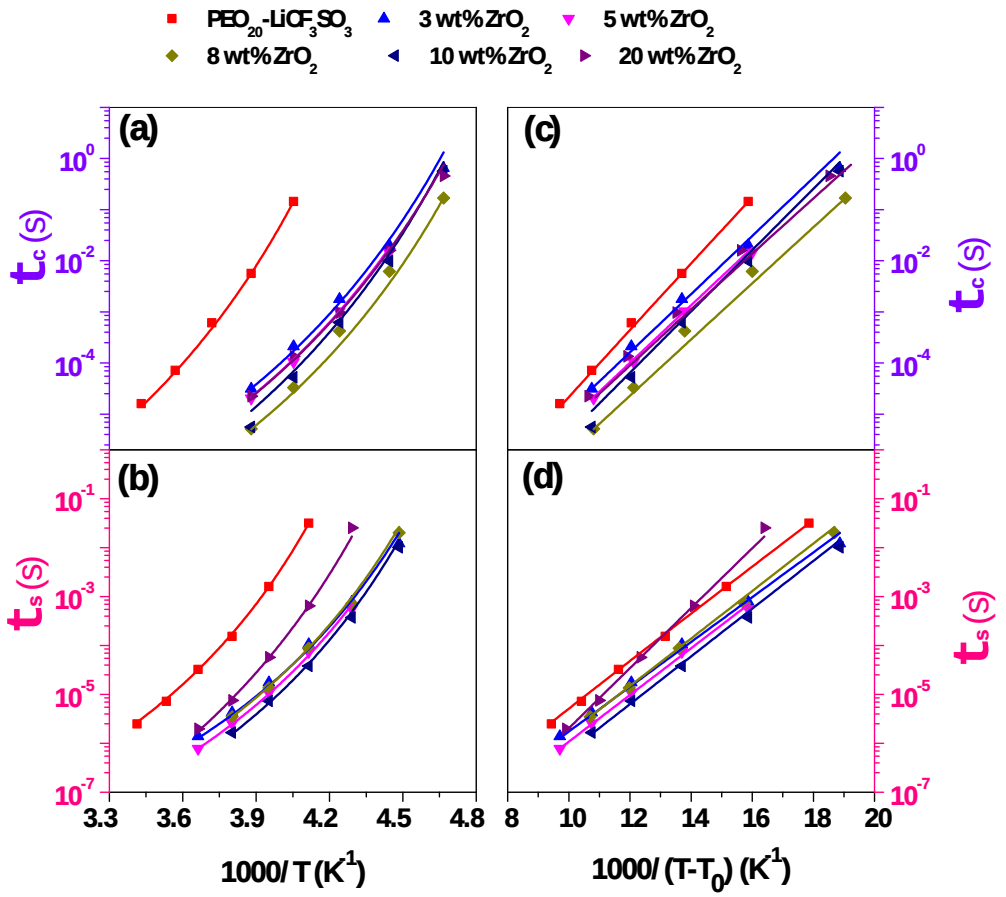

Figure 4.7: (a) Conductivity relaxation time and (b) segmental relaxation time as a function of inverse of temperature in absolute scale. (c) Conductivity relaxation time and (d) segmental relaxation time as a function of inverse of reduced temperature in absolute scale.

Conductivity relaxation time (τ_c) and segmental relaxation time (τ_s), obtained from electrical modulus analysis and dc conduction free dielectric loss formalism,[212] are analysed further to get more idea about the conduction process in PNCEs. Conductivity relaxation time and segmental relaxation time are plotted as a function of inverse of temperature as shown in figure (4.7a) and (4.7b) respectively. It is clear from the plot that with increase in temperature both, τ_c and τ_s decreases and these two relaxation time follow VFT behaviour given by the following equation[199, 211]

$$\tau = \tau_0 \, exp\left\{\frac{E_v}{k_B(T - T_0))}\right\} \tag{4.7}$$

where, τ is the relaxation time, τ_0 is the pre-exponential factor, k_B is the Boltzmann's constant, T is temperature in absolute scale, T_0 is the Vogel temperature and E_v is the pseudo activation energy. The temperature dependent τ_c and τ_s are fitted using the above mentioned

VTF equation and the best fitted parameters *i.e.* values of pseudo-activation energy (E_v) and Vogel temperature (T_0) are presented in table (4.1). A good agreement between the experimental data and fitted curve can be observed in figure (4.7a) and (4.7b). Conductivity relaxation time and segmental relaxation time are further represented as a function of reduced temperature *i.e.* $(T - T_0)$ in figure (4.7c) and (4.7c). In inverse of reduced temperature scale, variation of τ_c and τ_s appear like a straight lines. It also suggested that conductivity and segmental relaxation process follow VTF behaviour.[212] Moreover τ_c and τ_s in inverse of reduced temperature tends to overlap with each other for different composition of PNCEs. This finding states that, T_0 plays an important role in ion conduction process. Thermal energy in excess to T_0 is mainly responsible for the mobility of ions in these PNCEs causing macroscopic conductivity. To find the probable correlation between the conductivity and segmental relaxation processes, these two relaxation processes will be further explored in section (4.3.9).

Table 4.1: VTF fitted parameters obtained from temperature dependent conductivity, conductivity relaxation time and structural relaxation time plots of PSC and PNCE compositions. Maximum error limit obtained are stated in parenthesis for each set of parameters.

Composition (x wt.% ZrO_2)	σ VTF Fit		τ_c VTF Fit		τ_s VTF Fit	
	E_A(eV) ($\pm$0.002)	T_0(K) ($\pm$1)	E_A(eV) ($\pm$0.002)	T_0(K) ($\pm$1)	E_A(eV) ($\pm$0.002)	T_0(K) ($\pm$1)
x = 0	0.151	195	0.136	189	0.101	187
x = 3	0.135	179	0.112	170	0.091	170
x = 5	0.133	178	0.113	170.5	0.094	170
x = 8	0.128	173	0.110	169.5	0.094	169.5
x = 10	0.134	173	0.113	170.5	0.096	170
x = 20	0.161	175	0.114	170	0.125	172

4.3.8 Kramer - Krönig Relation and Nearly Constant Loss

From frequency dependent ac conductivity, shown in figure (4.4a), the presence of NCL can be observed at sufficiently low temperatures in PSC and PNCEs. In the NCL region, σ' spectra become parallel to the dotted guide line, showing linear behaviour between σ' and f in logarithmic plot. In order to explore the role of UDR and NCL in the ion conduction process Kramer - Krönig formalism has been used.[190] Kramer - Krönig representation gives a better understanding of the variation of power law exponent in UDR and NCL region.

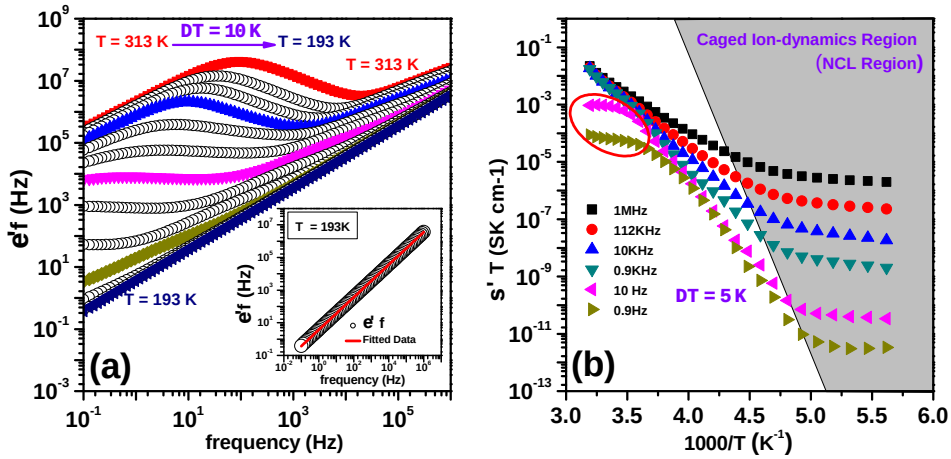

Figure 4.8: (a) Variation of $\epsilon' f$ as a function of frequency at different temperatures for PEO_{20}-$LiCF_3SO_3$- 8 wt.% ZrO_2 PNCE composition(representative). Inset showing the Kramer-Krönig fit at 193K. (b) Variation of $\sigma' T$ as a function of inverse of temperature in absolute scale.

Real part of permittivity (ϵ') is proportional to f^{m-1}, which can be written as,

$$\epsilon' f = B f^m \tag{4.8}$$

Therefore for a given temperature, a straight line with a slope of m should be obtained in a logarithmic plot of $\epsilon' f$ and f.[190]

In figure (4.8a) $\epsilon' f$ has been plotted as a function of frequency in logarithmic scale at different temperature. At sufficiently low temperatures, nature of the spectra become linear throughout the frequency range of investigation. The value of exponent $'m'$ is found 0.9975 at T = 193 K, which is close to unity. It suggests the clear dominance of NCL over UDR at sufficiently low temperatures. With increasing temperature this linear nature of spectra can only be seen at high frequency regions and the value of $'m'$ also tends to decrease. At T = 223 K, $'m'$ become 0.9865. This is attributed to the increasing contribution of UDR over NCL at relatively higher temperature and above T = 223 K UDR is mainly governing the ion conduction processes. Therefore it can be concluded that UDR and NCL in combination describes the dynamics of ion conduction process and segmental motions in PNCEs for the entire range of temperatures. We have already stated that UDR is attributed to hopping motion of charge carriers. However to find out the origin of NCL further investigation is required. Keeping this in mind a plot of $\sigma' T$ as a function of inverse of temperature has been shown in figure (4.8b). It can be observed that for a particular frequency below a critical temperature, $\sigma' T$ assumes nearly constant value. This critical temperature differentiate the dominance of UDR or NCL behaviour in ion conduction process. The activation energy obtained in the NCL region, $E_{NCL} = (0.045 \pm 0.015)$ eV (within the experimental window) which is much lower than that of the activation energy obtained from dc conductivity spectra

($E_{dc} = 0.128$ eV) for the same PNCE composition *i.e.* PEO_{20}-$LiCF_3SO_3$ - 8 wt. % ZrO_2. This result is expected for NCL phenomena, as it arises due to caged ion with small probability to hop towards the neighbouring sites and leave the cage at sufficiently low temperatures and/or high frequencies. The low value of activation energy for NCL region (E_{NCL}) correspond to the actual energy barrier that mobile lithium ions have to overcome to leave their cages and move to a favourable vacant site. The activation energy obtained from dc conduction E_{dc} is found comparatively higher than E_{NCL}. This finding reflects that mobile ions for long range diffusion process has to overcome caged ion dynamics effect (E_{NCL}) along with other interactions such as ion-ion interaction, ion-polymer interaction, ion filler interaction, the unsuccessful ion hops etc. Therefore caged ion dynamics formalism proposed by Ngai et. al. can be used successfully to explain this kind of behaviour in $\sigma' T$ isofrequency spectra. According to this concept at low temperatures, NCL is arising due to slowing down of ionic motion in the cage like potential landscape of small activation energy. The collective interactions mentioned above can be the reason for getting comparatively higher values of dc activation energy.[95, 217] In figure (4.8b) at very low frequency and relatively high temperatures a deviation from linear dispersion in conduction region can be observed. These deviations are arising due to electrode electrolyte interfacial issue, which can not be avoided in the present study.[186]

4.3.9 Scaling of Conductivity and Electric Modulus

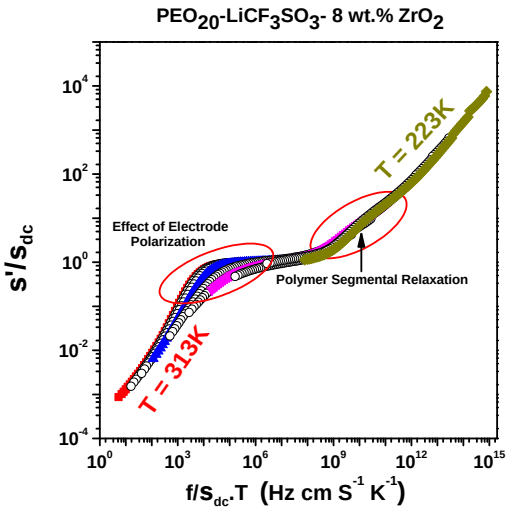

Figure 4.9: Conductivity scaling using Summerfield approach for PEO_{20}-$LiCF_3SO_3$- 8 wt.% ZrO_2 PNCE composition (representative).

Scaling studies of experimentally measured quantities are in general important. It gives better insight to the common underlying reasons for a particular physical property.[140, 191] In figure (4.4a) we observed strong frequency dependence of σ' spectra. With increasing temperature, onset of conductivity dispersion shifts towards higher frequency values. In

such cases changing both the conductivity and frequency values, the conductivity spectra can be scaled to obtain a superimposed master curve for all isotherms. This scaling procedure is also known as time temperature superposition principle and its purpose is to probe whether conduction mechanism is temperature dependent or not. Figure (4.9) shows the scaling of conductivity data using Summerfield approach. The detail scaling formalism is described in chapter (3) in section (3.5.1). It can be observed that scaled conductivity curves tend to superimpose onto each other, giving hints of temperature independent nature of ion conduction mechanism. Low frequency conductivity values show deviations from the expected low frequency plateau of the master curve(marked in figure (4.9)). This phenomena is attributed to the EP effects usually observed for ion conducting materials.[218] Another marked anomaly can be observed in comparatively the high frequency region. The frequency corresponding to this anomaly for each scaled conductivity isotherms (marked by an arrow in figure (4.9)) are very close to the segmental relaxation time. Therefore following Summerfield scaling formalism it is also not appropriate to conclude that the relaxation phenomena in PNCEs are temperature dependent or independent dynamic possess. Failure of Summerfield scaling approach confirms that polymer (used as host in the PNCEs) segmental dynamics and ion association both are independent processes and having crucial role on ion conduction mechanism.[218] To get a more comprehensive picture about the role of temperature on ion conduction process in PNCEs, scaling of M'' spectra need to be explored.

In section (4.3.6) the presence of two relaxation phenomena is already described, one correspond to conductivity relaxation and the other to segmental relaxation process. In figure (4.10a) the imaginary part of electrical modulus is plotted as a function of frequency for different temperatures. Form this, it is quite evident that M'' spectra consists of two relaxation process but they can not be superimposed or scaled together and the formation of a master curve is not possible. Figure (4.10b) is depicting the deconvolution of segmental relaxation and conductivity relaxation of PEO_{20}-$LiCF_3SO_3$- 8 wt. % ZrO_2 PNCE at $T = 243$ K. De-convoluted M'' spectrum are obtained as per the process discussed using equation (4.6) in section (4.3.6). In figure (4.10c) the de-convoluted conductivity relaxation peaks of modulus spectra are superimposed over each other forming a master curve. Scaling of conductivity relaxation modulus peak (M''_c) confirm that conductivity relaxation in PNCEs under investigation are temperature independent, whereas polymer segmental relaxation phenomena is temperature dependent process within the experimental window.[215] It can also be observed that with decrease in temperature the position of segmental relaxation peak is shifting towards higher frequency values. This indicates the presence of decoupling between the conductivity and segmental relaxation processes and the decoupling strength is increasing with decreasing temperature.[215] It also concludes that in PNCEs at relatively high temperatures ion conduction process is favoured by segmental relaxation of polymer host. In brief we can infer decoupling between conductivity and segmental relaxation process and temperature dependent segmental relaxation phenomena is favouring the microscopic

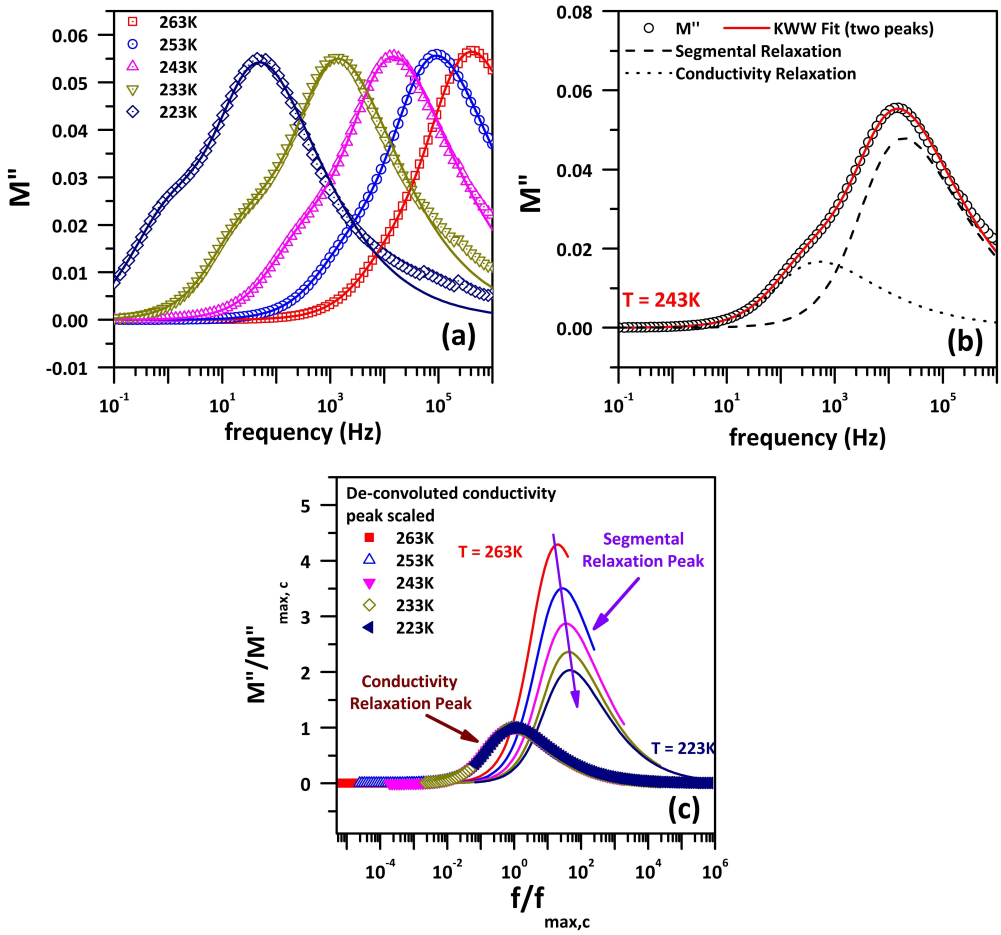

Figure 4.10: (a) Variation of imaginary part of electrical modulus as a function of frequency at different temperatures for PEO_{20}-$LiCF_3SO_3$-8 wt.% ZrO_2 PNCE composition. Solid lines representing Kohlrausch-Williams-Watts (KWW) fitted results. (b) Deconvolution of segmental and conductivity relaxation peak at T = 243 K for PEO_{20}-$LiCF_3SO_3$-8 wt.% ZrO_2. (c) Scaled conductivity relaxation process for PEO_{20}-$LiCF_3SO_3$-8 wt.% ZrO_2 at different temperatures.

conduction process in PNCEs under investigation.

4.4 Conclusions

A series of polymer nano-composites electrolytes are synthesised using conventional solution casting method. Polymer salt complexation and composite formation upon adding nano-crystalline ZrO_2 to PSC is confirmed using XRD analysis. Surface morphology is studied using FE-SEM. Vibrational characterization is carried out in mid IR region. Temperature dependent electrical measurements are carried out using broadband dielectric spectroscopy. The important observation of this study are as follows:

- Temperature dependent dc conductivity, conductivity relaxation time as well as

segmental relaxation time following VTF behaviour suggesting strong correlation between ion conduction process and polymer segmental relaxation process.

- At 303 K the maximum value of dc conductivity (σ_{dc})is found to be 2.04×10^{-5} Scm^{-1} for PEO_{20}-$LiCF_3SO_3$-8 wt.% ZrO_2 composition.
- Observations of first universality (UDR) and second universality (NCL) are explained with the help of $\sigma'(f)$ and $\epsilon''(f)$ spectra and the boundary between NCL and UDR is drawn using temperature dependent dielectric loss (ϵ'') spectra. Kramer - Krönig approach is used to explain the origin of NCL. The origin of NCL is due to caged ion dynamics feature *i.e.* at sufficiently high frequency and/or low temperature most of the ions do not posses enough thermal energy to overcome the caged potential landscape barrier and remain trapped.
- Summerfield scaling approach is used to explore the effect of temperature on ion conduction mechanism.
- It is found that the segmental relaxation is temperature dependent phenomena, but conductivity relaxation *i.e.*, ionic conduction process is independent of temperature.
- Decoupling between conductivity and segmental relaxation process is observed. Segmental relaxation phenomena is one of the causes for increased dc conductivity value in PNCEs.

Chapter 5

Relaxation Dynamics and Coupled Ionic Transport Mechanism in PEO_{20}-$LiCF_3SO_3$-TiO_2 Based Ion Conducting Polymer Nano-Composite Electrolytes

5.1 Introduction

In chapter (4) a detailed discussion on ion conduction mechanism in PNCEs films are carried out where nano-crystalline ZrO_2 is used as filler. In the present chapter electrical properties of titania-based PNCEs are investigated. Titania also acts as a passive filler but it can weakly attract the free cations.[219, 220] This series of PNCE will give us idea about how the overall acidic or basic filler can affect the ionic conductivity values. When electrical properties are investigated as a function of frequency and temperature, titania-based PNCEs also show the distinct signature of universal dielectric response and nearly constant loss feature.[221] With careful analysis of electrical modulus spectra, it can be observed that the segmental relaxations are non-Debye in nature. From relaxation mapping, it can be inferred that ion dynamics are coupled to polymer segmental relaxation which is also studied with Ratner's classical coupling formalism.[196]

In the present work, polymer nanocomposite electrolytes are prepared using polyethylene oxide as polymer host, lithium triflate as salt and nano-crystalline anatase polymorph of titania, having a tetragonal crystal structure, as ceramic filler. PNCEs films are synthesized using solution casting technique having compositions PEO_{20}-$LiCF_3SO_3$ - x wt.% TiO_2, with $x = 0, 2, 3, 5, 8, 10$ & 15. Phase purity of used titania filler is first checked by X-ray diffraction technique, before using it as the filler for the composite electrolyte. Structural, vibrational, surface morphological and temperature dependent electrical properties are investigated using X-ray diffraction, FTIR, FE-SEM and broadband dielectric spectroscopic technique respectively. In this chapter, the emphasis is given on the ion conduction mechanism of PNCEs using different formalisms. With the help of MIGRATION concept

temperature dependent dc conductivity behaviour is explained.

5.2 Experimental Procedure

Polyethylene oxide of $M_w = 6 \times 10^5$, lithium trifluoromethanesulfonate, tetragonal phased anatase titanium dioxide (TiO_2, used as filler) and analytical grade acetonitrile (used as common solvent) are used for preparation of PSC and a series of PNCE having compositions PEO_{20}-$LiFC_3SO_3$-$x$wt.% TiO_2 (x= 2, 3, 5, 8, 10 &15). PNCE samples are prepared using conventional solution casting technique. X-ray diffraction (XRD) is carried out using Rigaku Ultima IV X-Ray diffractometer operating at 40 kV and 40 mA; producing Cu $K_{\alpha 1}$ radiation having wavelength 1.5405 Å. The XRD patterns are recorded with a scanning rate of 3° per minute and a scanning step of 0.002°. Nova Nano SEM 450 is used to record FE-SEM micrographs. Bruker Alpha-E spectroscope is used to collect FTIR data from 4000 cm^{-1} to 550 cm^{-1} wavenumber range with 2 cm^{-1} wavenumber resolution. Dielectric measurements are carried out using Novo-Control GMBH Alpha analyzer over a wide range of frequency, 10^{-1} to 10^6 Hz with potential of 10 mV. Novo-Control Quattro Cryo-system is used to control the temperature of the samples under investigation in a liquid nitrogen gas based sample holding assembly.

5.3 Results and Discussion

5.3.1 Structural Study

Polymer salt complexation, composite formation and crystalline-amorphous nature of the prepared samples are studied using XRD technique. The observed XRD patterns of PEO, PSC and PNCE compositions are presented in figure (5.1). Inset of figure (5.1) shows the XRD pattern of tetragonal phased anatase TiO_2 (JCPDF NO: 21-1272) synthesized using polymer template technique. Co-existence of an amorphous hump from 15° to 28° along with several characteristic crystalline peaks can be observed in the XRD patterns of the samples (a set of dotted lines are used as a guide to the eye to show amorphous hump). Therefore it can be concluded that the samples are semi-crystalline in nature. XRD pattern of PEO film show characteristic crystalline peaks at 2θ = 19.2°, 23.4°, 26.3° and 27°, corresponding to the (120), (112)/(032), (21$\bar{1}$) and (040) reflections respectively.[222] The characteristic crystalline reflections of PEO mentioned here can be observed in PSC as well as in all compositions of PNCEs. The nature of these reflections does not undergo any significant change with the addition of $LiFC_3SO_3$ or anatase TiO_2 into host polymer of PEO. It indicates that structure of host polymer remains unaffected during polymer-salt complex formation or composite electrolyte formation.[174] On comparison of XRD pattern of PEO, PSC and PNCEs, it can be observed that no additional reflection arises due to $LiFC_3SO_3$ (JCPDF NO: 81-0813) in PSC and PNCEs. This indicates a proper dissolution of $LiFC_3SO_3$ into

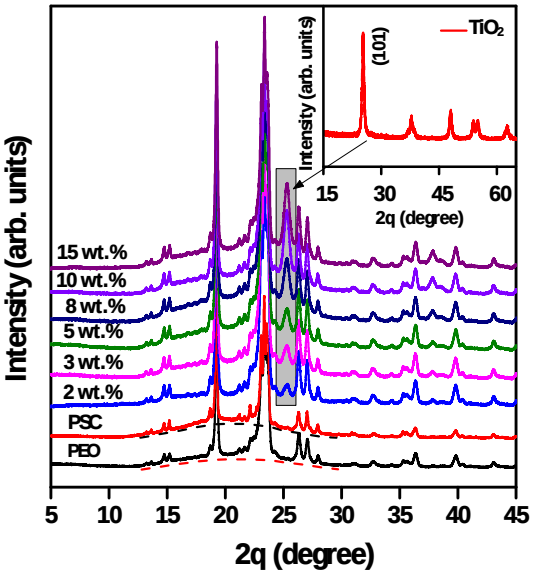

Figure 5.1: X-Ray diffraction pattern of polyethylene oxide, polymer salt complex and different PNCE films having following compositions PEO_{20}-$LiCF_3SO_3$- x wt.% TiO_2 (x = 2, 3, 5, 8, 10 & 15). Inset showing the anatase polymorph of TiO_2 used as filler. A dotted set of lines are used as a guide to eye to show amorphous hump present in each samples under investigation.

host polymer PEO.[199, 223] Characteristic reflection of TiO_2 can be observed in the XRD patterns of PNCEs with its most prominent peak (101) at $2\theta = 25°$ and its intensity tend to increase with an increase in the concentration of TiO_2. Since the characteristic signature of both PEO and TiO_2 are found in the XRD patterns of PNCEs, it can be safely concluded that the prepared PNCE samples are composite in nature.

5.3.2 Surface Morphology

Figure (5.2) shows SEM micrographs of the polymer salt complex and different PNCEs having compositions PEO_{20}-$LiCF_3SO_3$- x wt.% TiO_2 ($x = 3, 5, 8, 10\&15$). The scanning electron micrographs of the polymer-salt complex are shown in figure (5.2a). The presence of distinct spherulites and characteristics lamellar microstructure can be observed in PSC as well as different PNCEs. The average size of the spherulites observed in PSC and different compositions of PNCEs is around $60 - 70$ μm in diameter. These morphologies suggest the semi-crystalline nature of the samples, where lamellar structured spherulites represent crystalline domain and the boundaries represent the amorphous regions. TiO_2 is a dispersed phase filler; hence it is expected to be evenly distributed throughout the polymer matrix. With the addition of TiO_2 filler no substantial change in the morphological feature *i.e.*, spherulite texture can been observed as shown in from figure (5.2b) to (5.2f). It can also be observed that filler particles are clearly embedded in the host polymer forming composite

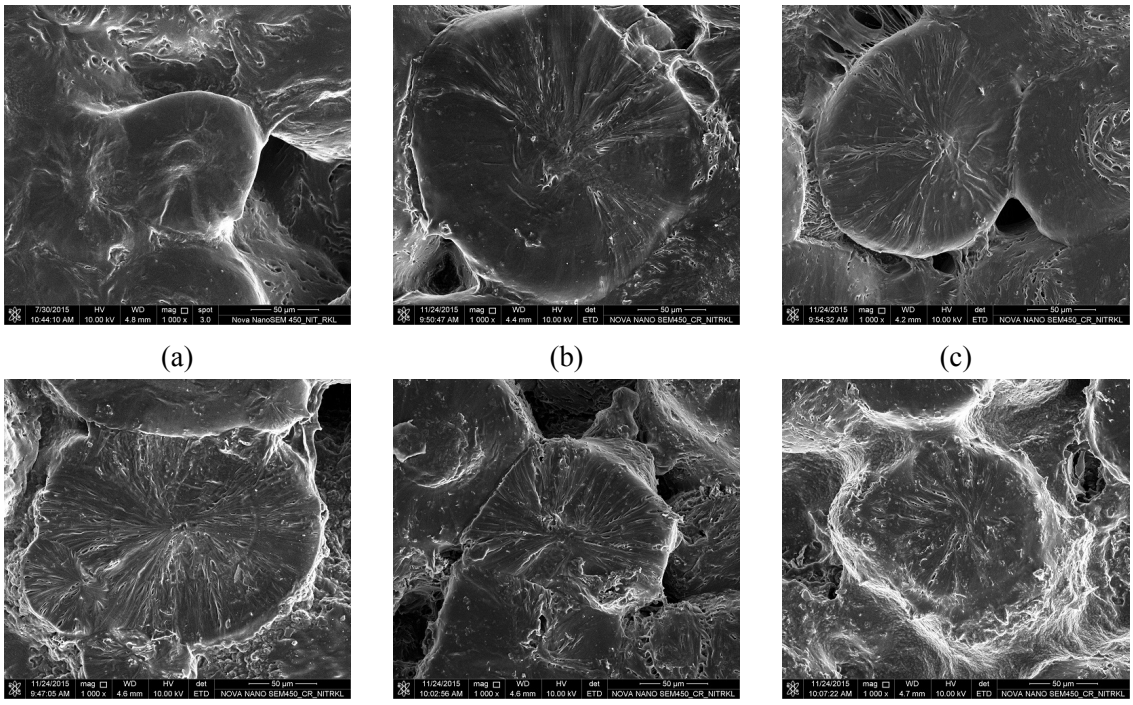

(a) (b) (c)

(d) (e) (f)

Figure 5.2: Scanning electron micrographs of PSC and titania based polymer nano-composite electrolyte samples. (a) Polymer salt complex, (b) 3 wt.% TiO_2, (c) 5 wt.% TiO_2, (d) 8 wt.% TiO_2, (e) 10 wt.% TiO_2 and (f) 15 wt.% TiO_2 based compositions.

polymer electrolyte sample. The semi-crystalline behaviour of the samples as suggested by XRD analysis is also supported from the surface morphology of SEM micrographs.

5.3.3 Vibrational Study

Infrared (IR) spectroscopy is used to study interactions between the ions and host polymer. FTIR studies can help to study the effect of additive concentration on polymer-salt complex. The characteristic bands of PSC and PNCEs are idex as follows; band around 638 cm^{-1} corresponds to cis C-H wagging mode, 842 cm^{-1} corresponds to cis C-H_2 wagging, 962 cm^{-1} corresponds to stretching of ether bond (C-O) of polymer, 1032 cm^{-1} corresponds to symmetric stretch SO_3 vibration of $LiCF_3SO_3$, 1100 cm^{-1} corresponds to stretching of ether bond (C-O) of polymer, 1242 cm^{-1} corresponds to C-F and CF_2- stretching, 1282 cm^{-1} corresponds to CH_2 twisting vibration of polymer and 1467 cm^{-1} corresponds to CH_2 scissoring mode.[200, 202] With varying concentration of ceramic additives focus is to be given on 1032 cm^{-1} and 1055 cm^{-1} bands, These bands correspond to symmetric stretch SO_3 vibration of $LiCF_3SO_3$ under complexation.[201] Band around 1032 cm^{-1} represents free anions and solvent separated pair vibrations whereas around 1055 cm^{-1} represents $Li_2CF_3SO_3^+$ aggregates.[203] The presence of both the bands can be observed in all these IR spectra, which suggests that dissociated ions do take part in enhancing the ionic conductivity of the composite electrolytes. No significant change in the position of various bands can be

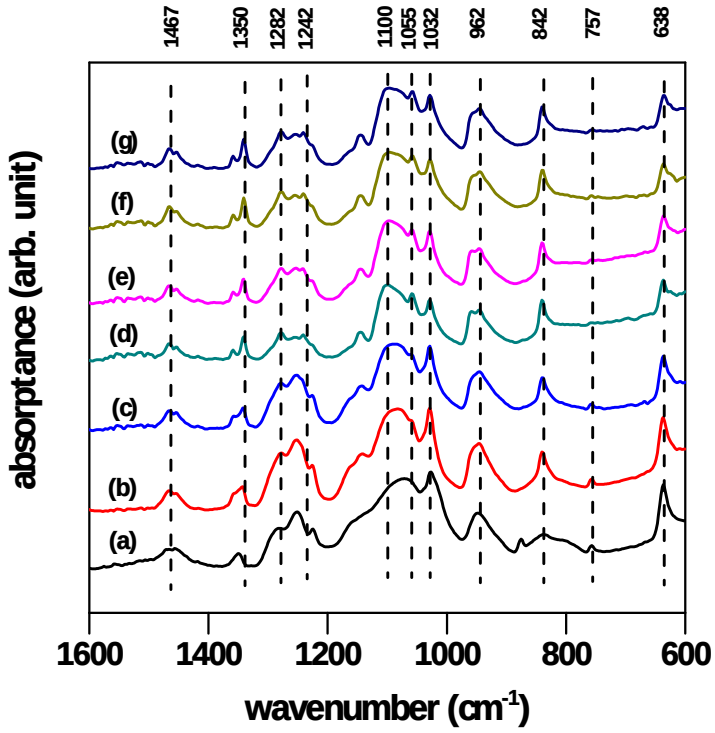

Figure 5.3: FTIR spectra of composite polymer electrolytes having composition PEO_{20}-$LiCF_3SO_3$- x wt.% TiO_2 (a) $x = 0$ *i.e.* PSC, (b) $x = 2$ (c) $x = 3$, (d) $x = 5$, (e) $x = 8$, (f) $x = 10$ and (g) $x = 15$

observed in different composite samples. However, small changes in the relative intensity of different bands can be observed, which suggests that the local environment of PSC, at the microscopic level, is modified with the addition of filler.[204]

5.3.4 AC Conductivity Study

Ion dynamics of the PSC and PNCEs have been investigated using complex electrical conductivity spectra. In figure (5.4a) a plot of the real part of ac conductivity as a function of frequency over a temperature range from 323 K to 203 K with 10 K interval for PEO_{20}-$LiCF_3SO_3$- 8 wt.% TiO_2 PNCE composition is shown as representative. The real part of ac conductivity, σ', as a function of frequency show three distinct regions at ambient temperature, (i) high frequency dispersion region which is attributed to short range ion hopping, (ii) frequency independent plateau region attributed to long-range ionic motion reflecting as dc conductivity (σ_{dc}) and (iii) low frequency dispersion attributed to fast ion migration reflecting as EP. With a decrease in temperature, the overall ac conductivity decreases and the high-frequency dispersive region is found to cover a larger part of the frequency range of investigation. Here the cross-over frequency between high-frequency dispersive region and frequency independent plateau region termed as hopping crossover frequency marks the onset of conductivity relaxation. Hopping cross-over frequency is

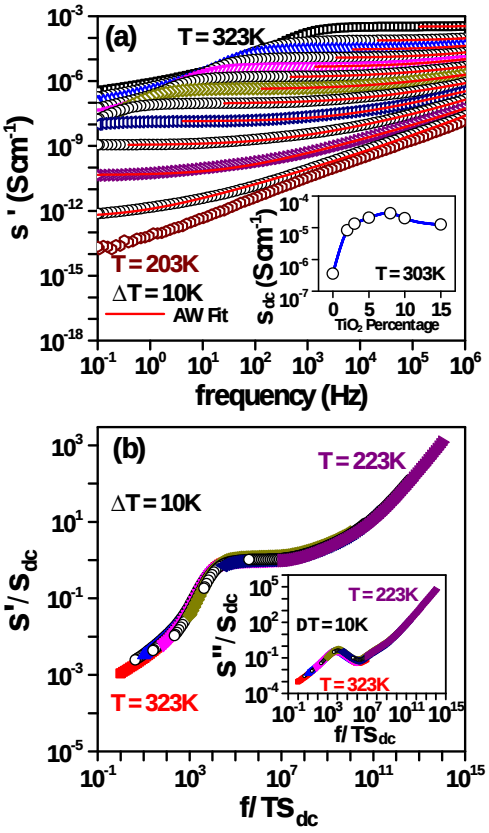

Figure 5.4: (a) AC conductivity as a function of frequency for the PNCE composition PEO_{20}-$LiCF_3SO_3$- 8 wt.% TiO_2, at temperature ranging from 203 K to 323 K with an interval of 10 K between each isotherms. Inset showing the variation of dc conductivity as a function of filler concentration at T = 303 K (b) Scaled real part of conductivity spectra with inset showing the scaled imaginary part of conductivity spectra using Summerfield scaling approach for PNCE composition PEO_{20}-$LiCF_3SO_3$- 8 wt.% TiO_2, at temperature ranging from 223 K to 323 K with an interval of 10 K between each isotherms.

observed to be shifted towards lower values with decreasing temperature. While temperature is decreased, at first low-frequency dispersive region go below the frequency range of investigation, then plateau region and finally around 203 K only high-frequency dispersive region prevail throughout the experimental frequency range. Therefore a strong frequency dependence of σ' isotherms can be observed with varying temperature. Other samples in this PNCE series under investigation show similar behaviour.

A quantitative description of ion conduction process can be presented analyzing the frequency independent plateau and high-frequency dispersion regions of real part of ac conductivity isotherm. At relatively high temperature and/or low frequency, σ' can be represented using Almond-West power law given by the following equation[107]

$$\sigma' = \sigma_{dc}[1 + (f/f_c)^n] \tag{5.1}$$

where, σ_{dc} is the dc conductivity, f is frequency and n is power law exponent having value

within $0 < n < 1$. For ionic conductors, in general the value of "n"is found between 0.4 and 0.7.[174] For the temperature range 323 K to 233 K a reasonably good fit is observed when the experimental data is fitted with equation (5.1) excluding the regions of EP. This behaviour is known as first universality or universal dielectric response (UDR). At very low temperature it can be observed that conductivity isotherms become nearly linear in nature, and using equation (5.1) a good fitting can not be achieved. In low-temperature regime, another term, which is having an approximately linear dependence on frequency is added to AW power law. Modified Almond-West equation is given below,[191]

$$\sigma' = \sigma_{dc}[1 + (f/f_c)^n] + Af^m \tag{5.2}$$

where, A is weakly temperature dependent and m is power law exponent whose value is found very close to 1. This added term in the isothermal spectra of the real part of ac conductivity corresponds to frequency independent dielectric loss. We found that in the present study, below 233 K, $\sigma'(f)$ spectra give a reasonably good fit only with equation (5.2). This observation suggests that below 233K temperature NCL phenomenon dominates over UDR. The cause of the presence of NCL phenomenon is already described in chapter (4) with the help of Ngai Coupling model and Kramer-Krönig formalism. Inset of figure (5.4a) shows the variation of dc conductivity at T = 303 K as a function of filler concentration. This plot indicates that with the addition of TiO_2 filler initially σ_{dc} increases up to 8 wt.% of TiO_2 PNCE composition and thereafter it decreases. For pure PSC, at T = 303 K, σ_{dc} value is found 3.760×10^{-7} Scm^{-1}, whereas at the same temperature for 8 wt.% of TiO_2 PNCE composition obtained σ_{dc} value is 3.174×10^{-5} Scm^{-1}. Hence, in terms of dc conductivity, an increase in nearly two orders of magnitude can be observed when 8 wt.% of TiO_2 is added to PSC.

The conductivity isotherms may be scaled using time-temperature superposition principle, as it can be observed from figure (5.4a), that the complex ionic conductivity exhibits a temperature independent profile.[224] For ionic conduction, the process of conductivity scaling indicates a common physical mechanism irrespective of various intrinsic physical parameters associated with it like temperature. Scaling procedure, in general, can be represented as[225]

$$\sigma'/\sigma_{dc} = F(f/f^*) \tag{5.3}$$

where, f^* is the scaling parameter. In the present investigation Summerfield scaling approach is used, where $f^* = \sigma_{dc}T$ is chosen as the scaling parameter. This scaling approach is very much straight forward as directly accessible physical parameters such as σ_{dc} and temperature is used to perform this time temperature superposition principle based conductivity scaling. Formation of master curve using Summerfield scaling approach for PNCE composition PEO_{20}-$LiCF_3SO_3$- 8 wt.% TiO_2 is shown in figure (5.4b). Due to the

effects of EP, at low frequency and high-temperature region, a small deviation is observed. Summerfield scaling suggests that although, there exist a strong temperature dependence for the crossover between subdiffusive to diffusive ionic conduction phenomenon, as a whole the ionic transport mechanism is independent of temperature.

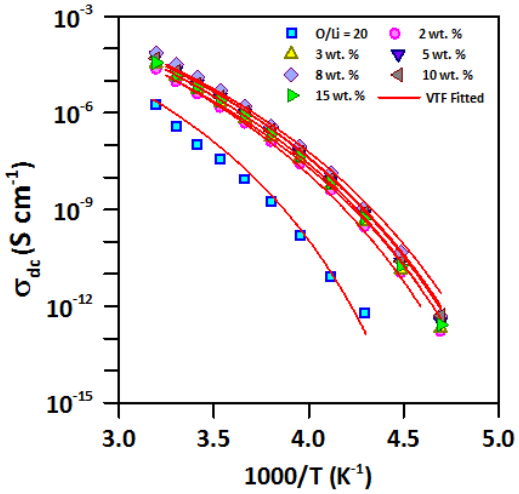

Figure 5.5: Temperature dependent dc conductivity in inverse temperature scale for PSC and PNCE compositions PEO_{20}- $LiCF_3SO_3$- x wt.% TiO_2 (x = 2, 3, 5, 8, 10 & 15).

Temperature dependent dc conductivity for different compositions of PNCE obtained from modified AW formalism is shown in figure (5.5). It is clear that the samples exhibit non-Arrhenius dependence and can be best represented by Vogel-Tammann-Fulcher (VTF) relation.[223, 226]The solid lines in figure (5.5) show the VTF fitted results to the dc conductivity data. The close agreement between VTF fitted and experimentally obtained results over a wide temperature range imply the close coupling among the polymer chain relaxation and the ionic conductivity of the PNCE.

5.3.5 Relaxation Dynamics and Electrical Modulus Formalism

Complex electrical modulus, M^* and complex dielectric permittivity, ε^* are having an inverse relationship. Using M^* spectra, conductivity relaxation phenomenon is studied. In figure (5.6a) real, M', and in figure (5.6b) imaginary, M'', part of electrical modulus spectra are represented as a function of frequency over a temperature range 263 K to 213 K for the PNCE composition PEO_{20}-$LiCF_3SO_3$- 8 wt.% TiO_2. From figure (5.6a), it can be observed that with the increase in frequency, there is a gradual increase in M' isotherm. At high-frequency values, M' tend to get saturated but due to the experimental constraint of frequency range proper saturation of M' spectra is not observed at ambient temperature. However, at low temperatures a near saturation behaviour can be seen for M' isotherms. When imaginary part of M^* isotherms are considered, shown in figure (5.6b), they show relaxation peaks. These peaks indicate that there exist a transition from short range (high

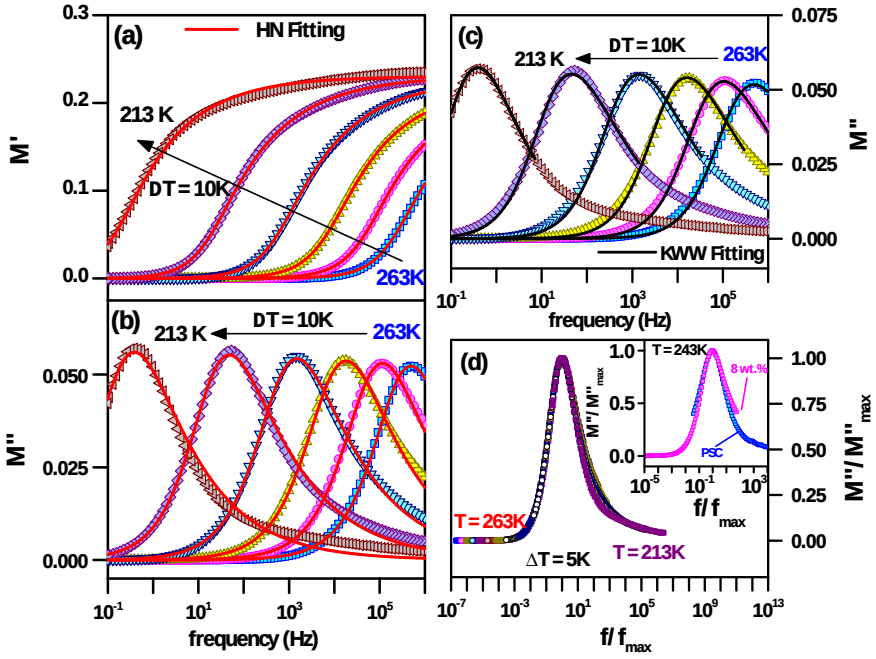

Figure 5.6: (a) Real and (b) imaginary part of electrical modulus analyzed with HN approach, having $\Delta T = 10$ K between each isotherms. (c) Imaginary part of electrical modulus analyzed with Bergman modified Kohlarsch-William-Watts approach, having $\Delta T = 10$ K between each isotherms. (d) Scaled imaginary part of electrical modulus for the PNCE composition PEO_{20}-$LiCF_3SO_3$- 8 wt.% TiO_2, having temperature interval $\Delta T = 5$ K. Inset of (d) showing the scaling of PSC and 8 wt.% TiO_2 PNCE composition at T = 243 K.

frequency) to long range (low frequency) ion mobility. The frequency related to the peak of M'' spectra corresponds to conductivity relaxation frequency, f_c. Using this frequency one can obtain the associated conductivity relaxation time using the relation $\tau_c = 1/2\pi f_c$. Observed peaks found in M'' spectra are asymmetric in nature and skewed towards the high-frequency side of the maxima in M'' spectra. With the increase in temperature, peak of M'' spectra is observed to shift towards high-frequency values. This suggests a decreased relaxation time with fast ionic motion and making ion conduction mechanism in polymer electrolytes a thermally activated phenomenon.[226]

Due to broad nature of M'' peaks, it is quite evident that conductivity relaxation is non-Debye type in nature. Hence for better understanding, complex modulus spectra are analyzed using Havriliak-Negami (HN) function as well as modified Kohlrausch-Williams-Watts (KWW) equation given by Bergmann. Havriliak-Negami (HN) function is represented by the following equation[171, 226]

$$M^* = M_\infty + \frac{(M_s - M_\infty)}{[1 + (j\omega\tau)^{\alpha}_{HN}]^{\gamma}_{HN}} \tag{5.4}$$

here, M_s and M_∞ are the low and high frequency limiting values of electrical modulus spectra respectively, α_{HN} and γ_{HN} are the shape parameters and τ corresponds to the

relaxation time. In general shape parameters, *i.e.* α_{HN} and γ_{HN}, has to satisfy the following relations $0 < \alpha_{HN} \leq 1$ and $0 < \alpha_{HN}\gamma_{HN} \leq 1$.[226] In case of ideal Debye type relaxation both the shape parameters should be 1 and in case of non-Debye type relaxation these deviate from unity. In figure (5.6a) and (5.6b) HN fitted results of complex modulus are shown by using solid lines. From the fitted results, the value of α_{HN} and γ_{HN} are calculated and they are found to be less than unity, suggesting a non-Debye type relaxation phenomenon.

In another approach, the modified KWW equation developed by Bergmann is used to analyze the imaginary part of electrical modulus spectra and the equation is given below as[107]

$$M'' = \frac{M''_{max}}{(1-\beta_{KWW})\left(\frac{\beta_{KWW}}{1+\beta_{KWW}}\right)\left[\beta_{KWW}(f_{max}/f) + (f/f_{max})^{\beta_{KWW}}\right]} \tag{5.5}$$

here, M''_{max}, β_{KWW} and f_{max} are the maxima of modulus spectra, the shape parameter, and frequency at which modulus maxima is observed respectively. Since KWW fit is not much successful at the high-frequency limits of M'' spectra, therefore, the fitting is focused around the M'' peak. KWW fitted M'' isotherms are shown in figure (5.6c). The value of β_{KWW} obtained from the fitting formalism is found between 0.45 to 0.55, which infer a non-Debye type behaviour of relaxation events as also found in HN analysis of complex electrical modulus. Low values of β_{KWW} suggest that the conductivity relaxation events are highly non-exponential in nature and Li^+ ion movement is a cooperative phenomenon in PSC and PNCEs. This infers that a mobile ion hopping from one favourable site to another can not be considered as an isolated event.[226] Havriliak-Negami and modified KWW approaches presented by Bergmann can be considered the same if HN and KWW fitting parameters follow the relation given by $\beta_{KWW}^{1.23} = \alpha_{HN}\gamma_{HN}$.[226] In the present investigation, we observed that the above-mentioned relation holds true for the obtained fitting parameters. Therefore any one of these representations is valid to discuss the complex modulus spectra and they bear the same physical interpretation to ion conduction mechanism. Scaling is performed to investigate the common underlying physical phenomena of ion conduction mechanism. It is already represented that using Summerfield conductivity scaling approach; conductivity isotherms can be scaled. Here the scaled M'' spectra are shown in figure (5.6d) for PEO_{20}-$LiCF_3SO_3$- 8 wt.% TiO_2 PNCE composition. A single master curve can be formed over a wide range of temperature using maxima normalization technique.[222] This property suggests that conductivity relaxation phenomena and ion conduction mechanism are thermally activated dynamic process but they remain independent of the temperature of the sample. Inset of figure (5.6d) show the process of scaling for PSC and 8 wt.% TiO_2 PNCE composition at T $= 243$ K. It can be observed that these M'' spectra are not superposing completely to form a master curve, hence can not be scaled using maxima normalization technique. It reflects that with the addition of filler, local environment is changing due to filler-polymer and filler-salt interaction.[107] This may be the reason for getting increased

ionic conductivity.

5.3.6 Relaxations and Concept of First and Second Universality

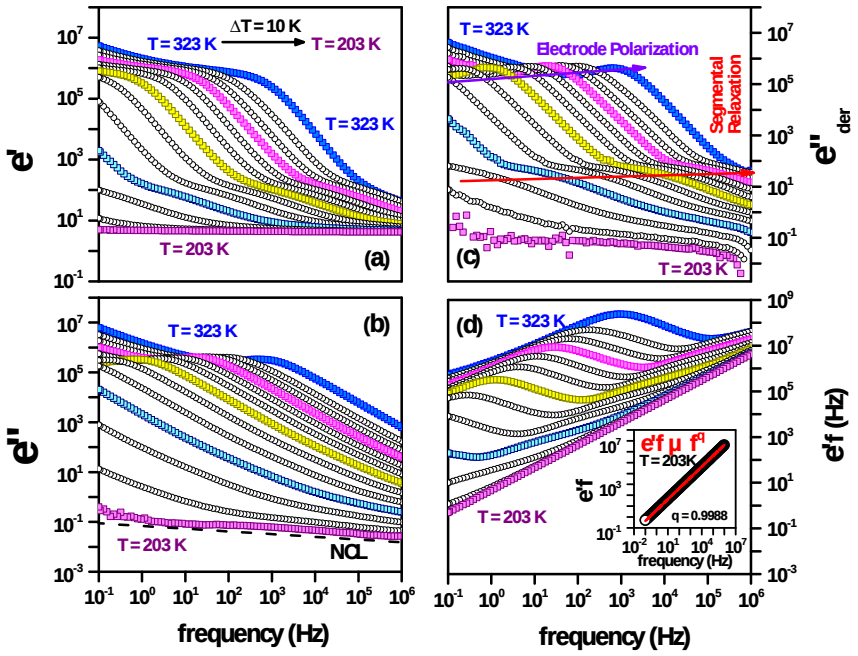

Figure 5.7: (a) Frequency dependent real part of permittivity, (b) frequency dependent imaginary part of permittivity, (c) DC conduction free dielectric loss and (d) $\varepsilon' f$ as a function of frequency with inset showing the fitted results at T =203 K for the PNCE composition PEO_{20}-$LiCF_3SO_3$- 5 wt.% TiO_2. Temperature interval between each isothermal spectra is $\Delta T = 10$ K.

Complex dielectric permittivity spectra can also provide information to interpret relaxation process and ionic conductivity in PSC and PNCEs. Real and imaginary component of complex permittivity spectra are shown in figure (5.7a) and (5.7b) respectively for the PNCE composition, PEO_{20}-$LiCF_3SO_3$- 5 wt.% TiO_2, over a temperature range of 323 K to 203 K having an interval of 10 K. The real part of the permittivity, ε', show nearly constant value at high-frequency regions and it is observed that with decreasing frequency it increases. Imaginary permittivity, ε'', increases monotonically with decreasing frequency and in the mid frequency region it is following the relation, $\varepsilon'' \propto f^{-1}$, which indicate the dc conductivity behaviour.[174] Due to the effects of EP at low-frequency regions ε'' show a sudden increase in magnitude. At very low temperature, T = 203 K, ε'' is found to assume nearly constant values, which indicate the presence of second universality or NCL in the case of PSC and PNCE. The dominance of UDR and NCL over each other will be discussed using Kramer-Krönig formalism. From conventional isothermal complex permittivity spectra, the segmental relaxation phenomena are not very clear as the relaxation events are masked by high ionic conductivity in PNCE. Therefore, to study segmental

relaxation, dc conduction-free dielectric loss approach is adopted and the obtained spectra are shown in figure (5.7c). In dc conduction-free dielectric loss approach, both segmental relaxation and EP become prominent at high and low-frequency regime respectively as observed in figure (5.7c). Segmental relaxation time can be calculated from each isotherm of dc conduction-free dielectric loss spectra using the relation $\tau_s = 1/2\pi f_s$, where f_s is the peak frequency of segmental relaxation.

For in depth analysis of NCL effect, Kramer-Krönig formalism is followed. In this formalism, ε' is found to be proportional to f^{q-1}, which can be written as[190]

$$\varepsilon' f = B f^q \tag{5.6}$$

where, q is the exponent. The value of q should be close to unity if ion conduction process is dominated by the second universality. In figure (5.7d), $\varepsilon' f$ has been plotted as a function of frequency for different temperatures. At very low temperatures $\varepsilon' f$ becomes nearly linear over the entire frequency range of investigation and with the increase in temperature the linear region is found to shift towards high-frequency regions. Inset of figure (5.7d) shows the fitted results at T = 203 K using equation (5.6). The value of exponent q is found 0.998, which is very close to unity. It indicates that the second universality governs the ion conduction process at low temperatures. The value of q is found to decrease with increase in temperature. This can be attributed to the increasing dominance of UDR over NCL in ion conduction process.[190] Therefore UDR and NCL together only can represent the ion conduction process in this class of material. The cause behind observing the NCL phenomena is considered to be the caged ion dynamics of the mobile ions. At the very low temperature and high frequency, there exists small probability for the mobile ions to hop towards a favorable neighboring site and leave the cage like potential landscape created at the microscopic level. On the other hand when temperature increases or at low frequencies, this caged ion become mobile and contribute to ion conduction process which is attributed as UDR.

5.3.7 Relaxation Mapping

Relaxation time can be obtained from the reciprocal of the angular frequency of relaxation events. Segmental relaxation time, τ_s and conductivity relaxation time, τ_c are obtained from dc conduction-free dielectric loss and electrical modulus formalisms respectively. Both τ_s and τ_c are shown as a function of temperature in form of a relaxation map in figure (5.8). It can be observed that both τ_s and τ_c can be best approximated by Vogel-Tammann-Fulcher (VTF) relation given by the following expression.[227]

$$\tau = \tau_0 \exp\left\{\frac{E_a}{k_B(T - T_0)}\right\} \tag{5.7}$$

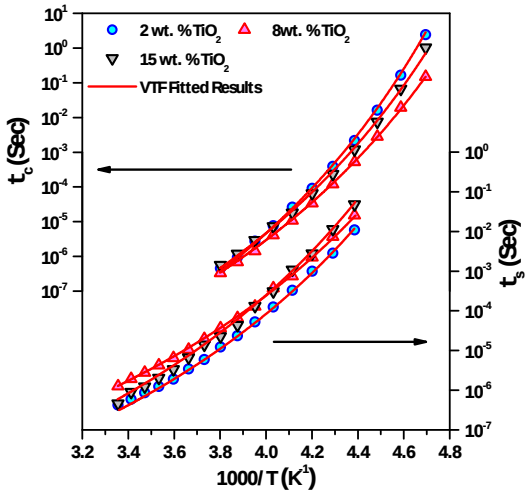

Figure 5.8: Variation of conductivity and segmental relaxation time for the PNCE compositions, PEO_{20}-$LiCF_3SO_3$- x wt.% TiO_2 (x = 2, 8, & 15). Solid lines represent VTF fitted results.

where, τ, τ_0, E_a, k_B, T and T_0 are relaxation time, pre-exponential parameter, pseudo-activation energy, Boltzmann's constant, absolute temperature and Vogel temperature respectively. Though VTF equation is an empirical relation, at present it is one of the widely accepted relation. Vogel temperature is considered as the temperature at which all molecular motion cease, or excess configuration entropy becomes zero. Generally in literature its range is found following the relation $60\ \text{K} \leq T_g - T_0 \leq 50\ \text{K}$, where T_g is equilibrium glass transition temperature.[174] A close correlation can be observed between experimentally obtained and fitted results, which suggest the ion conduction phenomena and segmental relaxation process in PSC and PNCE compositions are coupled in nature. As τ_c and τ_s are following VTF relation; therefore it can be considered that there exist a coupling between ionic conduction and segmental relaxation processes found in this class of materials. Calculated activation energies and Vogel temperature are tabulated in table (5.1).

5.3.8 Coupling

Coupled nature of ion conduction mechanism is explained using relaxation time mapping, different scaling approaches and Ratner's approach is used. The theoretical background of this analysis has been discussed in section (3.6) earlier. It can be observed from equation (3.23) that for a coupled system $-log\sigma_{dc}$ and $log\tau_s$ should follow similar behaviour. Figure (5.9a) represent $-log\sigma_{dc}$ and $log\tau_s$ as a function of temperature for the PNCE composition, PEO_{20}-$LiCF_3SO_3$- 8 wt.% TiO_2. For all other compositions in the present investigation, a similar trend can be observed (not shown here). σ_{dc} and τ_s follow VTF behaviour and the fitted spectra are shown in form of solid lines in the plot. In this context we have also

Table 5.1: VTF fitted parameters obtained from temperature dependent conductivity, conductivity relaxation time and structural relaxation time plots of PNCE compositions. Maximum error limit obtained are stated in parenthesis for each set of parameters.

Composition (x wt.% TiO_2)	σ VTF Fit		τ_c VTF Fit		τ_s VTF Fit	
	E_A(eV) ($\pm$0.002)	T_0(K) ($\pm$1)	E_A(eV) ($\pm$0.002)	T_0(K) ($\pm$1)	E_A(eV) ($\pm$0.002)	T_0(K) ($\pm$1)
x = 2	0.148	165	0.151	153	0.171	155
x = 3	0.136	162.5	0.148	152	0.170	152
x = 5	0.134	160	0.141	151	0.169	151
x = 8	0.127	152.5	0.136	151	0.161	149
x = 10	0.133	153	0.139	152	0.168	151
x = 15	0.146	154	0.150	153	0.164	152

examined $D\tau_s$ and $\sigma T\tau_s$. For coupled system, these two entities should remain constant as discussed earlier. These two parameters have been represented in figure (5.9b). Only one order of change in magnitude can be found in these plots for the entire range of investigation. This clearly indicates that ion conduction mechanism is a cooperative phenomenon of polymer segmental motion and thermally activated ion hopping. Hence ion conduction mechanism and segmental relaxation process are closely coupled.

5.3.9 Theoretical Model Analyzed DC Conductivity Results.

As described earlier; MIsmatch Generated Relaxation for the Accommodation and Transport of IONs (MIGRATION) concept based theoretical approach is getting more and more attention due to its conceptual representation of the whole ion conduction process. MIGRATION is a refined concept of the jump relaxation model, mismatch and relaxation model.[228] MIGRATION is an ion hopping based model for structurally disordered materials, especially in cases where ion conduction phenomena is a coupled process like the present investigation. So far VTF equation is used to describe temperature dependent dc conductivity which is an empirical relation and also possess a divergence at T = T_0, where T_0 is the Vogel temperature. According to this model, a short time ion hopping is always considered successful and termed as high-frequency conductivity. Ion hopping can be viewed as a collection of successful as well as unsuccessful forward-backward hopping over a larger period of time.[186] This forward-backward ion hopping is the cause behind the observed dispersion in the complex conductivity isotherms. Eventually only a small fraction of these ion hopping become successful and contribute towards dc conductivity.[229] According to this mechanism the key feature causing the non-Arrhenius behaviour of the dc conductivity is the constancy of the crossover angular frequency at the

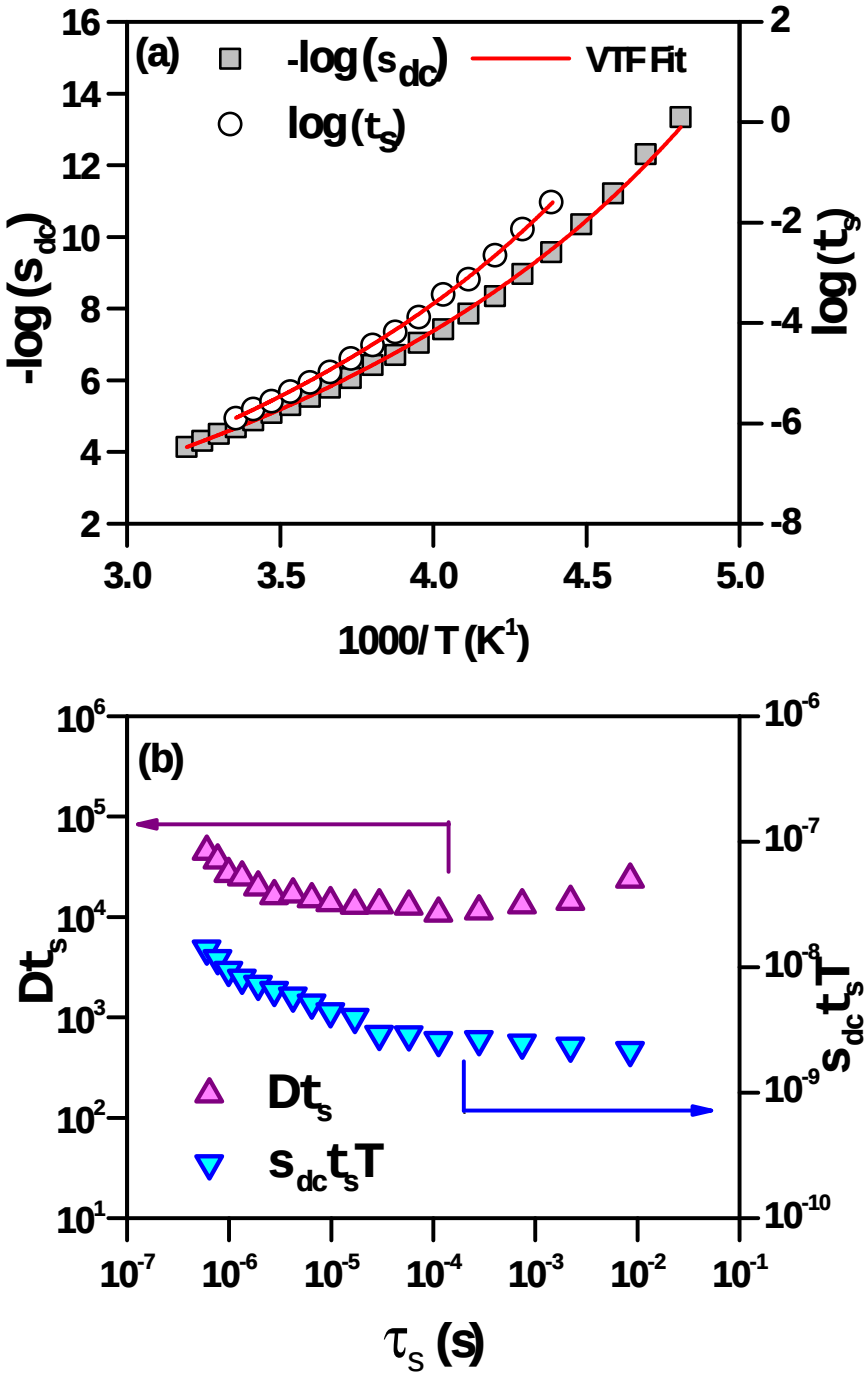

Figure 5.9: (a) Negative logarithm of dc conductivity and segmental relaxation time as a function of temperature for the PNCE composition PEO_{20}-$LiCF_3SO_3$- 8 wt.% TiO_2. Solid lines represent VTF fitted results. (b) variation of $D\tau_s$ and $\sigma D\tau_s$ as a function of segmental relaxation time for the PNCE composition PEO_{20}-$LiCF_3SO_3$- 8 wt.% TiO_2.

end of the dispersive regime. In general according to this model dc conductivity, σ_{dc} can be

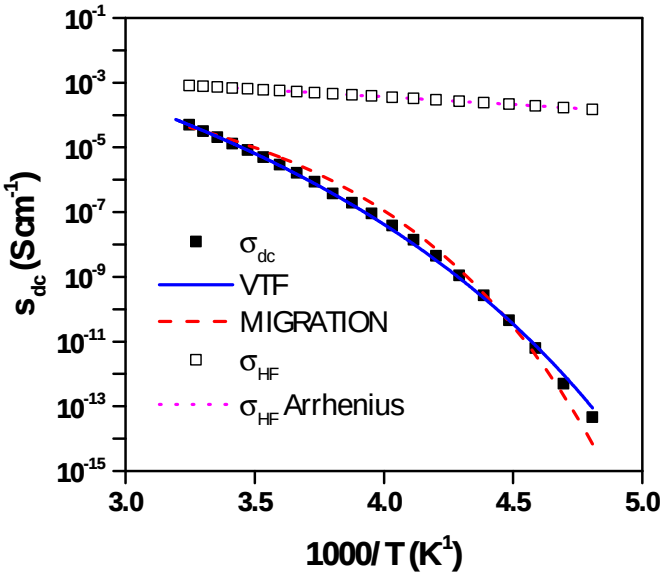

Figure 5.10: Study of temperature dependent dc conductivity using MIGRATION and VTF model approach for the PNCE composition PEO_{20}-$LiCF_3SO_3$- 8 wt.% TiO_2.

expressed as[230]

$$\sigma_{dc}(T) = \frac{\alpha}{\tau} \exp\left[-\frac{E^*}{k_B T} - \gamma \exp\left(\frac{E^*}{2k_B T}\right)\right] \tag{5.8}$$

where, α and γ are the pre-exponential factors, E^* is the activation energy for elementary displacive step. Figure (5.10) shows a comparative study between VTF and MIGRATION based concepts for PEO_{20}-$LiCF_3SO_3$-8 wt.% TiO_2 PNCE composition. A close agreement can be observed between experimentally obtained data and theoretically predicted results. Using VTF equation one can extract the information about the activation energy of ionic conductivity as well as Vogel temperature. At Vogel temperature, it is considered that molecular motion cease. Unlike VTF equation, MIGRATION concept does not have any singularity at temperature scale. MIGRATION based model is successfully reproducing the temperature dependent behaviour of dc conductivity and there exist no divergence temperature. Figure (5.10) also represents the evaluated ion hopping conductivity at high frequency range σ_{HF}. It can be observed from the plot that obtained σ_{HF} is Arrhenius activated. This σ_{HF} marks the transition from NCL to UDR as per the mapping of MIGRATION model to Ngai coupling model. A large displacive activation energy, obtained from fitted results E^* (0.1151 eV) represents the existence of the coupling between segmental motion of polymer host and ionic conduction. Observed dc conductivity behaviour as a function of temperature for the ion conducting PNCEs can be explained using MIGRATION model. It also supports the coupled nature of ion conduction mechanism as discussed in section (5.3.8), using modified Ratner's approach.[230]

5.4 Conclusions

At first, anatase polymorph of titania filler is synthesized using polymer template method. Phase formation and phase purity of the filler is analyzed using X-ray diffraction technique. Rietveld refinement is carried out to analyze the effect of calcination temperature on the phase purity of anatase polymorph of titania. Using conventional solution casting technique a series of ion conducting polymer nanocomposite electrolyte is prepared, using PEO as the polymer, $LiCF_3SO_3$ as salt and TiO_2 as filler. Polymer salt complex formation, phase formation of filler and composite nature of the proposed electrolytes are confirmed using XRD analysis. FE-SEM technique is employed to study the surface morphology of the prepared samples. Vibrational characterization is carried out in mid-IR region. Temperature dependent electrical measurements are carried out using broadband dielectric spectroscopy. The important observation of this study are as follows:

- Conductivity isotherms are analyzed using modified AW formalism. Universal dielectric response and nearly constant loss phenomena are clearly observed in this series of electrolytes.
- Temperature dependent dc conductivity, segmental relaxation time and conductivity relaxation time is following VTF behaviour suggesting a strong coupling between polymer segmental relaxation process and ion conduction process.
- Presence of both the first and second universality are shown with the help of conductivity spectra along with dielectric loss spectra. Kramer-Krönig approach explained that at low-temperature regime NCL dominates over UDR and with increasing temperature UDR become more prominent than NCL.
- Summerfield conductivity scaling approach and scaled electrical modulus spectra suggest that ion conduction mechanism is a temperature independent thermally activated dynamic process.
- With Ratner's approach, the coupled nature of polymer segmental motion and ion conduction mechanism is studied.
- A close agreement is observed between the experimentally obtained data and MIGRATION model predicted results. The high value of displacive activation energy, E^*, also represents the existence of a coupling between segmental motion of polymer host with that of ionic motion.
- At ambient temperature (T $= 303$ K) the maximum value of dc conductivity (σ_{dc})is found to be 3.17×10^{-5} Scm^{-1} for PEO_{20}-$LiCF_3SO_3$-8 wt.% TiO_2 PNCE composition, which is two orders of magnitude higher than polymer salt complex.

Chapter 6

Relaxation Dynamics and Ion conduction Process in PEO_{20} - $LiCF_3SO_3$ - modified Montmorillonite Clay Based Polymer Composite Electrolyte[1]

6.1 Introduction

So far ion conduction mechanism is discussed for two different types of filler based polymer nanocomposite electrolyte (PNCE) samples. In chapter (4) properties of zirconia filler based PNCEs are investigated whereas in chapter (5) properties of titania-based PNCEs are discussed. Zirconia is an inert passive filler, whereas anatase titania has the tendency to attract the free cations weakly.[219, 220] In comparison to both these ceramic fillers, Montmorillonite clay is very much different in various properties. Montmorillonite possesses a layer-like structure and is a high aspect ratio filler.[117, 231, 232] In addition to increased the ionic conductivity, this class filler also has the potential to reduce dual ion conduction phenomenon.[199] Motivations behind this particular study are as follows (i) investigation of the conductivity isotherms to analyse the ionic transport mechanism and correlate experimental data with existing suitable physical models or phenomenology, (ii) to correlate ionic transport with segmental relaxation of the polymer host and (iii) to get insight of the ionic transport process so that conductivity at ambient temperature of PNCEs can be increased further in future.

In view of the above, we have prepared a series of PNCEs by solution casting technique using polyethylene oxide (PEO), lithium trifluoromethanesulfonate (keeping $O:Li^+$ ratio 20) and modified hydrophobic montmorillonite (mMMT) clay as filler. For easy intercalation of polymers into the clay gallery, montmorillonite clay is organo-modified using cetyltrimethylammonium bromide modifier. The detail modification procedure is discussed in chapter (2). Structural, vibrational, surface morphological and temperature

[1]Content of this chapter is partially published in : Tapabrata Dam, S. S. Jena and D. K. Pradhan, "The ionic transport mechanism and coupling between the ion conduction and segmental relaxation processes of PEO_{20} - $LiCF_3SO_3$ based ion conducting polymer clay composites. ", Phys. Chem. Chem. Phys., 2016 (18) 19955-19965.

dependent electrical properties are investigated using X-ray diffraction, FTIR, FE-SEM and broadband dielectric spectroscopy respectively. In this chapter emphasis is given on a comparative study of two different physical model and phenomenology; random free energy barrier hopping model (RFEBM) and power law to depict the actual picture of ion conduction process at the microscopic level. In this process it is also examined whether segmental relaxation and ionic condition are coupled in nature or not.

6.2 Synthesis of Materials and Experimental Conditions

Polyethylene oxide of $M_w = 6 \times 10^5$, lithium trifluoromethanesulfonate, organo-modified montmorillonite clay and analytical grade acetonitrile (used as common solvent) are used for preparation of polymer salt complex (PSC) and a series of PNCE having compositions PEO_{20}-$LiFC_3SO_3$-$x$wt.% $mMMT_2$ (x = 2, 3, 5, 8, 10 &15). Synthesis procedure of PSC and PNCE films and modification of montmorillonite clay are already described in chapter (2). X-ray diffraction (XRD) of PNCEs are carried out using Rigaku Ultima IV X-ray diffractometer operating at 40 kV and 40 mA; producing Cu $K_{\alpha 1}$ radiation having wavelength 1.5405Å. The XRD patterns are recorded with a scanning rate of 3° per minute and a scanning step of 0.002°. FE-SEM micrographs are recorded using Nova NanoSEM 450/FEI electron microscope. FTIR spectroscopy is carried out using Bruker Alpha-E FTIR Spectroscope, with wavenumber ranging from 600 cm^{-1} to 4000 cm^{-1} having 1 cm^{-1} resolution. Dielectric measurements are carried out using Novo-Control GMBH Alpha analyzer over a wide range of frequency; 10^{-1} to 10^6 Hz with excitation potential of 10 mV. Novo-Control Quattro Cryo-system is used to control the temperature of the samples under investigation in a liquid nitrogen gas based sample holding assembly.

6.3 Results and Discussion

6.3.1 Structural Study

Structural evolution and the formation of PSC and PNCEs have been studied using X-ray diffraction technique and the patterns are shown in figure (6.1). Clay modification is already described in chapter (2), but the X-ray diffraction pattern of modified and unmodified montmorillonite clay is given in inset of figure (6.1). As mentioned earlier, increased interlayer spacing along with the hydrophobic nature of mMMT provide easy intercalation of polymer chain through clay layers.[199] It is evident from the XRD patterns that when mMMT is added to PSC the peak position of (001) clay plane is further shifting towards low values of 2θ (small amount of clay do not undergo intercalation, marked by '#' in XRD spectra), suggesting that polymer chains are intercalated within the clay layers. On comparison of the XRD patterns of PEO, PSC and different PNCE composition no characteristic peak of $LiCF_3SO_3$ (JCPDF number: 81-0813) is found, confirming the proper

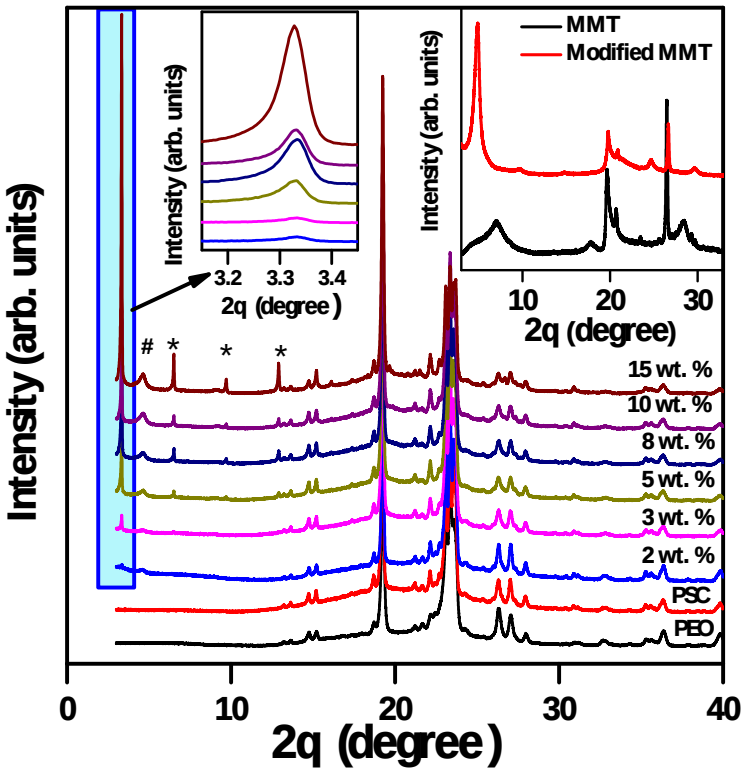

Figure 6.1: X-Ray diffraction patterns of polyethylene oxide, polymer salt complex and various compositions of polymer composite electrolytes [PEO_{20}- $LiCF_3SO_3$- x wt.% mMMT (x = 2, 3, 5, 8, 10 & 15)]. Inset show the unmodified and modified montmorillonite clay.

dissolution of salt into host polymer matrix. For the higher concentration of mMMT, higher order reflections of $(00l)$ clay planes are visible (marked by '$*$'). This is arising due to the ordered intercalation effect of PSC chains into clay layers.[110, 199, 233] It can also be observed that with increasing concentration of mMMT the intensity of (001) reflection is increasing. This increasing intensity is reflecting the increasing percentage of clay in PNCE samples. Characteristic peak of PEO does not show any significant change, confirming that due to intercalation phenomena there is no major change in the structure of PEO.[198] Finally as characteristic reflections of both PEO and mMMT are found in the XRD patterns of PNCE, *i.e.* the identity of both components are preserved; hence the PNCE samples are composite in nature.

6.3.2 Surface Morphology

Figure (6.2) shows SEM micrographs of the polymer salt complex, and different PNCEs having compositions PEO_{20}-$LiCF_3SO_3$- x wt.% mMMT ($x = 3, 5, 8, 10\&20$). The micrograph of the polymer-salt complex, shown in figure (6.2a), clearly shows the presence of distinct spherulites. Characteristics lamellar microstructure can be observed in the

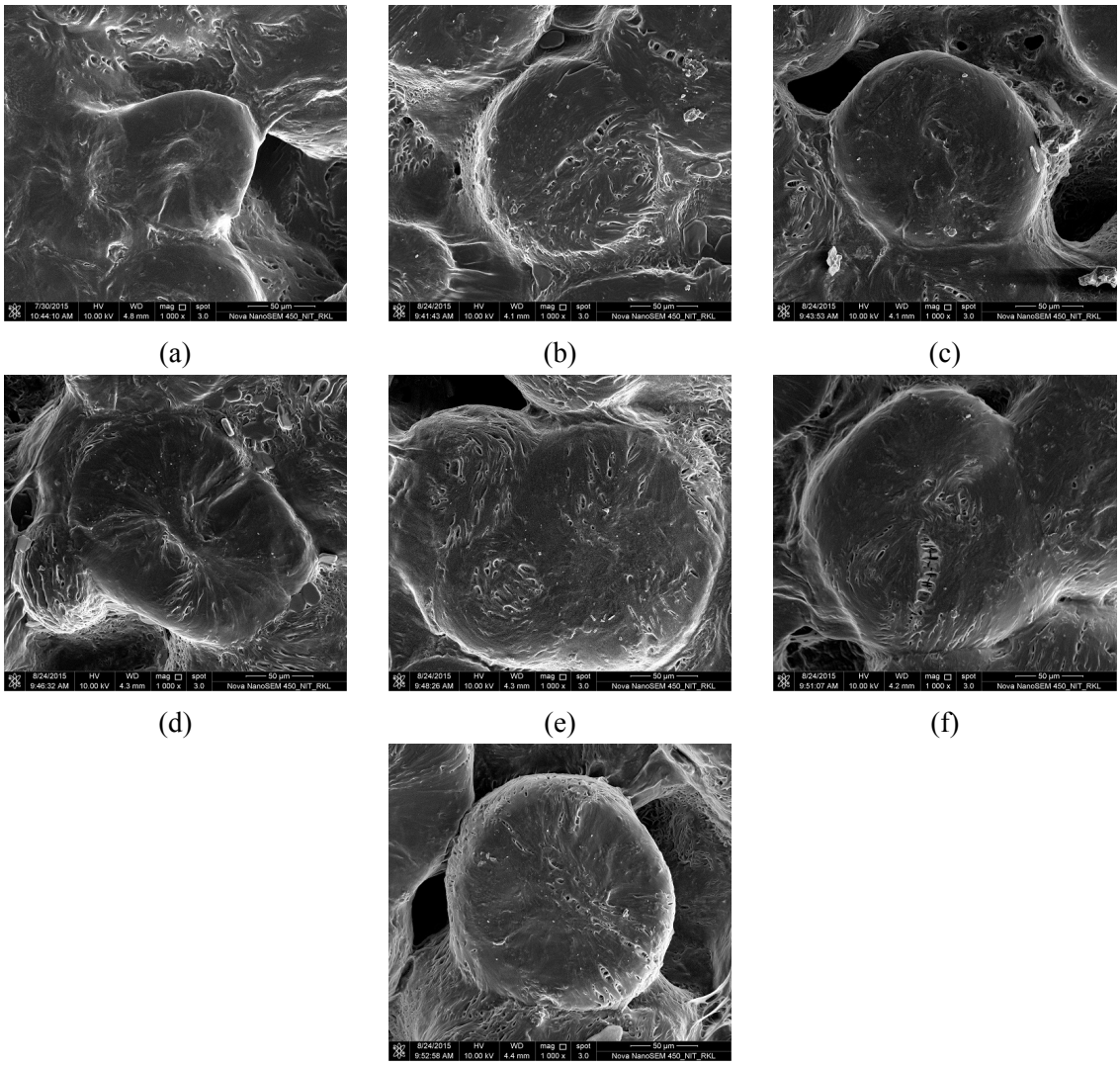

(a) (b) (c)

(d) (e) (f)

(g)

Figure 6.2: Scanning electron micrographs of PSC and mMMT clay based polymer nano-composite electrolyte samples. (a) Polymer salt complex, (b) $x = 2$, (c) $x = 3$, (d) $x = 5$, (e) $x = 8$, (f) $x = 10$ and (g) $x = 15$ wt.% mMMT clay based compositions.

spherulites and they represent the crystalline domain in the samples. The size of the spherulites is found around $60 - 70$ μm in diameter for PSC and PNCEs under investigation. The boundary between the spherulites represents the presence of amorphous phase in these samples.[234] With the addition of mMMT filler no substantial change in the morphological feature *i.e.*, spherulite texture can been observed as shown in figure (6.2b) to (6.2g). However, the fillers are found to be embedded in the polymer matrix forming composite samples. These surface micrographs of PNCEs, which reveal the presence of crystalline spherulites along with amorphous boundary region, indicate that the PNCE films are of semi-crystalline in nature.[234] This inference is also as suggested by X-ray diffraction patterns where co-existence of an amorphous hump and the characteristic peak of the crystalline region can be observed.[235]

6.3.3 Vibrational Study

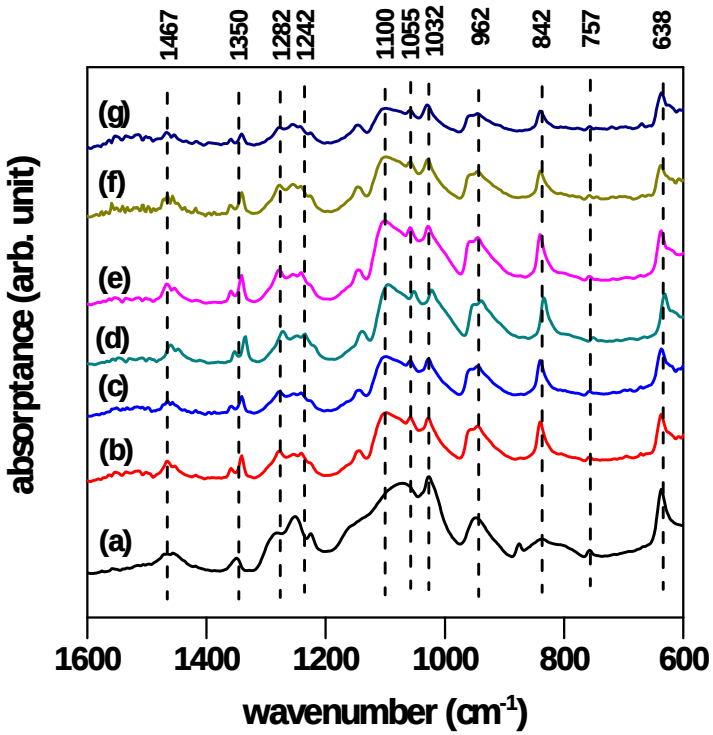

Figure 6.3: FTIR spectra of PSC and PNCEs having composition PEO_{20}-$LiCF_3SO_3$- x wt.% mMMT clay, where (a) $x = 0$ *i.e.* PSC, (b) $x = 2$ (c) $x = 3$, (d) $x = 5$, (e) $x = 8$, (f) $x = 10$ and (g) $x = 15$.

Interactions between the ions, host polymer and fillers can be studied using FTIR spectroscopy. FTIR studies can help to study the effect of additive concentration on polymer-salt complex. Polymer-salt complex and PNCEs exhibit characteristic bands of PEO mentioned here. Band around 638 cm^{-1} corresponds to cis C-H wagging mode, 842 cm^{-1} corresponds to cis C-H_2 wagging, 962 cm^{-1} corresponds to stretching of ether bond (C-O) of polymer, 1100 cm^{-1} corresponds to stretching of ether bond (C-O) of polymer, 1282 cm^{-1} corresponds to CH_2 twisting vibration of polymer and 1467 cm^{-1} corresponds to CH_2 scissoring mode. Similarly bads due to $LiCF_3SO_3$ are also identified. These are 1032 cm^{-1} corresponds to symmetric stretch SO_3 vibration of $LiCF_3SO_3$ and 1242 cm^{-1} corresponding to C-F and CF_2- stretching. Comparison of FTIR spectra of PSC and PNCEs reveal the characteristic bands of PEO as well as $LiCF_3SO_3$.[200–202] With varying concentration of ceramic additives focus is to be given on 1032 cm^{-1} to 1055 cm^{-1} band, which corresponds to symmetric stretch SO_3 vibration of $LiCF_3SO_3$ under complexation. Band around 1032 cm^{-1} represents free anions and solvent separated pair vibrations whereas around 1055 cm^{-1} represents $Li_2CF_3SO_3^+$ aggregates.[203] Presence of both the bands can be observed in all these IR spectra, which suggests that dissociated ions do take part in enhancing the ionic conductivity of the composite electrolytes.[204]

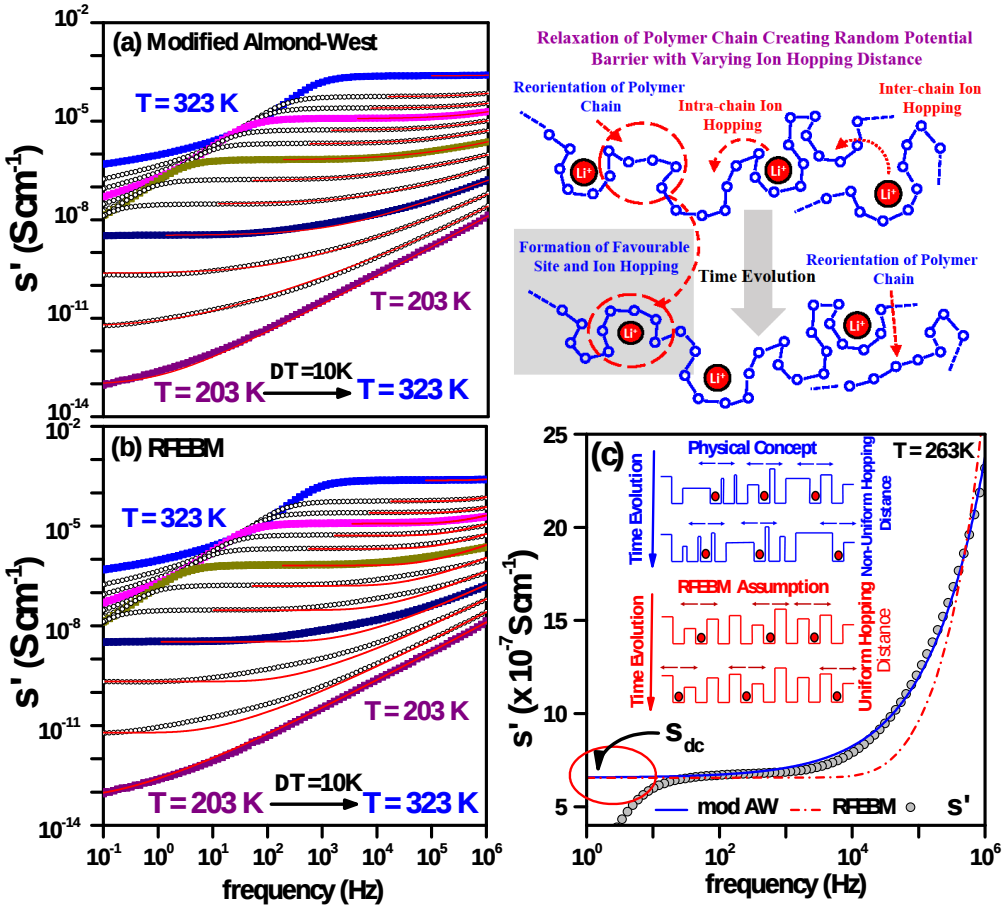

Figure 6.4: AC conductivity as a function of frequency for the PNCE composition PEO_{20}-$LiCF_3SO_3$- 8 wt.% mMMT at temperature ranging from 203 K to 323 K. (a) Phenomenological approach (Modified Almond-West) and (b) Random Free Energy Barrier Model used for analysing conductivity spectra. Represented curves are temperature dependent having interval of 10 K. (c) Comparison between Modified Almond-West and Random Free Energy Barrier Model approach at T = 263 K.

6.3.4 AC Conductivity Study

Electrical conductivity spectra provide information on ion dynamics in polymer electrolytes. Figure (6.4a) and (6.4b) represent the frequency dependent real part of ac conductivity spectra, σ' for PEO_{20}-$LiCF_3SO_3$- 8 wt.% mMMT over a temperature range from T = 203 K to 323 K and the conductivity data are analyzed and fitted using modified Almond-West (AW) and random free energy barrier hopping model (RFEBM) formalism as representative. Other compositions of the series under investigation show similar behaviour. The real part of ac conductivity spectra shows three distinct regions. Due to the accumulation of charge carriers at the electrode-electrolyte interphase sharp decrease in conductivity is observed in the low-frequency region of the spectra giving rise to electrode polarization phenomenon. In the mid-frequency region, σ' becomes nearly independent of frequency and corresponds to dc conductivity. At higher frequencies due to increasing probability of short range ionic motion, σ' start to increase rapidly and a dispersive region is observed. With increasing

temperature, the crossover frequency from the dc conductivity to the dispersive nature of conductivity spectra is shifting towards higher frequencies. This crossover frequency indicates the beginning of conductivity relaxation process. It can also be observed that at very low temperature, σ' spectra become nearly linear over the entire frequency range under investigation. This behaviour of conductivity isotherm at low temperatures indicate the presence of second universality or NCL in PNCE. Real part of ac conductivity spectra is analysed using two different formalisms, (i) phenomenological modified double power law in Almond-West formalism[236, 237] and (ii) random free energy barrier model.[139] Double power law in Almond-West formalism is given below[191, 238]

$$\sigma' = \sigma_{dc}[1 + (f/f_c)^n] + Bf \tag{6.1}$$

Using this modified AW approach, σ' spectra are analysed and the fitted results, shown as solid lines, are given in figure (6.4a). Literature suggests a very close relation between the crossover frequency, f_c obtained from modified AW formalism and ion hopping frequency, f_H obtained from NE relation, *i.e.* $f_c \approx f_H$.[239]

$$\sigma_{dc} = \frac{nq^2\gamma\lambda^2}{k_B T} H_R \omega_H \tag{6.2}$$

where, n is the concentration of mobile charge carriers, q is the ionic charge, γ is a geometrical factor for ion hopping, λ is hopping distance, k_B is Boltzmann constant, ω_H ($= 2\pi f_H$) is hopping rate and H_R is Haven's ratio. In simplified form equation (6.2) can be expressed as

$$\sigma_{dc} = KT^{-1}\omega_H \tag{6.3}$$

The mobile concentration factor, $K(= \frac{nq^2\gamma\lambda^2}{k_B} H_R)$ can be evaluated using σ_{dc} and estimated hopping rates, ω_H.[107] The values of K for PEO_{20}-$LiCF_3SO_3$ and PEO_{20}-$LiCF_3SO_3$-5 wt.% mMMT at different temperatures are presented in table (6.1). With increase in temperature, K increases, which is attributed to the increased free Li^+ ion concentration. When compared, K is found higher in case of PEO_{20}-$LiCF_3SO_3$- 5 wt.% mMMT than that of PSC. This increased mobile concentration factor in the presence of mMMT indicates that addition of mMMT helps in creating a favourable environment for better ion dissociation resulting in increased dc conductivity.

On the other hand from the RFEBM fitted results, shown in figure (6.4b) it can be observed that at very low temperature the experimental data justify the RFEBM results quite well but with increasing temperature there is some difference between experimental data and predicted RFEBM results. RFEBM equation is given below[194, 240]

$$\sigma' = \frac{\sigma_{dc}\omega\tau_e \tan^{-1}(\omega\tau_e)}{1/4\left[ln(1+\omega^2\tau_e^2)\right]^2 + \left[\tan^{-1}(\omega\tau_e)\right]^2} \tag{6.4}$$

A comparative discussion between modified AW and RFEBM is required to get more

Table 6.1: Mobile Concentration Factor for PSC and PEO_{20}-$LiFC_3SO_3$-5wt.% mMMT.

Temperature	Mobile Concentration Factor	
(K)	PSC	5wt.% mMMT
283	1.291×10^{-10}	1.764×10^{-10}
273	1.024×10^{-10}	1.482×10^{-10}
263	6.580×10^{-11}	1.179×10^{-10}
253	2.004×10^{-11}	8.300×10^{-11}
243	3.908×10^{-12}	6.531×10^{-11}
233	7.011×10^{-13}	3.174×10^{-11}

precise information regarding the ionic transport mechanism in PNCE. Before going to the comparison, let us discuss the possible ways an ion can transport from one position to another. Those are as follows (i) ion jumps from one favourable site to another along the PEO backbone, (ii) ion jumps from one favourable site to another favourable site of a different PEO chain, (iii) at ambient temperature PEO chains are having thermal motion, which can create a new favourable site and destroy an existing favourable site. These possibilities are shown as schematic in figure (6.4). Apart from the above-mentioned transport process, there exist clay-polymer and clay-ion interactions. A lithium-ion do form coordinate bonds with ether oxygen of PEO; as a result charge carriers are facing energy barriers decomposed into the Coulombic interaction between the ions and host network.[241, 242] Therefore, the motion of ions is supposed to be coupled with dynamics of the host. These energy barriers are best represented using a multidimensional randomly changing potential landscape with varying hopping distances as shown in figure (6.4c)[236]. In RFEBM disorderliness is expressed by the distribution of jump frequencies with equal hopping distances and all the free energy barriers are equally likely. Comparing the fitted spectra in figure (6.4a) and (6.4b); it can be observed that at very low temperature both of them show good fitting to the experimentally obtained data but with an increase in temperature there exist some deviation in RFEBM fitted results as discussedearlier. In figure (6.4c) a comparative study between modified AW and RFEBM is shown for σ' at T $=$ 263 K. The frequency dependent ac conductivity data has been analysed using modified AW and RFEBM approach given by equation (6.1) and (6.4) respectively. Using these equations, the ac conductivity isotherms are fitted and various fitting parameters are obtained. The σ_{dc} values obtained from fitted results are found to be 6.558×10^{-7} Scm^{-1} and 6.557×10^{-7} Scm^{-1} respectively for modified AW and RFEBM approach. The obtained values of σ_{dc} are also indicated in figure (6.4c) using the simulated spectra. It can be observed that the σ_{dc} obtained from both the mechanisms are almost equal. This observation is correlated with the equal probability of successful hopping of Li^+ ions in both the mechanism. The difference between experimental and theoretical results may be arising due to the assumption considered in RFEBM approach,

which states that the ion hopping distance of Li^+ ions is equal.[240] This can hold true at very low temperature when host polymer chain becomes rigid, ordered and with the evolution of time a favourable site is neither created nor destroyed. With increasing temperature host polymer chain starts to relax and become flexible thus the ion hopping distance should be varying instead of being equal. Therefore, phenomenological modified AW approach is a better choice to explain the experimentally obtained σ' spectra in the case of PSC and PNCE. Besides, modified AW approach also projects the occurrence of first universality or UDR and second universality or NCL of ion conduction mechanism.[140] First term representing UDR and the second term representing NCL. In brief thermally activated ion hopping in a random potential framework with varying ion hopping distance is a more suitable physical assumption to explain ionic transport mechanism in PNCEs. In this regard, it should also be mentioned that modified AW formalism is not applicable at the very low as well as very high-frequency regime. At very low-frequency regime modified AW do not validate linear response theory, on the other hand, it is physically impossible to get monotonically increasing conductivity at high-frequency regime *i.e.* around terahertz range.[243] Co-existence and crossover from the first to the second universality will be further discussed using Kramer-Krönig approach.[190]

6.3.5 Dielectric Relaxations and Concept of First and Second Universality

Permittivity spectra provide information to understand dielectric relaxation process and ionic conductivity in PNCE. Real and imaginary part of permittivity spectra are shown in figure (6.5a) and (6.5b) respectively for the PNCE composition PEO_{20}-$LiCF_3SO_3$- 8 wt.% mMMT over the temperature range T = 323 K to T = 203 K. Real permittivity, ε' show nearly constant value at high-frequency regions and with decreasing frequency its value is increasing gradually. Imaginary permittivity, ε'' increases monotonically with decreasing frequency and in mid-frequency region it satisfies $\varepsilon'' \propto f^{-1}$ relation, showing dc ion conduction region.[240] At low frequency due to the effects of EP, ε'' shows a sudden rise in magnitude. From conventional complex permittivity analysis, the relaxation phenomena are not clear as relaxation events are masked by high conductivity values of PNCE. Therefore, dc conduction-free dielectric loss approach described in equation (6.5) is adopted and the obtained spectra are shown in figure (6.5c). DC conduction-free dielectric loss formalism is given by the following expression

$$\epsilon''_{der} = -\pi/2 \times \partial\epsilon'/\partial(ln\omega) \approx \epsilon'' \tag{6.5}$$

At very low temperature it can be observed that the dielectric loss is becoming nearly constant as a function of frequency, giving the indication of the presence of second universality or NCL in the case of PSC and PNCE. In order to understand the effect of NCL, Kramer-Krönig

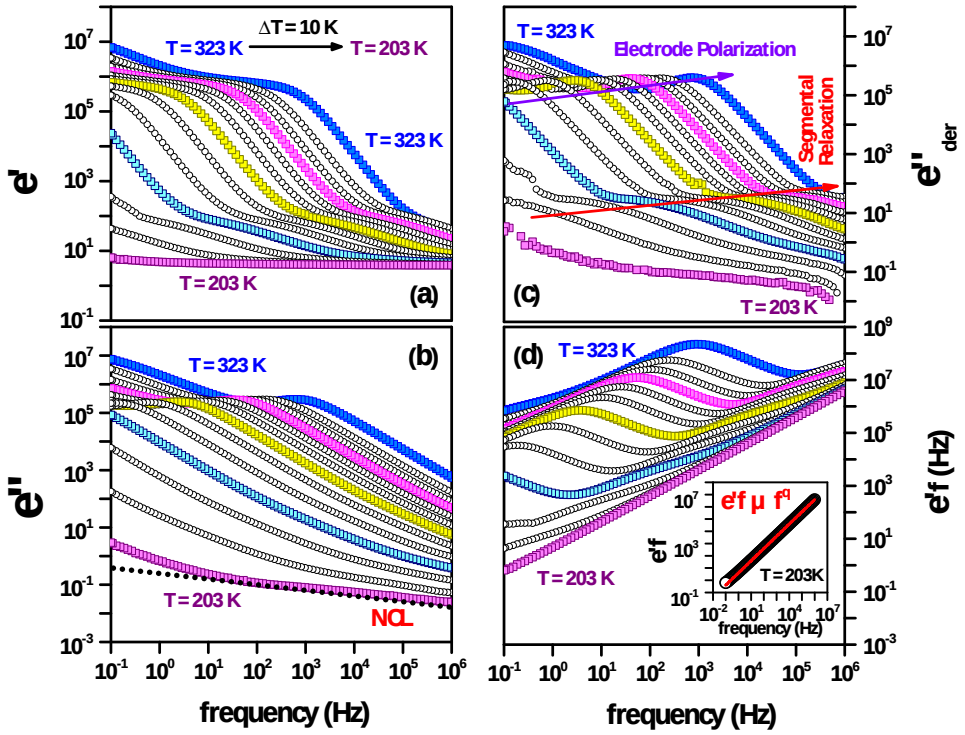

Figure 6.5: Frequency dependent (a) real and (b) imaginary part of permittivity, (c) DC conduction free dielectric loss and (d) $\varepsilon' f$ as a function of frequency for the PNCE composition PEO_{20}- $LiCF_3SO_3$- 5 wt.% mMMT. Represented curves are temperature dependent having interval of 10 K. Inset of panel (d) showing the fitted results at T =203 K.

formalism is used. In this approach, ε' is proportional to f^{q-1}, which can be expressed as[190]

$$\varepsilon' f = B f^q \tag{6.6}$$

where, q is the exponent. If the second universality is dominating over the first universality in ion conduction process; the value of q should be close to unity. In figure (6.5d) $\varepsilon' f$ has been plotted as a function of frequency for different isotherms. At sufficiently low temperatures $\varepsilon' f$ becomes nearly linear in nature over the entire frequency range of observation. With increasing temperature the linear region is shifting towards high-frequency regions. Inset of figure (6.5d) shows the fitted results using equation (6.6) at T $= 203$ K. The value of exponent q is found 0.998, which is very close to unity, indicates that at very low temperature the ion conduction process is governed mainly by the second universality. Again with increasing temperature the value of q is found to reduce, which is attributed to the increasing dominance of UDR over NCL in ion conduction process.[190] Therefore UDR and NCL together only can represent the ion conduction process in this class of material.

6.3.6 Temperature Dependence of DC Conductivity

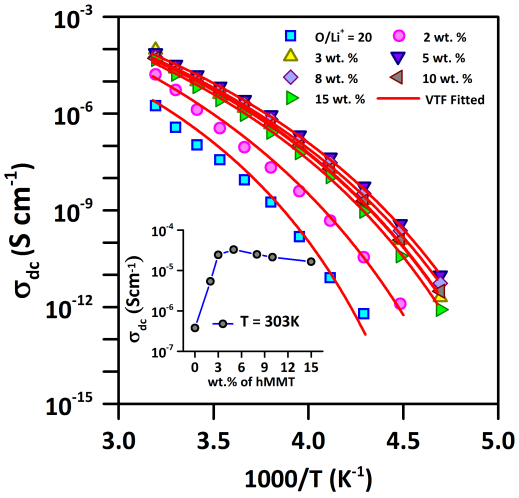

Figure 6.6: Temperature dependent dc conductivity in inverse temperature scale for polymer salt complex and PNCE compositions PEO_{20}- $LiCF_3SO_3$- x wt.% mMMT (x = 2, 3, 5, 8, 10 & 15). Inset showing the dc conductivity of various compositions of PNCE at T = 303 K.

Temperature dependent dc Conductivity for different compositions of PNCE obtained from modified AW formalism is shown in figure (6.6). It is clear that the samples exhibit non-Arrhenius dependence and can be best represented by Vogel-Tammann-Fulcher (VTF) relation given below.[223, 226]

$$\sigma_{dc} = \sigma_0 T^{-1/2} \exp\{-E_A/k_B(T - T_0)\} \tag{6.7}$$

where, σ_0 is the pre-exponential factor, E_A is the pseudo-activation energy, k_B is the

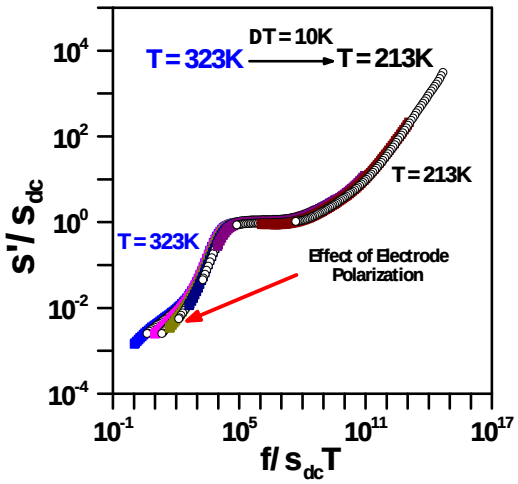

Figure 6.7: AC conductivity scaling with Summerfield approach for PNCE composition PEO_{20}-$LiCF_3SO_3$- 5 wt.% mMMT. Represented curves are temperature dependent having interval of 10 K.

Boltzmann's constant, T_0 the equilibrium glass transition temperature or Vogel temperature. At T $=$ T_0, excess configuration entropy becomes zero, *i.e.*, molecular motions cease. The solid lines in figure (6.6) show the VTF fitted results to the dc conductivity data. The close agreement between VTF fitted and experimentally obtained results over a wide temperature range imply the close coupling among the polymer chain relaxation and the ionic conductivity of the PNCE. Inset of figure (6.6) represents the compositional dependence of dc conductivity at temperature T $=$ 303 K. In the present study, it can be observed that PEO_{20}-$LiCF_3SO_3$- 5 wt.% mMMT show maximum dc conductivity among all composition of PNCE. At T $=$ 303 K dc conductivity of PNCE composition PEO_{20}-$LiCF_3SO_3$- 5 wt.% mMMT is 3.290×10^{-5} Scm^{-1} whereas at the same temperature conductivity of polymer salt complex PEO_{20}-$LiCF_3SO_3$ is 3.760×10^{-7} Scm^{-1}. Hence, with the addition of mMMT clay, σ_{dc} increase by nearly two orders of magnitude. It suggests, with the addition of mMMT clay, a suitable local environment is created for better ion dissociation and better ion mobility, which in turn resulting in higher conductivity. This phenomenon has already been correlated with the behaviour of mobile concentration factor.

6.3.7 Conductivity Scaling

From σ' spectra, it can be observed that there exist a strong frequency dispersion above the characteristics crossover frequency and it is found to be shifting towards higher values with increasing temperature. In addition, it can be observed that the frequency range of the mid frequency plateau region of σ' spectra depends strongly on temperature. This two observation suggest that multiple σ' isotherms can be superimposed to form a single master curve in a process known as time-temperature superposition principle (TTSP) or scaling.[194, 218] To understand the influence of an intrinsic thermodynamic parameter

(in present study temperature) on ion conduction mechanism TTSP is very useful. Scaling approach has already been discussed in chapter (3) section (3.5.1). Summerfield scaling approach is adopted in the present study, in which the scaling parameter is chosen as $\sigma_{dc}T$.[218] According to linear response theory, electrical conductivity is related to time dependent displacement of the mobile ions in thermal equilibrium.[244, 245] If mean square displacement, $< r^2(t) >$ is small or sub-diffusive in nature, ion dynamics are represented by a non-random forward-backward hopping process and in the case of the long-time regime, the ions behave like a random walker. Formation of master curve using Summerfield scaling approach for PNCE composition PEO_{20}-$LiCF_3SO_3$- 5 wt.% mMMT is shown in figure (6.7). A small deviation can be observed at high temperature and low-frequency region, which is due to EP effects. Summerfield scaling suggests that the crossover between sub-diffusive to diffusive behaviour strongly depend on temperature, but the ion conduction mechanism is independent of temperature.

6.3.8 Study of Conductivity Relaxation with Electrical Modulus Formalism

Electrical Modulus Formalism is a widely accepted technique to study the electrical relaxation phenomena as it helps in understanding the ion conduction mechanism and relaxation processes by suppressing the effects of electrode polarization mainly observed at low-frequency regions. Real, M' and imaginary, M'' part of electrical modulus spectra as a function of frequency for temperature range from 263 K to 213 K are shown in figure (6.8a) for PNCE composition PEO_{20}-$LiCF_3SO_3$- 8 wt.% mMMT. It can be observed that with increasing frequency, M' increases gradually. At very high frequency M' should get saturated, but due to frequency limiting of the experimental setup used, we do not observe proper saturation of M' spectra. However, at very low temperatures and high-frequency limits, M' spectra show nearly saturated behaviour. In the case of M'' spectra, we do observe a distinct peak, which corresponds to the conductivity relaxation process. Below the peak frequency, conducting mobile ions do exhibit long-range mobility and above this ions exhibit confined localized motion. With increasing temperature, the peak of M'' spectra is shifting towards higher frequency values, suggesting fast ionic motion leading to decrease in relaxation time. This observation also suggests that ion conduction process in SPE and PNCEs is thermally activated. It can also be observed that M'' spectra are asymmetric in nature and skewed towards higher frequency side of the maxima. For better understanding about the nature of the conductivity relaxation, complex modulus spectra are analyzed using Havriliak-Negami (HN) function given by[171, 226]

$$M^* = M_\infty + \frac{(M_s - M_\infty)}{[1 + (j\omega\tau)^{\alpha}_{HN}]^{\gamma}_{HN}} \tag{6.8}$$

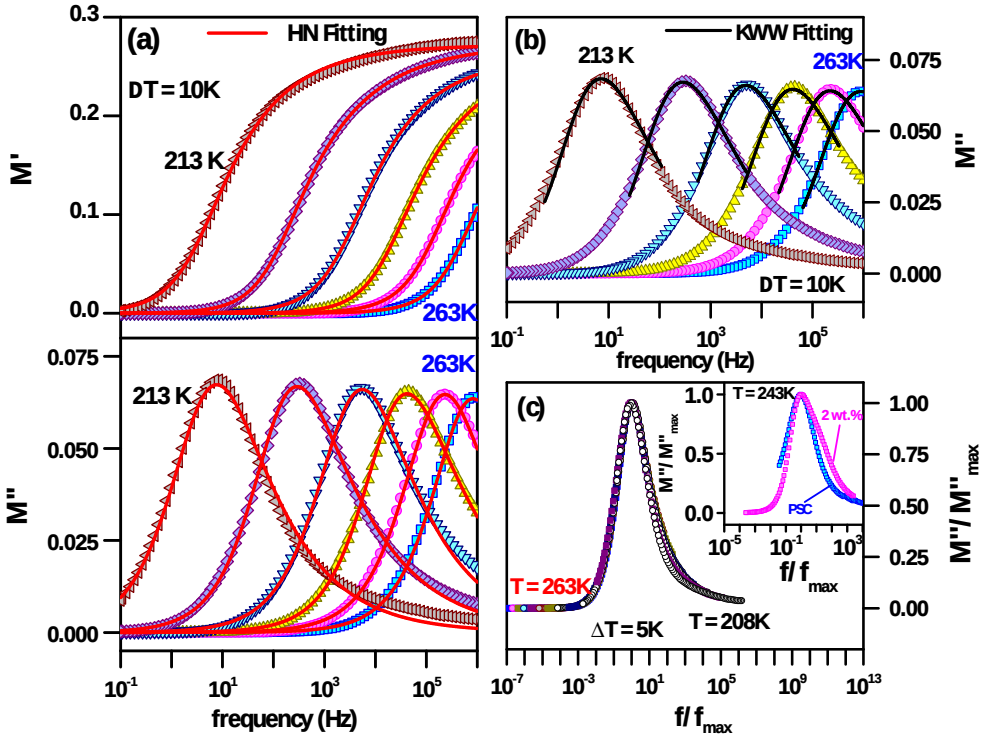

Figure 6.8: (a) Real and imaginary part of electrical modulus fitted with Havriliak-Negami (HN) approach, (b) Imaginary part of electrical modulus fitted with Bergman modified Kohlrausch-Williams-Watts approach. Represented curves are temperature dependent having interval of 10 K. (c) Scaled imaginary part of electrical modulus for the PNCE composition PEO_{20}-$LiCF_3SO_3$- 8 wt.% mMMT. Represented curves are temperature dependent having interval of 5 K. Inset showing scaled imaginary part of electrical modulus for the PSC and 2 wt.% mMMT PNCE composition at T = 243 K.

where, M_∞ and M_s are the high and low frequency limiting values of electrical modulus spectra respectively, τ corresponds to the relaxation time, α_{HN} and γ_{HN} are the shape parameters. For Debye type of interactions both the shape parameters should be unity; in general, they follow the relation $0 < \alpha_{HN} \leq 1$ and $0 < \alpha_{HN}\gamma_{HN} \leq 1$.[226] From the fitted results values of α_{HN} and γ_{HN} are calculated and found to be less than unity, suggesting non-Debye type in nature of the relaxation phenomena. The solid lines which are shown in figure (6.8a) are representing the HN fitted results of complex modulus. In another approach, Bergmann modified Kohlrausch-Williams-Watts (KWW) equation given below is used to analyze imaginary electrical modulus spectra.[107, 215]

$$M'' = \frac{M''_{max}}{(1-\beta_{KWW})\left(\frac{\beta_{KWW}}{1+\beta_{KWW}}\right)\left[\beta_{KWW}(f_{max}/f) + (f/f_{max})^{\beta_{KWW}}\right]} \tag{6.9}$$

where, β_{KWW}, M''_{max} and f_{max} are the shape parameter, maxima of modulus spectra and frequency at which modulus maxima is observed respectively. KWW fitted lines are shown in figure (6.8b). Literature suggests KWW fit is not very much successful for

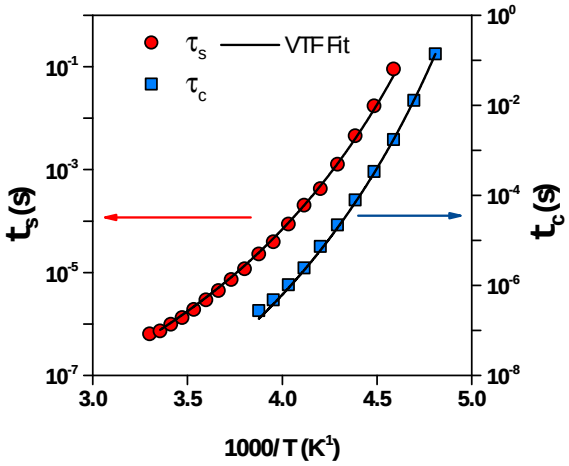

Figure 6.9: Temperature dependent conductivity and segmental relaxation time for the PNCE composition PEO_{20}- $LiCF_3SO_3$- 5 wt.% mMMT.

the high-frequency wing of M'' spectra.[246] Hence, fitting is focussed around the M'' peak. The value of β_{KWW} is found in the range of 0.45 to 0.55 inferring the nature of relaxation phenomena are of non-Debye type in nature as suggested by HN analysis of electrical modulus. The low values of β_{KWW} also suggest that the relaxations are highly non-exponential and Li^+ ion movement in PSC and PNCE is a cooperative phenomenon *i.e.* hopping off a mobile ion from one favourable site to another can not be considered as an isolated event.[226] Havriliak-Negami and Bergmann modified KWW approaches can be regarded as essentially the same if HN and KWW fitting parameters are following the relation $\beta_{KWW} = (\alpha_{HN}\gamma_{HN})^{1/1.23}$.[194, 226] In the present study it is found that the fitting parameters do obey the above-mentioned relation. Hence, either of the representation is valid to discuss complex modulus spectra and is having the same physical significance. The scaled M'' spectra is shown in figure (6.8c) for PEO_{20}-$LiCF_3SO_3$- 8 wt.% mMMT. Formation of a single master curve for a particular composition of PNCE over a wide range of temperature suggest that conductivity relaxation phenomenon is a temperature independent dynamic process. Inset of figure (6.8c) represents the same scaling approach in case of PSC and 2 wt.% mMMT composition at T = 243 K. Master curve formation in this regard is not successful and β_{KWW} parameter also found varying with different composition of PNCE. This indicates the presence of clay fillers modify the polymer chain arrangements and alter the local environment of host polymer in PNCE.[107]

6.3.9 Study of Temperature Dependent Relaxations Time

Relaxation time can be obtained by taking the reciprocal of the angular frequency of different relaxation peaks. Conductivity relaxation time, τ_c and segmental relaxation time,τ_s obtained from electrical modulus analysis and dc conduction-free dielectric loss formalism respectively,[212] are analysed further to get more idea about the conduction process in

PNCE. In figure (6.9) τ_c and τ_s for PEO_{20}-$LiCF_3SO_3$- 5 wt.% mMMT are plotted as a function of inverse of temperature in absolute scale. It is evident from the plot that, with decrease in temperature both, τ_c and τ_s increases and these two relaxation times follow VTF behaviour given by the following equation.[199, 211]

$$\tau = \tau_0 \, exp \left\{ \frac{E_A}{k_B(T - T_0))} \right\} \tag{6.10}$$

where, τ is relaxation time, τ_0 is pre-exponential factor, k_B is the Boltzmann's constant, T is absolute temperature, T_0 is Vogel temperature and E_A is the pseudo-activation energy. VTF behaviour of τ_c and τ_s infer a close correlation between ion conduction mechanism and segmental relaxation process in PSC and PNCEs. The obtained activation energy and Vogel temperatures for the VTF fitted results are shown in table (6.2)

Table 6.2: VTF fitted parameters obtained from temperature dependent conductivity, conductivity relaxation time and structural relaxation time plots of PNCE compositions. Maximum error limit obtained are stated in parenthesis for each set of parameters.

Composition (x wt.% mMMT)	σ VTF Fit		τ_c VTF Fit		τ_s VTF Fit	
	E_A(eV) ($\pm$0.002)	T_0(K) ($\pm$1)	E_A(eV) ($\pm$0.002)	T_0(K) ($\pm$1)	E_A(eV) ($\pm$0.002)	T_0(K) ($\pm$1)
x = 2	0.141	178	0.134	171	0.119	176
x = 3	0.132	169	0.126	168	0.114	169
x = 5	0.126	166	0.123	165	0.112	164
x = 8	0.131	170	0.128	167	0.118	170
x = 10	0.133	171	0.131	170	0.129	174
x = 15	0.143	172	0.139	173	0.145	174

6.3.10 Coupled Ionic Conduction Mechanism with Ratner's Classical Approach

In the case of coupled systems where ionic conduction process is coupled with the segmental relaxation equation (3.24) and equation (3.25) should hold true.[196] In figure (6.10), $D\tau_s$ and $\sigma_{dc}T\tau_s$ has been plotted as a function of relaxation time for PNCE composition PEO_{20}-$LiCF_3SO_3$- 8 wt.% mMMT. It can be observed from the plot that both $D\tau_s$ and $\sigma_{dc}T\tau_s$ remain nearly constant over a wide range of temperature. In fact, the variation of only one order is observed in both the case over the entire temperature range of investigation *i.e.* from T = 323 K to T = 203 K. Therefore from figure (6.10) it can be inferred that ionic transport mechanism is coupled with segmental relaxation. In other words, spatial rearrangements of polymer chains of host polymer are facilitating the ionic conductivity of PNCEs under

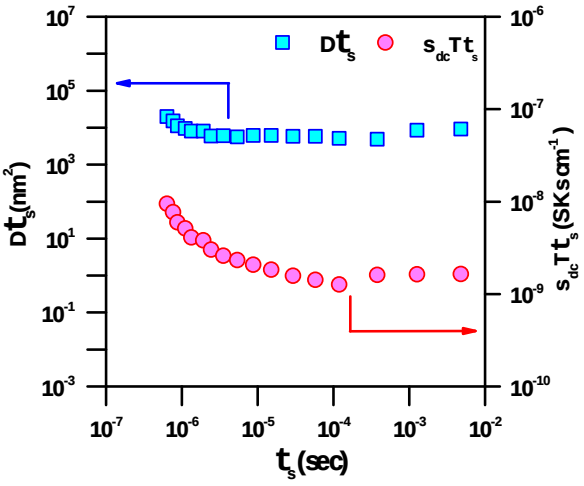

Figure 6.10: $D\tau_s$ and $\sigma_{dc}T\tau_s$ as a function of τ_s for the PNCE composition PEO_{20}-$LiCF_3SO_3$- 8 wt.% mMMT.

investigation.

6.4 Conclusions

A series of polymer nanocomposite electrolytes are synthesized using conventional solution casting technique. Polymer salt complexation and composite formation upon adding organo-modified montmorillonite clay to PSC are confirmed using XRD analysis. Surface morphology is studied using FE-SEM. Vibrational characterization is carried out in the mid-infrared region. Temperature dependent electrical measurements are performed using broadband dielectric spectroscopy. The important observations of this study are as follows

- Clay modification, PSC and PNCE formation are confirmed by XRD analysis.
- At 303 K the maximum value of σ_{dc} is found to be 3.29×10^{-5} Scm^{-1} for PEO_{20}-$LiCF_3SO_3$-5 wt.% mMMT clay composition, which is two order magnitude higher than pure polymer salt complex.
- Phenomenological modified Almond-West, and random free energy barrier model formalisms have been used to explain the behaviour of conductivity isotherms. A comparative study suggests that ion conduction takes place in a spatially varying random potential landscape with different ion hopping lengths in the case of PSC and PNCEs.
- Temperature dependent dc conductivity, conductivity relaxation time as well as segmental relaxation time follow VTF behaviour, suggesting a strong correlation between ion conduction process and polymer segmental relaxation process.

- The presence of both the first and second universality *i.e.* UDR and NCL are shown with the help of conductivity and dielectric loss spectra.
- By using Kramer-Krönig approach it is found that at the low-temperature regime, NCL dominates over UDR and at the high-temperature regime, UDR dominates over NCL.
- Summerfield scaling approach is used to explore the effect of temperature on ion conduction mechanism. It is found that the ion conduction mechanism is independent of temperature.
- Scaled modulus spectra also support the inference drawn from conductivity scaling *i.e.* ion conduction mechanism is a temperature-independent process though it is a thermally-activated phenomenon.
- The coupled nature of ion conduction mechanism and polymer segmental motion has been studied with classical Ratner's approach in combination with Stokes-Einstein relation. As a whole ion conduction and segmental relaxation are coupled phenomena *i.e.* ionic transport process is favoured with spatial rearrangements of polymer chains of host polymer in the case of PSC and PNCE.

Chapter 7

Ion conduction Process in PMMA and PVDF-HFP Blend based Gel Polymer Electrolyte.

7.1 Introduction

So far in previous chapters focus is given on explaining the ion conduction mechanism of composite polymer electrolytes comprising of different classes of filler. It can be observed that using different types of fillers; ionic conductivity can be improved by two orders of magnitude as compared to pure polymer salt complex at room temperature. Apart from the composite formation, another way to increase the ionic conductivity is by using the concept of gel polymer electrolyte.[247–249] At the macroscopic level, gels show solid like properties and at the microscopic level it shows liquid-like properties.[250, 251] Among different possible combinations found in literature, a blend based system is chosen to prepare gel polymer electrolyte. Optimizing blend composition, the physical properties of microporous membranes can be controlled easily.[252] Using phase inversion technique a series of polymers microporous membranes are prepared.[253] These microporous membranes can absorb liquid electrolyte to obtain gel polymer electrolyte film. Literature suggests that gel polymer electrolytes prepared by phase inversion technique can exhibit better ionic conductivity only if it is capable of absorbing more amount of liquid electrolyte during gel formation.[254] Thus the liquid uptake capability of the polymer blend films needs to be optimized by maximizing their micro-porosity.[255, 256] Liquid electrolyte absorption and retention capability of microporous membranes depend mainly on the porous nature of the membrane, pore size and pore distribution. Prior importance should also be provided for the compatibility of blending polymers while preparing gel polymer electrolyte in phase inversion technique.

Polymethyl methacrylate (PMMA) is widely used as a polymer matrix to prepare microporous gel polymer electrolytes. PMMA possess good compatibility with the liquid component entrapped in its matrix.[257] However, it suffers the problem of poor mechanical stability. This poor mechanical strength can be improved by blending PMMA with poly (vinylidene fluoride-co-hexafluoropropylene) (PVdF-HFP).[258] In various polymer

blends, PMMA can act as an interpenetrating phase, which prevents the absorbed electrolyte from leakage.

In this study, PVdF-HFP and PMMA based blended polymer matrices are synthesized through the phase inversion technique. A mixture of acetone and N, N-dimethylformamide is used as a solvent, taken in $1:1$ volumetric ratio. The stoichiometric amount of polymers are added to the mixed solvent and stirred for 12h. In this process, a clear solution of polymers is prepared, which is then cast on a glass petri dish and vacuum dried for another 12h to obtain a free-standing film. The prepared blend polymer membranes are then soaked in 1 molar $LiCF_3SO_3$ solution of ethylene carbonate and diethyl carbonate mixture, taken in $1:1$ volumetric ratio, for 12h to make the microporous gel polymer electrolyte. At first, the effect of the proportion of PVdF-HFP to PMMA on the properties of the microporous membrane, such as surface morphology, porosity and the liquid uptake capability are systematically studied. Thereafter, the focus is given on optimizing the ionic conductivity of these gel polymer electrolytes for different blend ratio of the polymers. Ion conduction mechanism of these gel polymer electrolytes is also discussed using the experimental observations of broadband dielectric spectroscopy.

7.2 Synthesis of Materials and Experimental Conditions

Polymer blend based gel polymer electrolytes are synthesized using phase inversion technique. The detailed synthesis procedure is given in chapter (2). The composition of the gel polymer electrolytes under investigation can be represented as $(100-x)$ PVDF-HFP- x PMMA- 1M $LiCF_3SO_3$ in $(1:1)$ EC and DEC. (x = 30, 40, 50, 60 and 70). Porous blended films are analyzed using X-ray diffraction and scanning electron microscopy to study the blend formation and porous nature of the host polymer matrix. FTIR characterization of gel polymer electrolytes is carried out in the mid-infrared region to analyze band structures. Bruker Alpha-E FTIR spectroscope is used for the FTIR analysis. FTIR spectra are recorded in the range of wavenumber from $550\ cm^{-1}$ to $4000\ cm^{-1}$ with $2\ cm^{-1}$ resolution. Broadband dielectric spectroscopy is carried out using PSM-1735 impedance analyzer around ambient temperature, to study the electrical properties and ion conduction mechanism of the gel polymer electrolytes.

7.3 Results and Discussion

7.3.1 X-Ray Diffraction Analysis

Figure (7.1) show the X-ray diffraction patterns of pure PVdF-HFP, PMMA and blend polymer membranes prepared using phase inversion technique. XRD pattern of PVdF-HFP show various characteristic sharp crystalline peaks along with a broad hump around 2θ value $20°$ and $40°$; this observation clearly indicates the semi-crystalline nature of PVdF-HFP. On

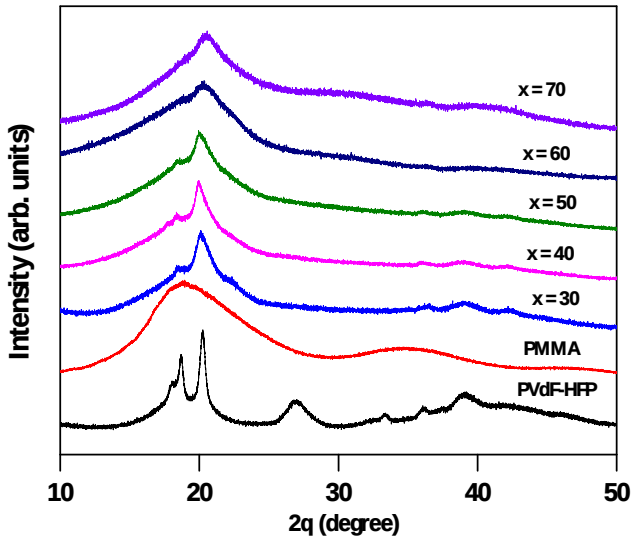

Figure 7.1: X-ray diffraction pattern of micro-porous membranes for pure PVdF-HFP, PMMA and different blending composition of these two polymers, $(100 - x)$ PVDF-HFP-x PMMA (x = 30, 40, 50, 60 and 70).

the other hand, PMMA shows mainly the amorphous characteristics with broad amorphous hump around 2θ value 20° and 35°. With increasing concentration of PMMA in the blend polymer matrices, the amorphous behaviour of the microporous membranes keeps on increasing. Sharp crystalline peaks lose its intensity, but the characteristic presence of both PVdF-HFP and PMMA in the blend microporous membranes can be observed in XRD patterns of all blend polymer membranes.

7.3.2 Surface Morphology and Electrolyte Holding Capability

The surface morphology of the prepared microporous membranes is shown by scanning electron micrographs from figure (7.2a) to (7.2e). It can be observed that the membrane porosity increases with increasing ratio of PMMA in the microporous host polymer membranes. Figure (7.2f) show the cross-sectional view of the microporous host polymer membrane for x = 60 blend polymer electrolyte composition. It can be observed that up to 60 wt.% PMMA composition, porosity increases and thereafter it start to reduce. The decrease in porous nature may be due to the increased physical cross-linking between PVdF-HFP and PMMA.[255] In figure (7.3) the ability to absorb liquid electrolyte by microporous host polymer membranes is plotted. To calculate the electrolyte uptake, the weight of a dry microporous membrane is measured. Thereafter the membrane is submerged in the liquid electrolyte solution for 12h. In this step the dry membrane absorbs electrolyte and gel formation occur. These gel electrolytes are then sandwiched in tissue paper to get rid of excess electrolytes. A weight of 100g is also applied to ensure that additional liquid is

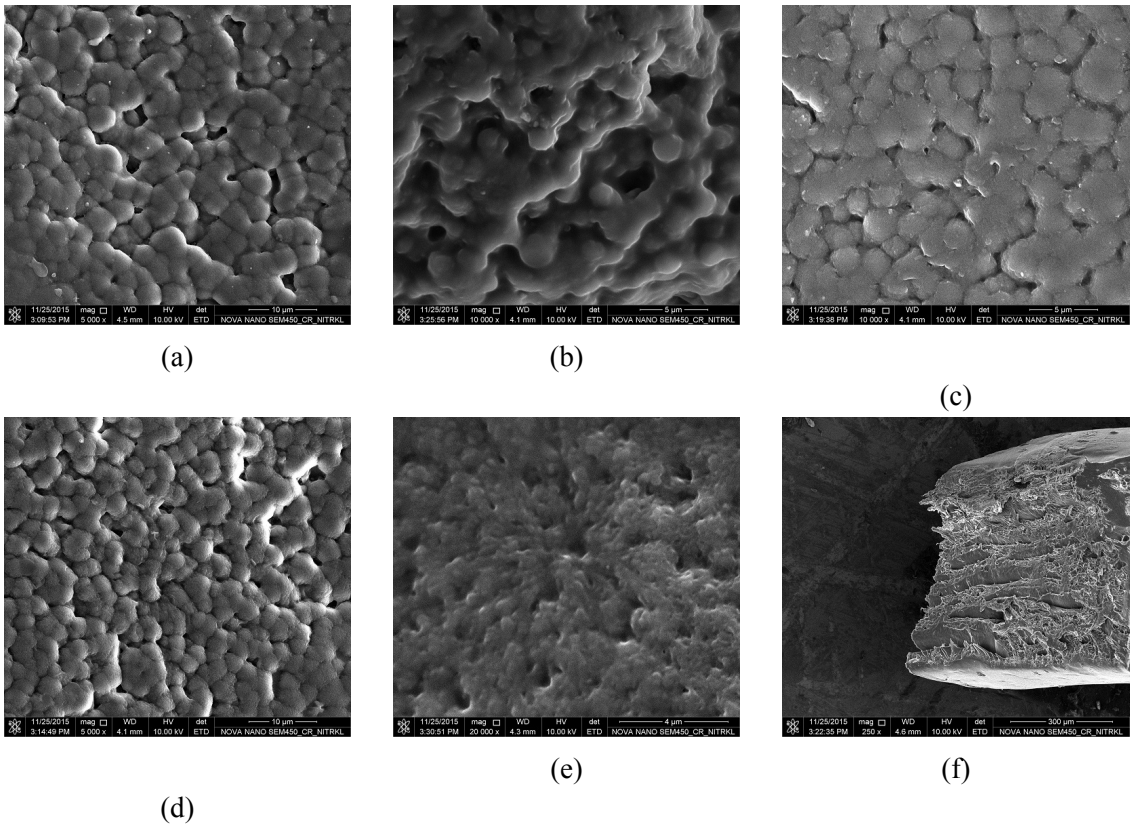

Figure 7.2: FE-SEM micrographs of blend polymer films $(100-x)$ PVDF-HFP- x PMMA. Surface view of (a) x = 30, (b) x = 40, (c) x = 50, (d) x = 60 and (e) x = 70 compositions. (f) Cross-sectional view of x =60 composition.

completely dried from the surface of the gel electrolyte films. Finally, the weight of the gel electrolytes are measured and its liquid electrolyte uptake capacity is calculated using the following relation[258]

$$EU = \frac{W_{gel} - W_{por}}{W_{por}} \times 100 \tag{7.1}$$

where, EU, W_{por} and W_{gel} stands for electrolyte uptake, the weight of porous membrane and weight of gel electrolyte respectively. To get the final result, the same procedure is repeated for thrice, and an average is calculated from the observations. As already mentioned that from FE-SEM micrographs it can be observed that 60 wt.% PMMA composition has maximum pores. Therefore, it should be capable of absorbing and holding the highest amount of liquid electrolytes to form a gel electrolyte. This inference is well correlated with electrolyte uptake results. It is worth mentioning that, the liquid electrolyte uptake capability of the blend polymer matrix is showing the same trend as the change in observed porosity from scanning electron microscopy results.

7.3.3 Vibrational Study

FTIR spectroscopy of $(100 - x)$ PVDF-HFP- x PMMA- 1M $LiCF_3SO_3$ in $(1 : 1)$ EC and DEC. (x = 30, 40, 50, 60 and 70), polymer gel electrolytes are shown in

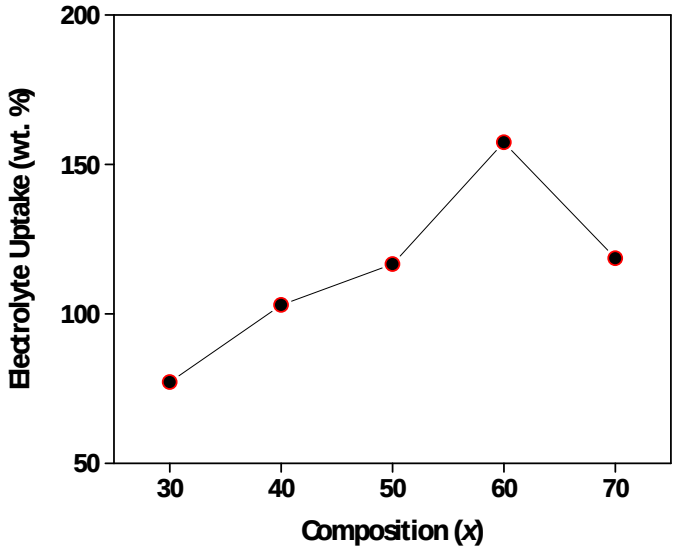

Figure 7.3: Liquid electrolyte uptake capacity as a function of blend polymer electrolyte composition $(100 - x)$ PVDF-HFP- x PMMA- 1M $LiCF_3SO_3$ in $(1 : 1)$ EC and DEC. (x = 30, 40, 50, 60 and 70).

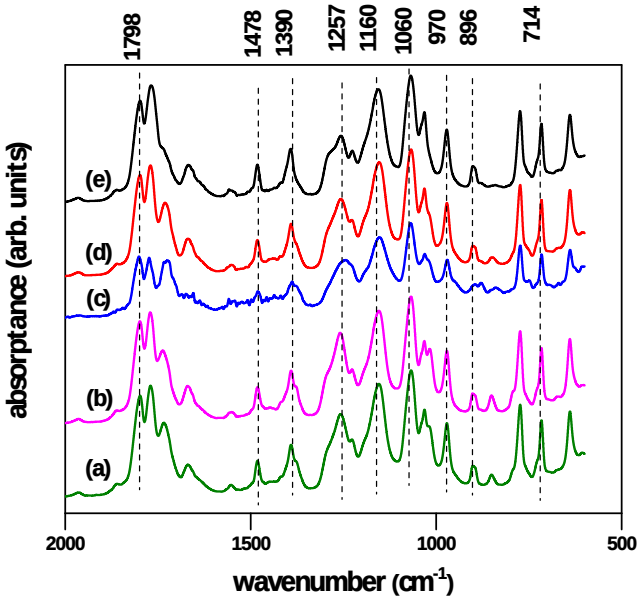

Figure 7.4: FTIR spectra of blended gel polymer electrolytes. $(100 - x)$ PVDF-HFP- x PMMA- 1M $LiCF_3SO_3$ in $(1 : 1)$ EC and DEC. (a) x = 30, (b) x = 40, (c) x = 50, (d) x = 60 and (e) x = 70

figure (7.4). Gel polymer electrolytes exhibit characteristic bands around 1798 cm^{-1} corresponding to C-O stretching, 1478 cm^{-1} corresponding to CH_2 bending, 1390 cm^{-1} corresponding to CH_2 wagging, 1160 cm^{-1} and 970 cm^{-1} corresponding to skeletal stretch, 1060 cm^{-1} and 896 cm^{-1} corresponding to ring breathing and 714 cm^{-1} corresponding to C-O bending modes.[202, 259, 260] Apart from the above mentioned bands around 1257

cm^{-1} characteristic presence of ionized free anions $CF_3SO_3^-$ and ion agglomeration like $Li^2CF_3SO_3^+$ can also be observed.[203] The presence of both PVdF-HFP, PMMA, EC, DEC, $LiCF_3SO_3$ in all composition leads to a near identical observation for FTIR spectrum of all specimens. On closer observation of it can be observed that the relative intensity of $CF_3SO_3^-$ and $Li^2CF_3SO_3^+$ slightly vary from one composition to another one. This may be also a reason for getting different values of ionic conductivity from various gel polymer electrolytes.

7.3.4 AC Conductivity Study

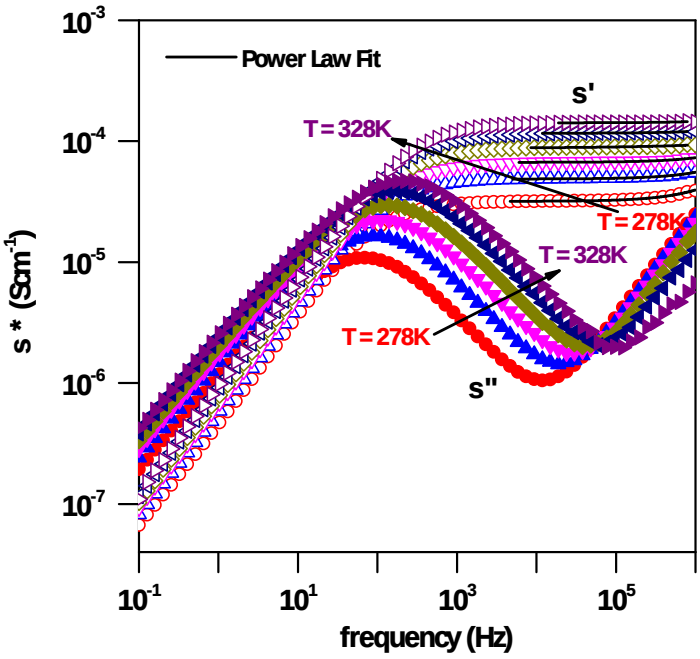

Figure 7.5: Real and imaginary part of ac conductivity spectra for (40) PVDF-HFP- 60 PMMA- 1M $LiCF_3SO_3$ in (1 : 1) EC and DEC, GPE composition over a temperature range from 338 K to 278 K with 10 K interval.

Ion dynamics of the gel polymer electrolyte, samples are investigated using complex electrical conductivity spectra. The real and imaginary part of ac conductivity as a function of frequency over a temperature range from 338 K to 278 K with 10 K interval for 40 PVDF-HFP- 60 PMMA- 1M $LiCF_3SO_3$ in (1 : 1) EC and DEC composition is shown in figure (7.5) as representative. Other composition in the series under investigation show similar behaviour. As mentioned in earlier chapters for composite polymer electrolytes, real part of ac conductivity spectra show three distinct region (i) low frequency dispersive region arising due to electrode polarization, (ii) mid frequency plateau region arising due to long-range ionic motion reflecting as dc conductivity (σ_{dc}) and (iii) high-frequency dispersive region arising due to short range ion hopping. A similar observation is also found

in the present study. A quantitative description of ion conduction process can be presented analyzing the frequency independent plateau and high-frequency dispersion regions of the real part of ac conductivity isotherm. Around ambient temperature, σ' can be fitted using Almond-West power law given by the following equation[107]

$$\sigma' = \sigma_{dc}[1 + (f/f_c)^n] \tag{7.2}$$

where, σ_{dc} is the dc conductivity, f is frequency and "n"is power law exponent having value within $0 < n < 1$. For ionic conductors, in general the value of "n"is found between 0.4 and 0.7.[174] A reasonably good fit is observed when the experimentally obtained data is fitted using equation (7.2). Fitting is carried out excluding the low-frequency regions having the effects of electrode polarization. For 60 wt.% PMMA composition, at T = 303 K, σ_{dc} value is found to be 7.723×10^{-5} Scm^{-1}. The imaginary part of ac conductivity shows a peak representing the electrode polarization phenomenon.[172] The occurrence of peaks in the imaginary part of the complex ac conductivity is reflected as a low-frequency dispersion region in real part of the complex ac conductivity spectra.[261]

7.3.5 Temperature Dependence of DC Conductivity

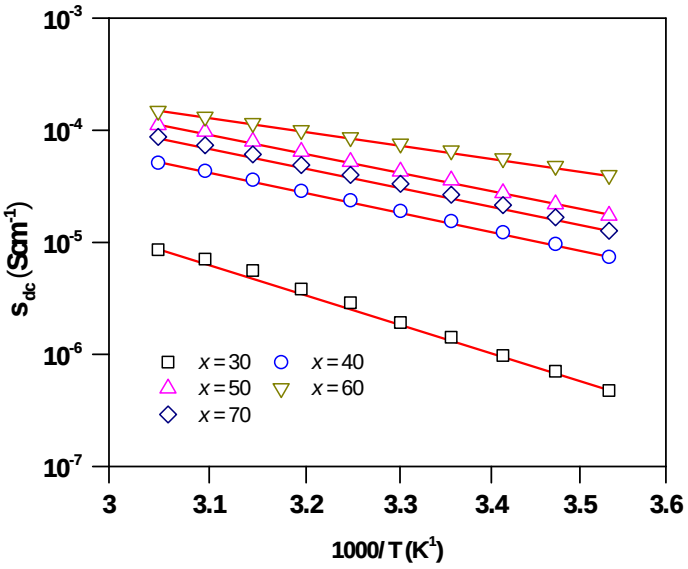

Figure 7.6: Temperature dependent dc conductivity as a function of inverse of temperature in absolute scale for the gel electrolyte compositions $(100 - x)$ PVDF-HFP- x PMMA- 1 M $LiCF_3SO_3$ in $(1 : 1)$ EC and DEC, where x = 30, 40, 50, 60 and 70.

There exist three possible ways for ion migration in the microporous gel polymer electrolytes; these are (i) through liquid electrolytes absorbed and entrapped by host polymer matrix in its micropores, (ii) along the host polymer chains and (iii) through amorphous domain at blend inter-phase of two polymers. Ion migration along the host polymer chains

and through amorphous polymer interphase domain is slower in comparison to that of through liquid electrolytes.[258] Therefore, uptake and entrapment of liquid electrolytes in the microporous polymer membranes plays an important role on the ionic conductivity of gel polymer electrolytes. The dc conductivity values as a function of the inverse of temperature in absolute scale is shown in figure (7.6). It can be observed that σ_{dc} as a function of temperature is showing Arrhenius behaviour given in equation (7.3), instead of VTF behaviour.[262]

$$\sigma_{dc} = \sigma_0 \exp(E_a/K_bT) \tag{7.3}$$

The Arrhenius equation is used to calculate the activation energy, which is the minimum energy required for all ions transportation across the membrane. The variation of activation energy for different composition, obtained from fitting the experimentally observed data using equation (7.3), is shown in table (7.1). It clarifies that ion transport process predominantly occurred through the liquid electrolyte phase trapped in the porous polymer host.

Table 7.1: Activation energy of different compositions of gel polymer electrolytes ($(100-x)$ PVDF-HFP- x PMMA- 1M $LiCF_3SO_3$ in $(1:1)$ EC and DEC, where x = 30, 40, 50, 60 and 70) calculated from dc conductivity results using Arrhenius fitting formalism.

Composition (x)	Activation Energy (eV)
30	0.46
40	0.38
50	0.33
60	0.24
70	0.36

7.3.6 Conductivity Scaling

It can be observed from figure (7.5) that the complex ionic conductivity exhibits a temperature independent profile. Therefore, using time-temperature superposition principle frequency dependent ionic conductivity can be scaled. The scaled spectra are shown in figure (7.7).[224] From the viewpoint of the ionic transport mechanism, the process of conductivity scaling indicates a common physical mechanism irrespective of various intrinsic physical parameters associated with it like temperature. The detailed description of time-temperature superposition principle is given in chapter (3). Here Summerfield scaling formalism is adopted to scaled the frequency dependent ac conductivity results. As mentioned earlier, Summerfield scaling formalism considers dc conductivity and temperature for formation of

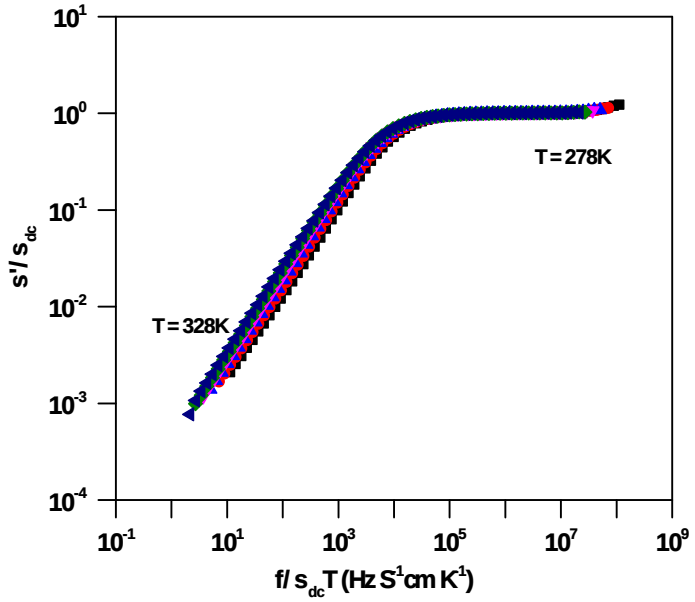

Figure 7.7: Scaled ac conductivity spectra for $x = 60$ GPE composition over a temperature range from 328 K to 278 K with 10 K interval.

master curve, which can be stated in the form of equation given below

$$\sigma'/\sigma_{dc} = F(f/\sigma_{dc}T) \tag{7.4}$$

Scaled ac conductivity spectra are shown in figure (7.7). A successful realization of scaled spectra *i.e.* overlapping of individual spectrum suggest that the ion conduction process is independent of temperature.

7.3.7 Electrical Modulus Analysis

Electric modulus is usually investigated to analyze the conductivity relaxation phenomena in the polymer electrolyte. Modulus formalism of analyzing frequency dependent data has the advantage of eliminating the electrode polarization effects in particular where ionically conducting samples are characterized with blocking electrodes. Figure (7.8a) show the imaginary part of the electrical modulus spectra for 30 wt.% PMMA composition with a temperature range from 278K to 328K. The peak frequency corresponds to the characteristic conductivity relaxation time. With the increase in temperature, the peak observed in the imaginary part of electrical modulus spectra is found to shift towards the higher frequency region. The region where the peak occurs is the indicative point of transition from long range to short range mobility of the charge carriers. The frequency region below peak frequency of modulus spectra determines the range in which charge carriers are mobile over long distances and above the peak frequency the carriers are considered to be confined in potential wells, *i.e.* short range hopping. The imaginary part of electrical modulus is fitted using modified

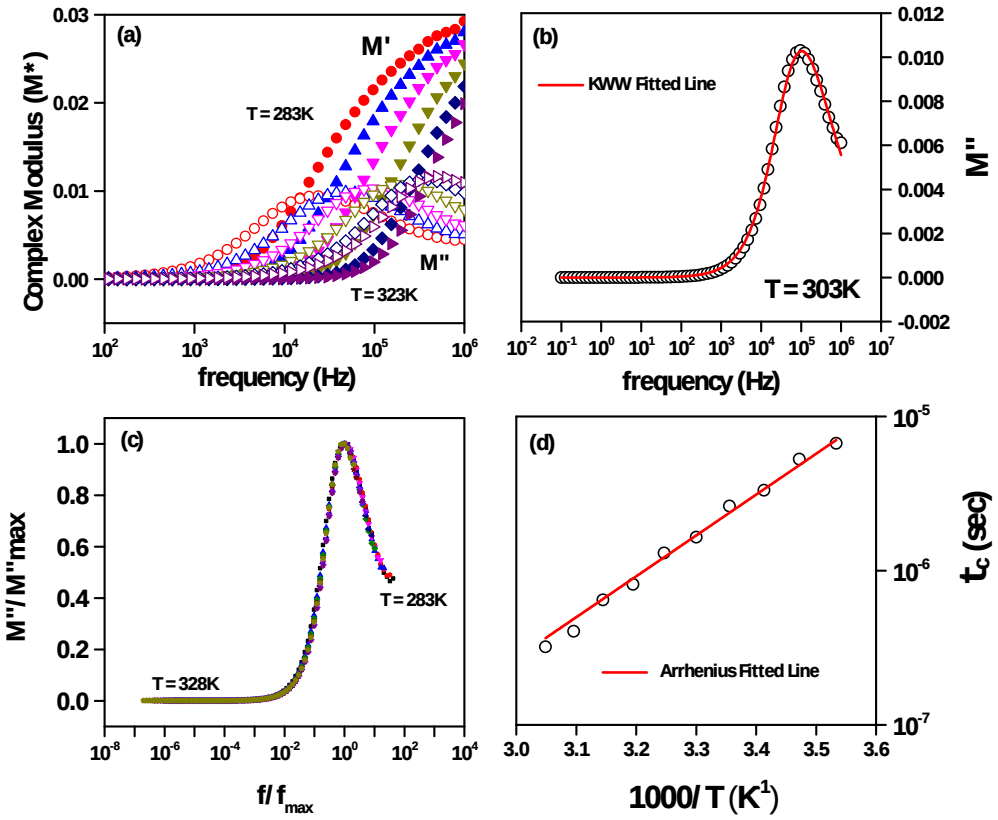

Figure 7.8: (a) Real (filled symbol) and imaginary part (hollow symbol) of electrical modulus as a function of frequency for x = 30 GPE composition over a temperature range from 328 K to 278 K with 10 K interval. (b)KWW fitted imaginary part of electrical modulus spectra at T = 303 K for the same composition. (c) Scaled imaginary part of electrical modulus data over a temperature range from 328 K to 283 K with 10 K interval. (d) Arrhenius fitted results of conductivity relaxation time for the same GPE composition.

KWW equation given by[263]

$$M''(f) = \sum_n \frac{M''_{max,n}}{(1-\beta_n) + \beta_n/(1+\beta_n)[\beta_n(f_{max,n}/f) + (f/f_{max,n})^{\beta_n}]} \tag{7.5}$$

Figure (7.8b) shows the fitted imaginary part of electrical modulus data for 30 wt.% PMMA sample at 288K. The value of stretching parameter β is found 0.59. This suggests the relaxations are non-Debye type in nature.[264] Scaling helps to find the common physical conditions and mechanism of the ionic transport process. Figure (7.8c) show the scaled imaginary part of modulus spectra. A proper overlapping of modulus spectrum suggests ion conduction mechanism is independent of temperature.[265] Figure (7.8d) shows the variation of relaxation time as a function of an inverse of temperature in absolute scale. The variation of relaxation time is found to follow Arrhenius relation. Using Arrhenius fitted results the activation energy for the sample is calculated and the effective activation energy is found to be 0.32eV. For any other compositions, conductivity relaxation time can not be

evaluated as they fall beyond the experimental frequency range of investigation.

7.3.8 Study of the Relative Permittivity and Segmental Relaxation

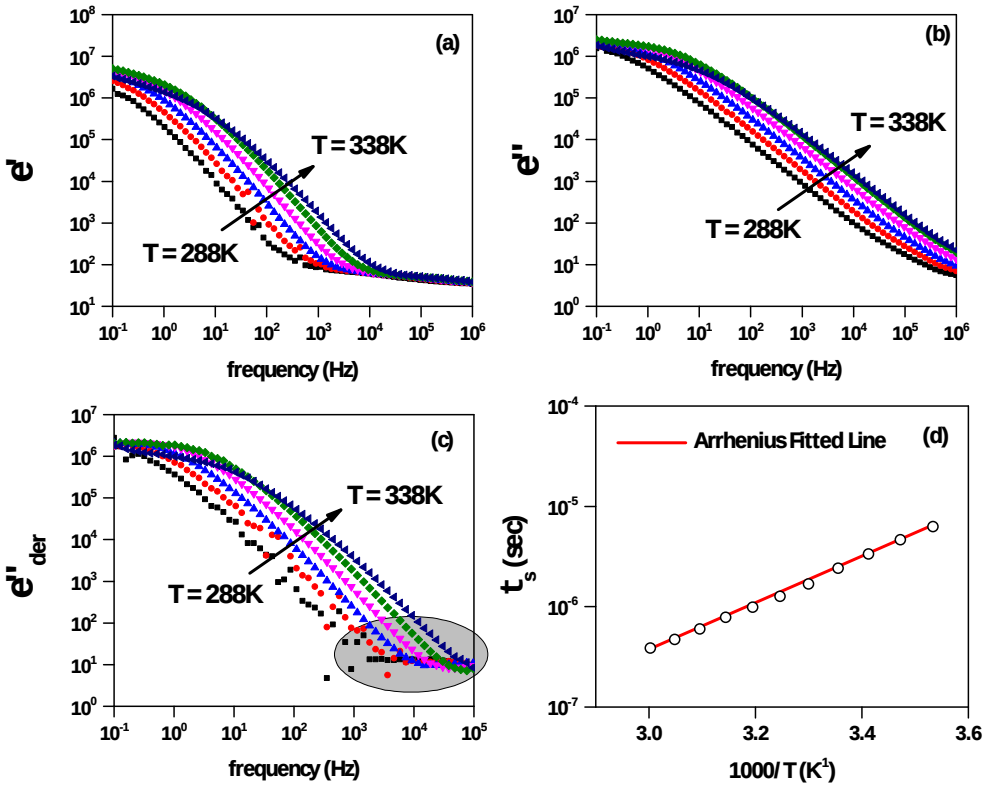

Figure 7.9: (a) Real and (b)Imaginary part of dielectric permittivity, (c) DC conduction free dielectric loss for $x = 30$ GPE composition. (d) Arrhenius fitted results for high frequency relaxation time for $x = 30$ GPE composition.

Relative permittivity exhibits complex behavior in alternating electric fields and can be expressed by $\varepsilon^* = \varepsilon' - j\varepsilon''$, where ε' and ε'' are the real and imaginary parts of the relative permittivity respectively.[264, 266, 267] Figure (7.9a) and (7.9b) represent the real and imaginary part of complex dielectric permittivity for 30 wt.% PMMA composite over the temperature range 288 K to 338 K at an interval of 10 K. The imaginary part of the relative permittivity helps in studying electrode polarization phenomena and different relaxations observed in gel polymer electrolytes. It can be observed that the high-frequency relaxation phenomenon is not clear in the plot of imaginary part of dielectric permittivity plot as a function of frequency. Therefore, to study the high-frequency relaxation phenomena, dc conduction-free dielectric loss approach is adopted, which is shown in figure (7.9c). In dc conduction-free dielectric loss approach, both the relaxation phenomenon *i.e.* low-frequency electrode polarization and high-frequency polymer segmental relaxation are clearly visible.[268] From the high-frequency segmental relaxation process, the relaxation

time is calculated and are represented as a function of absolute temperature in figure (7.9d). Relaxation time is found obeying Arrhenius relationship, which indicates that ion conduction mainly takes place through the liquids electrolytes entrapped in host polymer matrix. Polymer host does not play any significant role in ion conduction phenomena. The presence of high-frequency relaxation can only be observed for 30 wt.% composition. For other compositions of the GPE series, the high-frequency relaxation falls beyond the limit of the investigation.

7.4 Conclusions

The gel polymer electrolyte based on microporous PVdF-HFP and PMMA blend polymer membrane is synthesized and characterized using various experimental conditions with a wide range of investigation limits. Organic liquid electrolyte made of ethylene carbonate and diethyl carbonate is taken in $1:1$ volumetric ratio having 1 molar $LiCF_3SO_3$ dissolved in it and is used to charge the microporous membranes to prepare the gel electrolytes. The effect of the ratio of PVdF-HFP to PMMA on surface morphology, membrane porosity and the liquid uptake and retention capability of the microporous membrane are systematically studied. Temperature dependent electrical properties and ion conduction mechanism are also studied for the gel polymer electrolytes. The important observations of this study are as follows

- By varying the ratio of polymers microporous films can be prepared with different surface morphology, porosity, electrolyte absorb capability etc.
- PMMA is capable of working as an interpenetrating polymer network, which helps in increasing the porous nature of electrolyte samples.
- Ionic conductivity is optimized as a function of blending ratio. For 40 wt.% PVdF-HFP and 60wt.% PMMA the maximum ionic conductivity can be observed having value 7.77×10^{-5} Scm^{-1} at 303K.
- Liquid electrolyte uptake capacity is correlated with ionic conductivity of the gel polymer electrolytes.
- Ion conduction mainly takes place through the liquid electrolytes entrapped into the gel polymer matrix.
- DC conductivity and observed relaxations are found to follow Arrhenius relationship, which suggests host polymer relaxation do not play a crucial role in ion conduction process. Polymer host does provide the mechanical strength and ion conduction mainly take place through the liquid electrolyte entrapped in host polymer matrix in gel polymer electrolyte membranes.

Chapter 8

Conclusions and Future Scope

8.1 Conclusions

In the present investigation, electrical properties and relaxation dynamics of polymer composite electrolytes and gel polymer electrolytes are studied. Ionic conductivity of composite polymer electrolytes are optimized based on the filler concentration, whereas for gel polymer electrolytes it is optimized based on the blend ratio of the host polymer matrix. Ion conduction mechanism of both composite polymer electrolytes and gel polymer electrolytes are investigated using different formalisms.

Based on the optimization conditions, characterization and experimental results of the analyzed data, the following conclusions are drawn:

- Single phase nanocrystalline ceramic fillers are synthesized using chemical synthesis routes. Auto-combustion technique is used for the preparation of tetragonal zirconia and for anatase titania synthesis acrylamide gel polymer template technique is employed. The synthesis of pure phase materials is confirmed using X-ray powder diffraction analysis.

- Cation exchange reaction is carried out to modify montmorillonite clay. Organo-modified montmorillonite clay is used as a layered clay filler for the preparation of composite polymer electrolyte. CTAB (cetyltrimethylammonium bromide) in protonic medium is used as modifier in the cation exchange reaction. In this technique Na^{+} and Mg^{2+} ions are replaced by the cetyltrimethylammonium ions in the channel region of montmorillonite clay layers.

- Polymer composite electrolytes are prepared using polyethylene oxide (PEO) as host polymer, lithium triflate ($LiCF_3SO_3$) as salt and nano-crystalline zirconia, anatase titania and organo-modified montmorillonite clay as filler. Among the fillers, zirconia and titania are used for making dispersed phase composite electrolytes while montmorillonite makes intercalation type polymer electrolyte. Titania is having the tendency to weakly attract the anions. The composite and semi-crystalline nature of these materials are studied using X-ray diffraction techniques. Surface morphology is investigated using FE-SEM technique. Broadband dielectric spectroscopy is used

to examine the ionic conductivity and relaxation dynamics over a wide range of temperature and frequency.

- Among zirconia based polymer composite electrolytes, 8 wt.% composition show maximum ionic conductivity at room temperature (RT) (T = 303 K) having value 2.04×10^{-5} Scm^{-1}. For titania based polymer composite electrolyte 8 wt.% composition show maximum ionic conductivity at RT having value 3.17×10^{-5} Scm^{-1}. Finally, for organo-modified montmorillonite polymer composite electrolytes 5 wt.% composition shows maximum ionic conductivity at RT having value 3.29×10^{-5} Scm^{-1}. A comparative study of dc conductivity as a function of filler loading for three series of polymer composite electrolytes are carried out for RT, T = 303 K, and shown in figure (8.1). It can be observed that maximum dc conductivity can be observed for minimum filler addition of intercalation based montmorillonite clay filler, which may be due to high aspect ratio property of montmorillonite clay.

- Temperature dependent dc conductivity is following the VTF behaviour, which indicates the presence of coupling between ionic conductivity and polymer segmental relaxation.

- Frequency dependent ac conductivity show the presence of universal dielectric response behaviour at high temperature and the low-frequency region of ac conductivity spectra. At very low temperature, the dominance of universal dielectric response behaviour is found decreasing, and conduction process is mainly dominated by nearly constant loss phenomena.

- The probable cause behind nearly constant loss phenomena is associated with caged ion dynamics motion based on the activation energy values for universal dielectric response region and nearly constant loss region.

- Ion conduction mechanism is also explained with different models like Ngai Coupling model, Random Free Energy Barrier model, MIGRATION model etc. A comparative study is carried out using these various formalisms to analyze the ion conduction mechanism for polymer nanocomposite electrolytes. From comparative analysis it is shown that the ionic conductivity is favoured by polymer segmental relaxation. The ionic conductivity and segmental relaxation are coupled in nature, and the conduction process is co-operative in nature.

- The dielectric analysis has shown the presence of electrode polarization effects due to space charge polarization at lower frequencies. Analyzing the frequency dependent imaginary part of dielectric data using Havriliak-Negami approach, it can be observed that the relaxation associated with the electrode polarization is nearly non-interactive in nature as the shape parameters are found very close to unity.

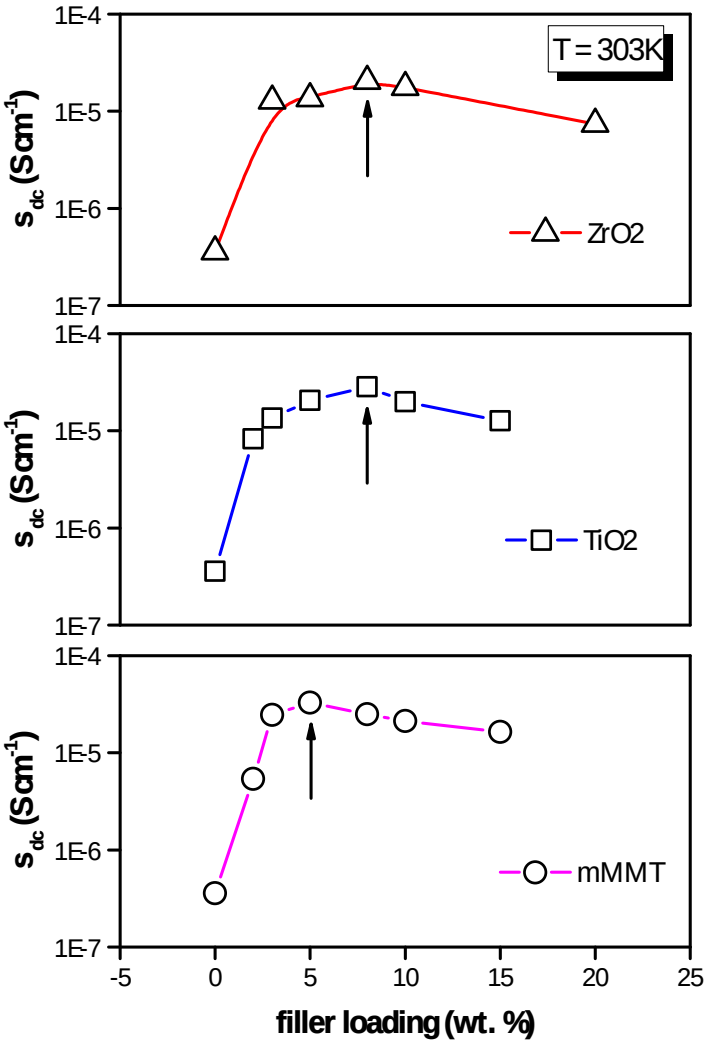

Figure 8.1: DC conductivity for different PNCE compositions as a function of filler loading percentage at temperature T = 303 K.

- The dielectric analysis also reveal the presence of segmental relaxation at a comparatively high frequency and high temperature region. Upon analyzing with Havriliak-Negami approach, the observed relaxation phenomenon associated with segmental relaxation are found to be non-Debye type in nature. The shape parameters are obtained in the range 0.7 to 0.75 for segmental relaxation.

- Using phase inversion technique, a series of blend based polymer gel electrolytes is prepared. The ionic conductivity of the series is optimized and found that for 40 wt.% PVdF-HFP and 60 wt.% PMMA blends composition, room temperature, T = 303 K, ionic conductivity is found maximum with its value 7.77×10^{-5} Scm^{-1}. It is also observed that the polymer blend matrix with the same composition is also capable of holding the maximum amount of liquid electrolytes. It indicates that ion conduction in

gel polymer electrolytes mainly occurs through the liquid electrolytes trapped within the host polymer matrix.

- DC conductivity and the relaxation times are following Arrhenius relation, which suggests that ionic transport process in gel polymer electrolyte occur predominantly through liquid electrolytes trapped in the host polymer matrix of gel polymer electrolyte membrane.

8.2 Future Scope

A lot of further studies on different aspects is possible to explore fundamental interest as well as possible device based applications. In the present investigation ternary polymer composite electrolytes and a blend based gel polymer electrolyte are studied. Ionic conductivity of these materials are found $\approx 10^{-5}$ S cm^{-1}, which still can be improved with further optimization of polymer electrolytes using different filler, salt, plasticizer, blend polymeric host etc. The followings are the future scope of the present work.

- Study of ionic transport mechanism for quaternary systems, mainly hybrid polymer electrolytes, need to be explored. It may consist of polymer blend as polymer host, a mixture of low molecular weight and high molecular weight polymers at various ratio for varying segmental mobility.

- The Ionic transport mechanism for composite polymer electrolytes to be studied with positron annihilation spectroscopy (PAS). Using PAS a better representation of ion conduction mechanism in terms of free volume theory can be achieved. A correlative study of free volume theory and MIGRATION can be attempted.

- Dual ion conduction phenomenon in polymer composite films need to be addressed. This can be attempted by using bulky anion based salt and layer structured fillers or by using polyelectrolyte membranes.

- Neutron scattering experiment can be carried out to study the influence of polymer architecture on ion conduction mechanism.

- Mechanical spectroscopy or dynamical mechanical analysis can be performed to correlate the ionic conductivity and mechanical properties of polymer electrolytes.

References

[1] M. J. Bradshaw, *Global Energy Dilemmas*, Polity, 2014.

[2] B. Bagley, D. Moulioukova and H. S. Kassab, *The Impact of Emerging Economies on Global Energy and the Environment*, Lexington Books, Lanham, 2015.

[3] V. C. Nelson, *Introduction to Renewable Energy*, CRC Press, Boca Raton, 2011.

[4] D. Craddock, *Renewable Energy Made Easy: Free Energy from Solar, Wind, Hydropower and Other Alternative Energy Sources*, Atlantic Publishing Group, Florida, 2008.

[5] T. B. Johansson, H. Kelly, A. K. N.Reddy and R. H. Williams, *Renewable Energy: Sources for Fuels and Electricity*, Island Press, Washington, 2008.

[6] G. Boyle, *Renewable Energy: Power for a Sustainable Future*, Oxford University Press, Oxford, 2012.

[7] J. Zhang, L. Zhang, H. Liu, A. Sun and R.-S. Liu, *Electrochemical Technologies for Energy Storage and Conversion*, Wiley VCH Verlag and Co., Boschstr, 2012.

[8] C. Liu, Z. G. Neale and G. Cao, *Materials Today*, 2016, **19**, 109 – 123.

[9] R. Wagner, N. Preschitschek, S. Passerini, J. Leker and M. Winter, *Journal of Applied Electrochemistry*, 2013, **43**, 481–496.

[10] M. Armand and J. M. Tarascon, *Nature*, 2008, **451**, 652–657.

[11] B. Scrosati, *Modern Batteries (Second Edition)*, Butterworth-Heinemann, Oxford, 1997, pp. 198 – 242.

[12] F. M. Gray, *Solid Polymer Electrolytes: Fundamentals and Technological Applications*, CRC Press, London, 1991.

[13] F. M. Gray, *Polymer Electrolytes*, Royal Society of Chemistry, London, 1997.

[14] L. Merhari, *Hybrid Nanocomposites for Nanotechnology*, Springer, Limoges, 2009.

[15] J. Fang, J. Qiao, D. P. Wilkinson and J. Zhang, *Electrochemical Polymer Electrolyte Membranes*, CRC Press, Boca Raton, 2000.

[16] T. Christen and M. W. Carlen, *Journal of Power Sources*, 2000, **91**, 210 – 216.

[17] D. P. Dubal, O. Ayyad, V. Ruiz and P. Gomez-Romero, *Chem. Soc. Rev.*, 2015, **44**, 1777–1790.

[18] J. Nunes-Pereira, C. Costa and S. Lanceros-Méndez, *Journal of Power Sources*, 2015, **281**, 378 – 398.

[19] H. Lee, M. Yanilmaz, O. Toprakci, K. Fu and X. Zhang, *Energy Environ. Sci.*, 2014, **7**, 3857–3886.

[20] D. Scherson, *Fundamentals of Energy Storage and Conversion: ECS Transactions*, ECS, New Jersey, 2008.

[21] T. P. J. Crompton, *Battery Reference Book*, Newnes, Oxford, 2000.

[22] L. Long, S. Wang, M. Xiao and Y. Meng, *J. Mater. Chem. A*, 2016, **4**, 10038–10069.

[23] B. Scrosati and C. A. Vincent, *MRS Bulletin*, 2000, **25**, 28–30.

[24] R. C. Agrawal and G. P. Pandey, *Journal of Physics D: Applied Physics*, 2008, **41**, 223001.

[25] H. S. Lee, X. Q. Yang, C. L. Xiang, J. McBreen and L. S. Choi, *Journal of The Electrochemical Society*, 1998, **145**, 2813–2818.

[26] H. S. Lee, Z. F. Ma, X. Q. Yang, X. Sun and J. McBreen, *Journal of The Electrochemical Society*, 2004, **151**, A1429–A1435.

[27] Y. Zhu, X. Gao, X. Wang, Y. Hou, L. Liu and Y. Wu, *Electrochemistry Communications*, 2012, **22**, 29 – 32.

[28] Y. Zhu, X. Wang, Y. Hou, X. Gao, L. Liu, Y. Wu and M. Shimizu, *Electrochimica Acta*, 2013, **87**, 113 – 118.

[29] H. Nakajima and H. Ohno, *Polymer*, 2005, **46**, 11499 – 11504.

[30] K. M. Abraham, Z. Jiang, and B. Carroll, *Chemistry of Materials*, 1997, **9**, 1978–1988.

[31] W. Xu, J.-P. Belieres, and C. A. Angell, *Chemistry of Materials*, 2001, **13**, 575–580.

[32] Y. Liu, J. Y. Lee and L. Hong, *Journal of Applied Polymer Science*, 2003, **89**, 2815–2822.

[33] B. E. Conway and W. G. Pel, *Journal of Solid State Electrochemistry*, 2003, **7**, 637–644.

[34] L. L. Zhang and X. S. Zhao, *Chem. Soc. Rev.*, 2009, **38**, 2520–2531.

[35] J. Rodríguez, E. Navarrete, E. A. Dalchiele, L. Sánchez, J. R. Ramos-Barrado and F. Martín, *Journal of Power Sources*, 2013, **237**, 270 – 276.

[36] H. Gao and K. Lian, *RSC Adv.*, 2014, **4**, 33091–33113.

[37] N. H. Behling, *Fuel Cells*, Elsevier, 2013, pp. 423 – 600.

[38] M. Rikukawa and K. Sanui, *Progress in Polymer Science*, 2000, **25**, 1463 – 1502.

[39] F. Alcaide, P.-L. Cabot and E. Brillas, *Journal of Power Sources*, 2006, **153**, 47 – 60.

[40] V. Mehta and J. S. Cooper, *Journal of Power Sources*, 2003, **114**, 32 – 53.

[41] R. Mouazer, M. Persin, M. Cretin and A. Larbot, *Colloids and Surfaces A: Physicochemical and Engineering Aspects*, 2004, **244**, 95 – 104.

[42] S. Zhai, L. Li, F. Chen, Q. Jiao, C. Rüssel and C. Lin, *Journal of the American Ceramic Society*, 2015, **98**, 3770–3774.

[43] B. Sujatha, R. Viswanatha, B. K. Chethana, H. Nagabhushana and C. Narayana Reddy, *Ionics*, 2016, **22**, 563–571.

[44] N. J. Dudney, in *Glass and Ceramic Electrolytes for Lithium and Lithium-Ion Batteries*, ed. G.-A. Nazri and G. Pistoia, Springer US, Boston, MA, 2003, pp. 624–642.

[45] T. Suriwong, T. Thongtem and S. Thongtem, *Materials Science in Semiconductor Processing*, 2015, **39**, 348 – 354.

[46] D. Golodnitsky, G. Ardel, E. Strauss, E. Peled, Y. Lareah and Y. Rosenberg, *Journal of The Electrochemical Society*, 1997, **144**, 3484–3491.

[47] A. M. Stephan, K. S. Nahm, T. P. Kumar, M. A. Kulandainathan, G. Ravi and J. Wilson, *Journal of Power Sources*, 2006, **159**, 1316 – 1321.

[48] V. Aravindan and P. Vickraman, *Journal of Applied Polymer Science*, 2008, **108**, 1314–1322.

[49] R. tao Wang, X. ping Liang, Y. Peng, X. wei Fan and J. xin Li, *Journal of Ceramic Processing Research*, 2010, **11**, 173–175.

[50] E. Strauss, D. Golodnitsky, G. Ardel and E. Peled, *Electrochimica Acta*, 1998, **43**, 1315 – 1320.

[51] C. Vachon, C. Labreche, A. Vallee, S. Besner, M. Dumont and J. Prud'homme, *Macromolecules*, 1995, **28**, 5585–5594.

[52] M. Michael, M. Jacob, S. Prabaharan and S. Radhakrishna, *Solid State Ionics*, 1997, **98**, 167 – 174.

[53] Y. Kato, K. Hasumi, S. Yokoyama, T. Yabe, H. Ikuta, Y. Uchimoto and M. Wakihara, *Solid State Ionics*, 2002, **150**, 355 – 361.

[54] N. Kuznetsova, N. Bogino, L. Tsivinskaya and Y. Yavorskaya, *Polymer Science U.S.S.R.*, 1974, **16**, 2826 – 2829.

[55] S. Choi, S. Jo, W. Lee and Y.-R. Kim, *Advanced Materials*, 2003, **15**, 2027–2032.

[56] X. Wang, C. Gong, D. He, Z. Xue, C. Chen, Y. Liao and X. Xie, *Journal of Membrane Science*, 2014, **454**, 298 – 304.

[57] J. R. Kim, S. W. Choi, S. M. Jo, W. S. Lee and B. C. Kim, *Electrochimica Acta*, 2004, **50**, 69 – 75.

[58] P. Sun, Y. Liao, X. Luo, Z. Li, T. Chen, L. Xing and W. Li, *RSC Adv.*, 2015, **5**, 64368–64377.

[59] D. E. Fenton, J. M. Parker and P. V. Wright, *Polymer*, 1973, **14**, 589.

[60] P. V. Wright, *British Polymer Journal*, 1975, **7**, 319–327.

[61] P. G. Bruce and C. A. Vincent, *J. Chem. Soc., Faraday Trans.*, 1993, **89**, 3187–3203.

[62] D. Payne and P. Wright, *Polymer*, 1982, **23**, 690 – 693.

[63] J. Parker, P. Wright and C. Lee, *Polymer*, 1981, **22**, 1305 – 1307.

[64] D. Shriver, B. Papke, M. Ratner, R. Dupon, T. Wong and M. Brodwin, *Solid State Ionics*, 1981, **5**, 83 – 88.

[65] D. James, R. Wetton and D. Brown, *Polymer*, 1979, **20**, 187 – 195.

[66] J. Motomatsu, H. Kodama, T. Furukawa and Y. Tominaga, *Polymers for Advanced Technologies*, 2016.

[67] S. Klongkan and J. Pumchusak, *Electrochimica Acta*, 2015, **161**, 171 – 176.

[68] P. Pal and A. Ghosh, *Journal of Applied Physics*, 2016, **120**, 045108.

[69] M. N. Chai and M. I. N. Isa, *Scientific Reports*, 2016, **6**, 27328.

[70] S. Livi, J. Duchet-Rumeau, J.-F. Gérard and T. N. Pham, *Macromolecular Chemistry and Physics*, 2015, **216**, 359 – 368.

[71] C. W. Walker and M. Salomon, *Journal of The Electrochemical Society*, 1993, **140**, 3409–3412.

[72] M. Yahya and A. Arof, *European Polymer Journal*, 2003, **39**, 897 – 902.

[73] A. Mohamad and A. Arof, *Materials Letters*, 2007, **61**, 3096 – 3099.

[74] M. Kadir, S. Majid and A. Arof, *Electrochimica Acta*, 2010, **55**, 1475 – 1482.

[75] H. Mazor, D. Golodnitsky, E. Peled, W. Wieczorek and B. Scrosati, *Journal of Power Sources*, 2008, **178**, 736 – 743.

[76] H. Ohno and K. Ito, *Polymer*, 1995, **36**, 891 – 893.

[77] N. Shubha, H. Zhu, M. Forsyth and M. Srinivasan, *Polymer*, 2016, **99**, 748 – 755.

[78] X. Li, P. Yan, M. H. Engelhard, A. J. Crawford, V. V. Viswanathan, C. Wang, J. Liu and V. L. Sprenkle, *Nano Energy*, 2016, **27**, 664 – 672.

[79] H. Oh, K. Xu, H. D. Yoo, D. S. Kim, C. Chanthad, G. Yang, J. Jin, I. A. Ayhan, S. M. Oh and Q. Wang, *Chemistry of Materials*, 2016, **28**, 188–196.

[80] A. Chandra, P. C. Srivastava and S. Chandra, *Journal of Materials Science*, 1995, **30**, 3633–3638.

[81] W. Wieczorek, A. Zalewska, D. Raducha, Z. Florjańczyk, and J. R. Stevens, *The Journal of Physical Chemistry B*, 1998, **102**, 352–360.

[82] J. Zhou and P. S. Fedkiw, *Solid State Ionics*, 2004, **166**, 275 – 293.

[83] S. Srivastava, J. L. Schaefer, Z. Yang, Z. Tu and L. A. Archer, *Advanced Materials*, 2014, **26**, 201– 234.

[84] F. Croce, F. Bonino, S. Panero and B. Scrosati, *Philosophical Magazine B*, 1989, **59**, 161–168.

[85] J. Płocharski, W. Wieczorek, J. Przyłuski and K. Such, *Applied Physics A*, 1989, **49**, 55 – 60.

[86] M. Dissanayake, P. Jayathilaka, R. Bokalawala, I. Albinsson and B.-E. Mellander, *Journal of Power Sources*, 2003, **119–121**, 409 – 414.

[87] J. W. Park, E. D. Jeong, M.-S. Won and Y.-B. Shim, *Journal of Power Sources*, 2006, **160**, 674 – 680.

[88] J.-K. Lee, Y.-J. Lee, W.-S. Chae and Y.-M. Sung, *Journal of Electroceramics*, 2006, **17**, 941–944.

[89] S. Y. An, I. C. Jeong, M.-S. Won, E. D. Jeong and Y.-B. Shim, *Journal of Applied Electrochemistry*, 2009, **39**, 1573 – 1578.

[90] E. M. Masoud, A.-A. El-Bellihi, W. Bayoumy and M. Mousa, *Journal of Alloys and Compounds*, 2013, **575**, 223 – 228.

[91] G. Nagasubramanian, A. Attia, G. Halpert and E. Peled, *Solid State Ionics*, 1993, **67**, 51 – 56.

[92] W. Krawiec, L. Scanlon, J. Fellner, R. Vaia, S. Vasudevan and E. Giannelis, *Journal of Power Sources*, 1995, **54**, 310 – 315.

[93] J.-H. Ahn, G. Wang, H. Liu and S. Dou, *Journal of Power Sources*, 2003, **119–121**, 422 – 426.

[94] A. Ahmad, M. Rahman and M. Su'ait, *Physica B: Condensed Matter*, 2008, **403**, 4128 – 4131.

[95] S. Das and A. Ghosh, *Journal of Applied Physics*, 2015, **117**, 174103 (1–7).

[96] B. Scrosati, F. Croce and S. Panero, *Journal of Power Sources*, 2001, **100**, 93 – 100.

[97] H. Zhang, J. Wang, H. Zheng, K. Zhuo, and Y. Zhao, *The Journal of Physical Chemistry B*, 2005, **109**, 2610–2616.

[98] A. Bac, M. Ciosek, M. Bukat, M. Marczewski, H. Marczewska and W. Wieczorek, *Journal of Power Sources*, 2006, **159**, 405 – 411.

[99] Y. Chen-Yang, H. Chen, F. Lin, C. Liao and T. Chen, *Solid State Ionics*, 2003, **156**, 383 – 392.

[100] Z. Li, G. Su, D. Gao, X. Wang and X. Li, *Electrochimica Acta*, 2004, **49**, 4633 – 4639.

[101] M. Morita, H. Noborio, N. Yoshimoto and M. Ishikawa, *Solid State Ionics*, 2006, **177**, 715 – 720.

[102] P. Raghavan, X. Zhao, J. Manuel, G. S. Chauhan, J.-H. Ahn, H.-S. Ryu, H.-J. Ahn, K.-W. Kim and C. Nah, *Electrochimica Acta*, 2010, **55**, 1347 – 1354.

[103] W. Wieczorek, K. Such, S. H. Chung and J. R. Stevens, *The Journal of Physical Chemistry*, 1994, **98**, 9047–9055.

[104] A. S. Best, J. Adebahr, P. Jacobsson, D. R. MacFarlane, and M. Forsyth, *Macromolecules*, 2001, **34**, 4549–4555.

[105] M. Forsyth, D. MacFarlane, A. Best, J. Adebahr, P. Jacobsson and A. Hill, *Solid State Ionics*, 2002, **147**, 203 – 211.

[106] C. Karlsson, A. S. Best, J. Swenson, J. Kohlbrecher, and L. B'orjesson, *Macromolecules*, 2005, **38**, 6666–6671.

[107] B. K. Money, K. Hariharan and J. Swenson, *The Journal of Physical Chemistry B*, 2012, **116**, 7762–7770.

[108] I. Tanahashi, A. Yoshida and A. Nishino, *Journal of The Electrochemical Society*, 1990, **137**, 3052–3057.

[109] T. Kanbara, M. Inami and T. Yamamoto, *Journal of Power Sources*, 1991, **36**, 87 – 93.

[110] R. A. Vaia and E. P. Giannelis, *Macromolecules*, 1997, **30**, 8000 – 8009.

[111] H.-W. Chen and F.-C. Chang, *Polymer*, 2001, **42**, 9763 – 9769.

[112] S. Kim, E.-J. Hwang, Y. Jung, M. Han and S.-J. Park, *Colloids and Surfaces A: Physicochemical and Engineering Aspects*, 2008, **313–314**, 216 – 219.

[113] S. Kim and S.-J. Park, *Solid State Ionics*, 2007, **178**, 973 – 979.

[114] Y. Huang, M. Lee, M. Yang and C. Chen, *Applied Clay Science*, 2010, **49**, 163 – 169.

[115] S. Choudhary and R. J. Sengwa, *Ionics*, 2012, **18**, 379–384.

[116] H.-W. Chen, T.-P. Lin and F.-C. Chang, *Polymer*, 2002, **43**, 5281 – 5288.

[117] Y. Ma, L. Li, G. Gao, X. Yang and Y. You, *Electrochimica Acta*, 2016, **187**, 535 – 542.

[118] G. Feuillade and P. Perche, *Journal of Applied Electrochemistry*, 1975, **5**, 63 – 69.

[119] P. Vickraman and S. Ramamurthy, *Materials Letters*, 2006, **60**, 3431 – 3436.

[120] S. Rajendran, R. Babu and P. Sivakumar, *Journal of Applied Polymer Science*, 2009, **113**, 1651–1656.

[121] P. Meneghetti, S. Qutubuddin and A. Webber, *Electrochimica Acta*, 2004, **49**, 4923 – 4931.

[122] S. Ramesh and G. P. Ang, *Ionics*, 2010, **16**, 465–473.

[123] S. W. Choi, J. R. Kim, S. M. Jo, W. S. Lee and Y.-R. Kim, *Journal of The Electrochemical Society*, 2005, **152**, A989–A995.

[124] P. Carol, P. Ramakrishnan, B. John and G. Cheruvally, *Journal of Power Sources*, 2011, **196**, 10156 – 10162.

[125] P. Yan, Z. Huang, Y. Lin, X. Wu, Y. Yang, D. Wang, F. Chen, C. Zhang and D. He, *Ionics*, 2015, **21**, 593–599.

[126] E. Cznotka, S. Jeschke and H.-D. Wiemhöfer, *Solid State Ionics*, 2016, **289**, 35 – 47.

[127] S. Panero, D. Satolli, A. D'Epifano and B. Scrosati, *Journal of The Electrochemical Society*, 2002, **149**, A414–A417.

[128] Y. Liao, X. Li, C. Fu, R. Xu, L. Zhou, C. Tan, S. Hu and W. Li, *Journal of Power Sources*, 2011, **196**, 2115 – 2121.

[129] S.-H. Kim, K.-H. Choi, S.-J. Cho, E.-H. Kil and S.-Y. Lee, *J. Mater. Chem. A*, 2013, **1**, 4949–4955.

[130] W. K. Lee, J. F. Liu and A. S. Nowick, *Phys. Rev. Lett.*, 1991, **67**, 1559 –1561.

[131] K. Ngaí, *Solid State Ionics*, 1981, **5**, 27 – 33.

[132] J. R. Macdonald, *Journal of Applied Physics*, 1998, **84**, 812–827.

[133] K. L. Ngai and C. León, *Phys. Rev. B*, 2002, **66**, 064308(1–11).

[134] K. Funke, R. D. Banhatti and C. Cramer, *Phys. Chem. Chem. Phys.*, 2005, **7**, 157–165.

[135] S. D. Druger, M. A. Ratner and A. Nitzan, *Solid State Ionics*, 1983, **9**, 1115 – 1120.

[136] A. Maitra and A. Heuer, *Phys. Rev. Lett.*, 2007, **98**, 227802.

[137] M. A. Webb, B. M. Savoie, Z.-G. Wang and T. F. M. III, *Macromolecules*, 2015, **48**, 7346–7358.

[138] E. F. Hairetdinov, N. F. Uvarov, H. K. Patel and S. W. Martin, *Phys. Rev. B*, 1994, **50**, 13259 –13266.

[139] J. C. Dyre, *Journal of Applied Physics*, 1988, **64**, 2456–2468.

[140] J. C. Dyre and T. B. Schrøder, *Rev. Mod. Phys.*, 2000, **72**, 873–892.

[141] A. Auroux and J. Vedrine, *Catalysis by Acids and Bases*, Elsevier, 1985, vol. 20, pp. 311 – 318.

[142] T. A. Ring, *Fundamentals of Ceramic Powder Processing and Synthesis*, Academic Press, San Diego, 1996, pp. 95 – 138.

[143] T. A. Ring, *Fundamentals of Ceramic Powder Processing and Synthesis*, Academic Press, San Diego, 1996, pp. 139 – 178.

[144] D. Segal, *J. Mater. Chem.*, 1997, **7**, 1297–1305.

[145] H. Birol, C. Renato Rambo, M. Guiotoku and D. Hotza, *RSC Adv.*, 2013, **3**, 2873–2884.

[146] V. Mandic, E. Tkalcec, J. Popovic, S. Kurajica and J. Schmauch, *Journal of the European Ceramic Society*, 2016, **36**, 1285 – 1292.

[147] J. Li, X. Sun, S. Liu, X. Li, J.-G. Li and D. Huo, *Ceramics International*, 2015, **41**, 3283 – 3287.

[148] O. V. der Biest, J. Kwarciak, D. Dierickx, M. Dhalle, W. Boon and Y. Bruynseraede, *Physica C: Superconductivity*, 1991, **190**, 119 – 121.

[149] J. Ortiz-Landeros, C. Gómez-Yáñez, R. López-Juárez, I. Dávalos-Velasco and H. Pfeiffer, *Journal of Advanced Ceramics*, 2012, **1**, 204–220.

[150] R. Chu, Z. Xu, Z. Zhu, G. Li and Q. Yin, *Materials Science and Engineering: B*, 2005, **122**, 106 – 109.

[151] A. Sutka and G. Mezinskis, *Frontiers of Materials Science*, 2012, **6**, 128–141.

[152] X. Wang, J. Feng, Y. Bai, Q. Zhang and Y. Yin, *Chemical Reviews*, 0, **0**, null.

[153] J. W. Gilman, C. L. Jackson, A. B. Morgan, , R. H. Jr., E. Manias, E. P. Giannelis, , M. Wuthenow, D. Hilton, and S. H. Phillips, *Chemistry of Materials*, 2000, **12**, 1866–1873.

[154] H. Ishida, S. Campbell, and J. Blackwell, *Chemistry of Materials*, 2000, **12**, 1260–1267.

[155] M. Wang, F. Zhao, Z. Guo and S. Dong, *Electrochimica Acta*, 2004, **49**, 3595 – 3602.

[156] J.-M. Yeh, S.-J. Liou, C.-Y. Lin, C.-Y. Cheng, , Y.-W. Chang and K.-R. Lee, *Chemistry of Materials*, 2002, **14**, 154–161.

[157] R. Ashrafi, D. K. Sahu, P. Kesharwani, M. Ganjir and R. Agrawal, *Journal of Non-Crystalline Solids*, 2014, **391**, 91 – 95.

[158] M. Khanmirzaei and S. Ramesh, *Measurement*, 2014, **58**, 68 – 72.

[159] D.-W. Kang and J.-K. Kim, *Journal of Electroanalytical Chemistry*, 2016, **775**, 37 – 42.

[160] X. Luo, Y. Liao, H. Xie, Y. Zhu, Q. Huang and W. Li, *Electrochimica Acta*, 2016, **220**, 47 – 56.

[161] M. Liu, D. Zhou, Y.-B. He, Y. Fu, X. Qin, C. Miao, H. Du, B. Li, Q.-H. Yang, Z. Lin, T. Zhao and F. Kang, *Nano Energy*, 2016, **22**, 278 – 289.

[162] A. Guinier, *X-ray Diffraction in Crystals, Imperfect Crystals, and Amorphous Bodies*, Dover Publication, New York, 1994.

[163] B. E. Warren, *X-ray Diffraction*, Dover Publication, New York, 2012.

[164] E. J. Mittemeijer and P. Scardit, *Diffraction Analysis of the Microstructure of Materials*, Springer, New York, 2013.

[165] V. Pecharsky and P. Zavalij, *Fundamentals of Powder Diffraction and Structural Characterization of Materials*, Springer, New York, 2008.

[166] L. Reimer, *Scanning Electron Microscopy: Physics of Image Formation and Microanalysis*, Springer, New York, 1998.

[167] B. C. Smith, *Fundamentals of Fourier Transform Infrared Spectroscopy*, Springer, New York, 2011.

[168] F. Kremer and A. Schonhals, *Broadband Dielectric Spectroscopy*, Springer, Heidelberg, 2002.

[169] J. P. Runt and J. J. Fitzgerald, *Dielectric spectroscopy of polymeric materials*, American Chemical Society, New York, 1997.

[170] F. Croce, G. B. Appetecchi, L. Persi and B. Scrosati, *Nature*, 1998, **394**, 456–458.

[171] G. Molnár, S. Cobo, T. Mahfoud, E. J. M. Vertelman, P. J. van Koningsbruggen, P. Demont and A. Bousseksou, *The Journal of Physical Chemistry C*, 2009, **113**, 2586–2593.

[172] S. Samanta, K. Jana, K. Gupta, A. Nayak and U. C. Ghosh, *Materials Chemistry and Physics*, 2016, **182**, 173 – 181.

[173] A. Viswanathan and S. A. Suthanthiraraj, *Solid State Ionics*, 1993, **62**, 79 – 83.

[174] T. Dam, S. N. Tripathy, M. Paluch, S. S. Jena and D. K. Pradhan, *Electrochimica Acta*, 2016, **202**, 147 – 156.

[175] A. Rivera, C. León, J. Sanz, J. Santamaria, C. T. Moynihan and K. L. Ngai, *Phys. Rev. B*, 2002, **65**, 224302(1–6).

[176] W. Lee, B. Lim, J. Liu and A. Nowick, *Solid State Ionics*, 1992, **53**, 831 – 836.

[177] P. Jeevanandam and S. Vasudevan, *The Journal of Chemical Physics*, 1998, **109**, 8109–8117.

[178] T. Smith Sorensen, R. Diaz-Calleja, E. Riande, J. Guzman and A. Andrio, *J. Chem. Soc., Faraday Trans.*, 1997, **93**, 2399–2411.

[179] A. Schiraldi, P. Baldini and E. Pezzati, *Journal of thermal analysis*, 1985, **30**, 1343–1348.

[180] H. D. Rowland, W. P. King, G. L. W. Cross and J. B. Pethica, *ACS Nano*, 2008, **2**, 149 – 428.

[181] K. Ngai and O. Kanert, *Solid State Ionics*, 1992, **53**, 936 – 946.

[182] D. Diddens and A. Heuer.

[183] D. Knödler, P. Pendzig and W. Dieterich, *Solid State Ionics*, 1996, **86–88, Part 1**, 29 – 39.

[184] G. E. Murch and J. C. Dyre, *Critical Reviews in Solid State and Materials Sciences*, 1989, **15**, 345–365.

[185] K. L. Ngai, *The Journal of Chemical Physics*, 2015, **142**,.

[186] K. Funke and R. D. Banhatti, *Solid State Ionics*, 2006, **177**, 1551 – 1557.

[187] S. Dalgleish, L. Reissig, Y. Sudo and K. Awaga, *Chem. Commun.*, 2015, **51**, 16401–16404.

[188] N. Elfaleh and S. Kamoun, *Ionics*, 2015, **21**, 2685–2692.

[189] C. M. Mathew, K. Kesavan and S. Rajendran, *Polymer International*, 2015, **64**, 750–757.

[190] S. Ke, H. Huang, L. Ren and Y. Wang, *Journal of Applied Physics*, 2009, **105**, 096103 (1–3).

[191] B. Roling, C. Martiny and S. Murugavel, *Phys. Rev. Lett.*, 2001, **87**, 085901 (1–4).

[192] D. L. Sidebottom, *Rev. Mod. Phys.*, 2009, **81**, 999–1014.

[193] A. W. Imre, M. Schönhoff and C. Cramer, *Phys. Rev. Lett.*, 2009, **102**, 255901(1–4).

[194] S. N. Tripathy, Z. Wojnarowska, J. Knapik, H. Shirota, R. Biswas and M. Paluch, *The Journal of Chemical Physics*, 2015, **142**, 184504 (1–10).

[195] M. A. Ratner and D. F. Shriver, *Chemical Reviews*, 1988, **88**, 109–124.

[196] Y. Wang, A. L. Agapov, F. Fan, K. Hong, X. Yu, J. Mays and A. P. Sokolov, *Phys. Rev. Lett.*, 2012, **108**, 088303.

[197] R. Sengwa, P. Dhatarwal and S. Choudhary, *Electrochimica Acta*, 2014, **142**, 359 – 370.

[198] S. R. Mohapatra, A. K. Thakur and R. Choudhary, *Journal of Power Sources*, 2009, **191**, 601 – 613.

[199] T. Dam, N. K. Karan, R. Thomas, D. K. Pradhan and R. S. Katiyar, *Ionics*, 2015, **21**, 401–410.

[200] B. Laik, L. Legrand, A. Chausse and R. Messina, *Electrochimica Acta*, 1998, **44**, 773 – 780.

[201] N. Inoue, M. Xu and S. Petrucci.

[202] C. L. Angell, *Trans. Faraday Soc.*, 1956, **52**, 1178–1183.

[203] Z. Osman and A. Arof, *Electrochimica Acta*, 2003, **48**, 993 – 999.

[204] M. R. Johan, O. H. Shy, S. Ibrahim, S. M. M. Yassin and T. Y. Hui, *Solid State Ionics*, 2011, **196**, 41 – 47.

[205] J. Dygas, B. Misztal-Faraj, Z. Florjańczyk, F. Krok, M. Marzantowicz and E. Zygadło-Monikowska, *Solid State Ionics*, 2003, **157**, 249 – 256.

[206] A. A. Khamzin, I. I. Popov and R. R. Nigmatullin, *Phys. Rev. E*, 2014, **89**, 032303 (1–8).

[207] H. Jain and X. Lu, *Journal of Non-Crystalline Solids*, 1996, **196**, 285 – 290.

[208] C. León, A. Rivera, A. Várez, J. Sanz, J. Santamaria and K. L. Ngai, *Phys. Rev. Lett.*, 2001, **86**, 1279–1282.

[209] K. L. Ngai, *The Journal of Chemical Physics*, 1999, **110**, 10576–10584.

[210] S. D. Druger, *The Journal of Chemical Physics*, 1994, **100**, 3979–3984.

[211] N. Karan, D. Pradhan, R. Thomas, B. Natesan and R. Katiyar, *Solid State Ionics*, 2008, **179**, 689 – 696.

[212] S. Zhang, S. Dou, R. H. Colby and J. Runt, *Journal of Non-Crystalline Solids*, 2005, **351**, 2825 – 2830.

[213] M. Díaz-Guillén, M. Frechero, J. Díaz-Guillén, A. Fuentes and C.León, *Journal of Electroceramics*, 2015, **34**, 15–19.

[214] A. Rivera, J. Santamaría, C. León and K. Ngai, *Journal of Physics Condensed Matter*, 2003, **15**, S1633 – S1642.

[215] B. K. Money, K. Hariharan and J. Swenson, *Solid State Ionics*, 2014, **262**, 785 – 789.

[216] K. Ngai, R. Rendell and C. Leon, *Journal of Non-Crystalline Solids*, 2002, **307–310**, 1039 – 1049.

[217] M. R. Díaz-Guillén, J. A. Díaz-Guillén, A. F. Fuentes, J. Santamaría and C. León, *Phys. Rev. B*, 2010, **82**, 174304.

[218] S. Das and A. J. Bhattacharyya, *The Journal of Physical Chemistry Letters*, 2012, **3**, 3550–3554.

[219] Y.-X. Jiang, X.-M. Chen, Y.-F. Mo and Z.-F. Tong, *Journal of Molecular Catalysis A: Chemical*, 2004, **213**, 231 – 234.

[220] M. Manríquez, T. López, R. Gómez and J. Navarrete, *Journal of Molecular Catalysis A: Chemical*, 2004, **220**, 229 – 237.

[221] P. Pal and A. Ghosh, *Phys. Rev. E*, 2015, **92**, 062603.

[222] T. Dam, S. S. Jena and D. K. Pradhan, *Phys. Chem. Chem. Phys.*, 2016, **18**, 19955–19965.

[223] A. K. Thakur, D. K. Pradhan, B. Samantaray and R. Choudhary, *Journal of Power Sources*, 2006, **159**, 272 – 276.

[224] S. Murugavel and B. Roling, *Phys. Rev. Lett.*, 2002, **89**, 195902(1–4).

[225] S. Kabi and A. Ghosh, *EPL (Europhysics Letters)*, 2014, **108**, 36002.

[226] A. Karmakar and A. Ghosh, *Phys. Rev. E*, 2011, **84**, 051802(1–9).

[227] S. D. Druger, *The Journal of Chemical Physics*, 1994, **100**, 3979–3984.

[228] K. Funke, R. D. Banhatti, D. M. Laughmann, L. G. Badr, M. Mutke, S. Santic, W. Wrobel, E. M.Fellberg and C. Biermann, *Z. Phys. Chem.*, 2010, **224**, 1891–1950.

[229] D. M. Laughman, R. D. Banhatti and K. Funke, *Phys. Chem. Chem. Phys.*, 2010, **12**, 14102–14108.

[230] M. Kunze, Y. Karatas, H.-D. Wiemhöfer and M. Schönhoff, *Macromolecules*, 2012, **45**, 8328–8335.

[231] M. Purwanto, L. Atmaja, M. A. Mohamed, M. T. Salleh, J. Jaafar, A. F. Ismail, M. Santoso and N. Widiastuti, *RSC Adv.*, 2016, **6**, 2314–2322.

[232] R. J. Sengwa and S. Choudhary, *Journal of Applied Polymer Science*, 2014, **131**, 1097–4628.

[233] P. Aranda and E. Ruiz-Hitzky, *Chemistry of Materials*, 1992, **4**, 1395–1403.

[234] D. K. Pradhan, B. Samantaray, R. Choudhary and A. K. Thakur, *Journal of Power Sources*, 2005, **139**, 384 – 393.

[235] K. Sownthari and S. Suthanthiraraj, *Electrochimica Acta*, 2015, **174**, 885 – 892.

[236] K. Funke, *Progress in Solid State Chemistry*, 1993, **22**, 111 – 195.

[237] K. Funke, *Radiation Effects and Defects in Solids*, 1991, **119-121**, 463–468.

[238] D. P. Singh, K. Shahi and K. K. Kar, *Solid State Ionics*, 2013, **231**, 102 – 108.

[239] S. Bhattacharya and A. Ghosh, *Phys. Rev. B*, 2006, **74**, 184308(1–5).

[240] R. Murugaraj, G. Govindaraj and D. George, *Journal of Materials Science*, 2002, **37**, 5101–5106.

[241] B. Sun, J. Mindemark, E. Morozov, L. T. Costa, M. Bergman, P. Johansson, Y. Fang, I. Furo and D. Brandell, *Phys. Chem. Chem. Phys.*, 2016, doi:10.1039/C6CP00757K.

[242] J. R. MacCallum and C. A. Vincent, *Polymer electrolyte reviews Vol I*, Elsevier Applied Science, New York, 1987.

[243] Y. Hazama, J. Nakamura and A. Natori, *Journal of Materials Science*, 2010, **45**, 2843–2851.

[244] B. Roling, A. Happe, K. Funke and M. D. Ingram, *Phys. Rev. Lett.*, 1997, **78**, 2160–2163.

[245] R. Metzler, E. Barkai and J. Klafter, *Phys. Rev. Lett.*, 1999, **82**, 3563–3567.

[246] J. R. Macdonald, *Journal of Non-Crystalline Solids*, 1997, **212**, 95 – 116.

[247] Y. Yu, Y. X. Zuo, C. C. Zuo, Z. H. Liu and Z. Zhang, *Materials Research Innovations*, 2015, **19**, S10–168–S10–171.

[248] N. R. Chodankar, D. P. Dubal, A. C. Lokhande and C. D. Lokhande, *Journal of Colloid and Interface Science*, 2015, **460**, 370 – 376.

[249] P. Hu, J. Zhao, T. Wang, C. Shang, J. Zhang, B. Qin, Z. Liu, J. Xiong and G. Cui, *Electrochemistry Communications*, 2015, **61**, 32 – 35.

[250] T. Okubo, D. Suzuki and A. Tsuchida, *Colloid and Polymer Science*, 2012, **290**, 411–421.

[251] R. H. Guo, C. H. Hsu, C. C. Hua and S. A. Chen.

[252] J. Liu, W. Li, X. Zuo, S. Liu and Z. Li, *Journal of Power Sources*, 2013, **226**, 101 – 106.

[253] A. M. Stephan and Y. Saito, *Solid State Ionics*, 2002, **148**, 475 – 481.

[254] F. Boudin, X. Andrieu, C. Jehoulet and I. Olsen, *Journal of Power Sources*, 1999, **81–82**, 804 – 807.

[255] Y. Tong, M. Que, S. Su and L. Chen, *Ionics*, 2016, **22**, 1311–1318.

[256] X.-r. Pan, F. Lian, Y. He, Y.-f. Peng, X.-m. Sun, Y. Wen and H.-y. Guan, *Journal of Applied Polymer Science*, 2015, **132**, 1097–4628.

[257] R. Mani, T. Mani and J. R. Stevens, *Journal of Polymer Science Part A: Polymer Chemistry*, 1992, **30**, 2025–2031.

[258] D. Song, C. Xu, Y. Chen, J. He, Y. Zhao, P. Li, W. Lin and F. Fu, *Solid State Ionics*, 2015, **282**, 31 – 36.

[259] D. K. Singh and A. R. Ray, *Journal of Applied Polymer Science*, 1997, **66**, 869–877.

[260] S. Chintapalli and R. Frech, *Solid State Ionics*, 1996, **86**, 341 – 346.

[261] A. Lopes, C. Costa, R. S. i Serra, I. Neves, J. G. Ribelles and S. Lanceros-Méndez, *Solid State Ionics*, 2013, **235**, 42 – 50.

[262] X. Wang, Z. Liu, Q. Kong, W. Jiang, J. Yao, C. Zhang and G. Cui, *Solid State Ionics*, 2014, **262**, 747 – 753.

[263] D. K. Pradhan, N. Karan, R. Thomas and R. Katiyar, *Materials Chemistry and Physics*, 2014, **147**, 1016 – 1021.

[264] J. Menegotto, P. Demont and C. Lacabanne, *Polymer*, 2001, **42**, 4375 – 4383.

[265] J. Hazarika and A. Kumar, *Synthetic Metals*, 2014, **198**, 239 – 247.

[266] D. K. Pradhan, R. Choudhary and B. Samantaray, *Materials Chemistry and Physics*, 2009, **115**, 557 – 561.

[267] Y. Qing, Y. Mu, Y. Zhou, F. Luo, D. Zhu and W. Zhou, *Journal of the European Ceramic Society*, 2014, **34**, 2229 – 2237.

[268] K. Shehzad, Z.-M. Dang, M. N. Ahmad, R. U. R. Sagar, S. Butt, M. U. Farooq and T.-B. Wang, *Carbon*, 2013, **54**, 105 – 112.

Dissemination

Internationally Indexed Journals (*Web of Science, SCI, Scopus, etc.*)[1]

1. **Tapabrata Dam**, N. K. Karan, R. Thomas, D. K. Pradhan* and R. S. Katiyar*, "Observation of ionic transport and ion-coordinated segmental motions in composite (polymer-salt-clay) solid polymer electrolyte.", Ionics, 2015 (21) 401-410.

2. **Tapabrata Dam***, S. N. Tripathy, M. Paluch, S. S. Jena and D. K. Pradhan* , "Investigations of Relaxation Dynamics and Observation of Nearly Constant Loss Phenomena in PEO_{20} - $LiCF_3SO_3$ -ZrO_2 Based Polymer Nano-Composite Electrolyte.", Electrochimica Acta, 2016 (202) 147-156.

3. **Tapabrata Dam***, S. S. Jena and D. K. Pradhan* , "The ionic transport mechanism and coupling between the ion conduction and segmental relaxation processes of PEO_{20} - $LiCF_3SO_3$ based ion conducting polymer clay composites.", Phys. Chem. Chem. Phys., 2016 (18) 19955-19965.

Conferences

1. **Tapabrata Dam**, S. Jena and D. K. Pradhan*, "Equilibrium state of anatase to rutile transformation for nano-structured titanium dioxide powder using polymer template method.", *IOP Conference Series: MSE*, 115: 012038, 2016.
   In: *5^{th} NCPCM, Rourkela, India*, December 12–13, 2015.

2. **Tapabrata Dam**, Satya N. Tripathy, M. Paluch, S. Jena and D. K. Pradhan*, "Ionic Conduction In Polymer Composite Electrolytes.", *AIP Conference Proceedings*, 1731: 070027,2016.
   In: *60^{th} DAE SSPS, Noida, India*, December 21–25, 2015.

Article Under Preparation [2]

1. **Tapabrata Dam***, S. S. Jena and D. K. Pradhan* , "The ionic transport mechanism and coupling between the ion conduction and segmental relaxation processes of PEO_{20} - $LiCF_3SO_3$ based ion conducting polymer clay composites. "

[1] Articles already published, in press, or formally accepted for publication.
[2] Articles under review, communicated, or to be communicated.

Index